

**Aromatic Isophthalamides Aggregate in Lipid Bilayers – Evidence for
Cooperative Transport Mechanism**

S. N. Berry^a, N. Busschaert^a, C. L. Frankling^a, D. Salter^a and P. A. Gale^{a*}

^aChemistry, University of Southampton, Southampton, SO17 1BJ

Table of Contents

General Remarks	2
Synthesis.....	3
Spectra.....	6
Anion Transport Studies.....	13
Electrode Calibration	14
Conversion of Raw Potentiometric Data to Percentage Chloride Efflux.....	18
Cl⁻/NO₃⁻ Transport Studies.....	19
Hill Plots	28
Hill Analysis in POPC:Cholesterol Vesicles	42
Evidence for Antiport.....	43
Evidence for Aggregation	55
Anion Binding Studies.....	60
Fluorescence Studies	69
References	73

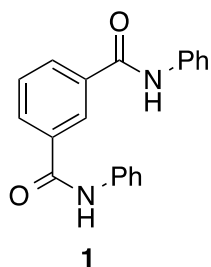
General Remarks

All starting materials and solvents were purchased from commercial sources and used without further purification unless stated otherwise.

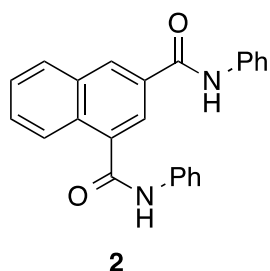
All NMR data were recorded on Bruker AVII400 or Bruker AVIHD400 FT-NMR spectrometers and references to the indicated solvent at 298 K. Chemical shifts reported on the delta scale and abbreviations used for spin multiplicity of peaks include: s = singlet, d = doublet, t = triplet, q = quartet, quin = quintet, m = multiplet, br = broad.

All receptor samples were submitted to the University of Southampton Institute for Applied Mass Spectrometry (**UoSIAMS**) for HRMS (ES). Samples were analysed using a MaXis (Bruker Daltonics, Bremen, Germany) mass spectrometer equipped with a Time of Flight (TOF) analyser. The sample was introduced via a Dionex Ultimate 3000 autosampler and uHPLC pump. Gradient 20% acetonitrile (0.2% formic acid) to 100% acetonitrile (0.2% formic acid) in five minutes at a flow rate of 0.6 mL/min. Column, Acquity UPLC BEH C18 (waters) 1.7 micron 50 x 2.1mm high. High resolution spectra was recorded using positive/negative electrospray ionization. Melting point (Mp) analyses were carried out using a Barnstead Electrothermal IA9100 melting point machine.

Synthesis

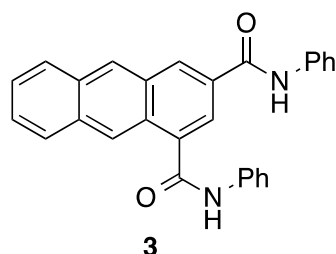


***N*¹,*N*³-diphenylisophthalamide (1)**¹ Isophthaloyl dichloride (812 mg, 4 mmol), triethylamine (1.12 mL, 8 mmol) and aniline (730 μ L, 8 mmol) were refluxed in acetonitrile (25 mL) at 55°C for 3 h. The resulting yellow precipitate was collected by vacuum filtration and triturated in warm methanol (15 mL) and the product was then dried *in vacuo*, giving the product as a pale yellow solid. Yield: 1.079 g, 3.41 mmol (85%). Mp = 286.9 – 287.5 °C. Spectra consistent with reported data.¹

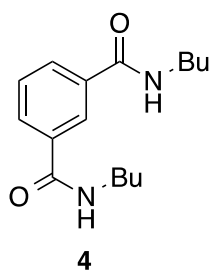


***N*¹,*N*³-diphenylnaphthalene-1,3-dicarboxamide (2)** DCM was distilled over CaH₂ overnight under nitrogen and all glassware was oven dried before use. Freshly distilled aniline (0.41 mL, 4.7 mmol, 2.6 eq) was dissolved in dry DCM (25 mL). 2M AlMe₃ solution in Toluene (2.35 mL, 4.7 mmol, 2.6 eq) was added to this solution dropwise before being stirred under nitrogen for half an hour. After this time, the diethyl naphthalene-1,3-dicarboxylate (synthesised from literature procedures)² (0.5 g, 1.8 mmol, 1 eq), dissolved in dry DCM (15 mL) under anhydrous conditions was added dropwise to the reaction mixture and the reaction heated at reflux for 5 days. The reaction was then allowed to cool before slow addition of HCl (aq) 1:10 v:v until the bubbling ceased. Water was added (50 mL) and the mixture left to stir for 30 mins. The organic phase was separated and washed with water (3 x 50 mL) and then dried with MgSO₄ before the solvent was removed under vacuum to give a yellow oil. This was subsequently purified by column chromatography (60% ethyl acetate in hexane as eluent) producing the pure product as an off-white solid.

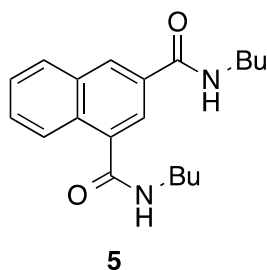
Yield: 0.232 g, 0.6 mmol, (35%). ^1H NMR (400 MHz, DMSO): δ = 10.70 (s, 1H, amide NH), δ = 10.53 (s, 1H, amide NH), δ = 8.75 (s, 1H, aromatic CH), δ = 8.31 (s, 1H, aromatic CH), δ = 8.27 (d, 1H, aromatic CH, J = 8.07 Hz), δ = 8.21 (d, 1H, aromatic CH, J = 7.34 Hz), δ = 7.84 (d, 4 H, aromatic CH x 4, J = 8.07 Hz), δ = 7.72 (m, 4H, aromatic CH x 4), δ = 7.14 (td, 2H, aromatic CH x 2, J_1 = 7.31, J_2 = 7.31, J_3 = 3.36). ^{13}C NMR (101 MHz, DMSO): 166.8 (amide CO), 164.8 (amide CO), 139.2 (aromatic C), 139.1 (aromatic C), 131.0 (aromatic C), 131.1 (aromatic C), 129.6 (aromatic C), 128.8 (aromatic C), 128.7 (aromatic C), 127.3 (aromatic C), 123.9 (aromatic C), 120.5 (aromatic C), 119.9 (aromatic C). LRMS ESI⁺ (m/z): 367.1 [M+H]⁺. HRMS ESI⁺ (m/z): 367.1437 [M+H]⁺, err. (ppm) 1.2. Mp 287-289.2 °C.



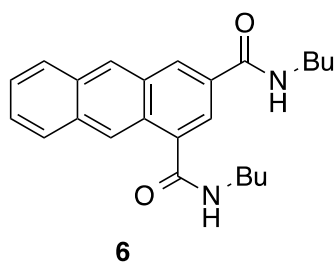
***N*¹,*N*³-diphenylanthracene-1,3-dicarboxamide (3)** has been previously reported by this group and spectra are consistent with reported data.³ Mp = 290.1–291 °C followed by immediate decomposition.



***N*¹,*N*³-dibutylisophthalamide (4)**⁴ Isophthaloyl dichloride (6.33 g, 0.031 mol) was added to a solution of n-butylamine (6.2 mL, 0.062 mol) in DMF (75 mL), which was stirred at room temperature for 30 minutes. The reaction mixture was then poured into water (300 mL). The product was precipitated as a white powder, which was washed three times with water (3x100 mL). The diamide then refluxed with water to remove any remaining DMF before being dried *in vacuo*. producing a white solid. Yield 6.087 g, 0.022 mol (71%). Mp = 127.3 – 128 °C Spectra consistent with reported data.⁴



***N*¹,*N*³-dibutyl-naphthalene-1,3-dicarboxamide (5)** DCM was distilled over CaH₂ overnight under nitrogen and all glassware was oven dried before use. n-butylamine (0.34 mL, 3.4 mmol, 2.6 eq) was dissolved in dry DCM (25 mL). 2M AlMe₃ solution in Toluene (1.8 mL, 3.6 mmol, 2.6 eq) was added to this solution dropwise before being stirred under nitrogen for half an hour. After this time, the diethyl naphthalene-1,3-dicarboxylate (synthesised from literature procedures)² (0.354 g, 1.3 mmol, 1 eq), dissolved in dry DCM (15 mL) under anhydrous conditions was added dropwise to the reaction mixture. This was then heated at reflux for 5 days. The reaction was then allowed to cool before slow addition of HCl (aq) 1:10 v:v until the bubbling ceased. Water was added (50 mL) and the mixture left to stir for 30 mins. The organic phase was separated and washed with water (3 x 50 mL) and then dried with MgSO₄ before the solvent was removed under vacuum to give a yellow oil. This was subsequently purified by column chromatography (60% ethyl acetate in hexane as eluent) producing the pure product as a white solid. Yield: (0.189 g, 50%). ¹H NMR (400 MHz, CDCl₃): d = 8.67 (br t, 1H, amide NH, J = 6.01 Hz), d = 8.58 (br t, 1H, amide NH, J = 5.5 Hz), d = 8.50 (s, 1H, aromatic CH), d = 8.18 (d, 1H, aromatic CH, J = 7.95 Hz), d = 8.06 (d, 1H, Aromatic CH, J = 7.34 Hz), d = 7.98 (d, 1H, aromatic CH, J = ~1 Hz), d = 7.64 (m, 2H, aromatic CH x 2), d = 3.32 (m, 4H, aliphatic CH₂ x 2 overlapping under H₂O peak), d = 1.55 (tq, 4H, aliphatic CH₂ x 2, J₁ = 14.5, J₂ = 7.26), d = 1.38 (tq, 4H, aliphatic CH₂ x 2, J₁ = 14.5, J₂ = 7.25 Hz), d = 0.93 (q, 6H, aliphatic CH₃ x 2, J = 7.54 Hz x 3). ¹³C NMR (101 MHz, CDCl₃): 168.9 (amide CO), 167.0 (amide CO), 135.3 (aromatic C), 133.0 (aromatic C), 131.4 (aromatic C), 131.1 (aromatic C), 129.2 (aromatic C), 129.0 (aromatic C), 128.7 (aromatic C), 127.2 (aromatic C), 125.5 (aromatic C), 122.8 (aromatic C), 40.1 (aliphatic C), 40.0 (aliphatic C), 31.7 (aliphatic C x 2), 20.2 (aliphatic C x 2), 13.8 (aliphatic C x 2). LRMS ESI⁻ (m/z): 325.1 [M-H⁺]⁻ HRMS ESI⁺ (m/z): 327.2070 [M+H⁺]⁺, err. (ppm) - 0.8. Mp = 144.8 –146.1 °C



*N*¹,*N*³-dibutylanthracene-1,3-dicarboxamide (**6**) has been previously reported by this group and spectra are consistent with reported data.³ Mp = 186.4 – 187.6 °C.

Spectra

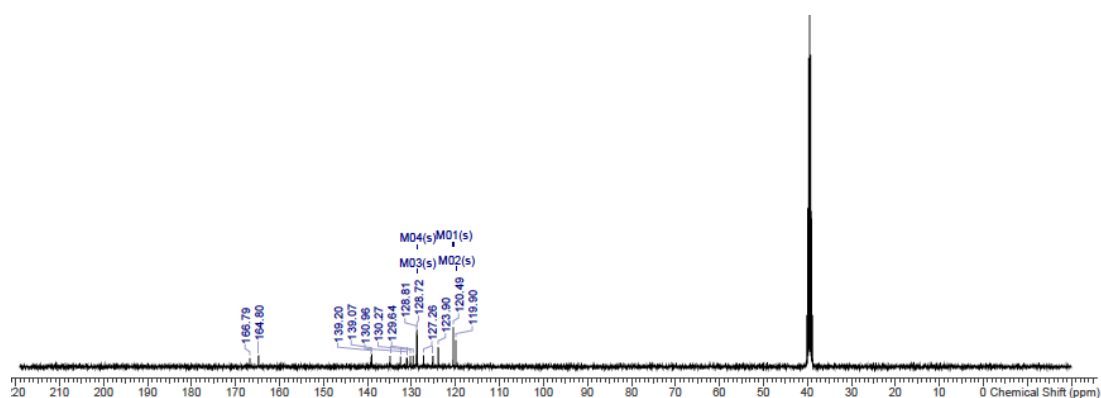


Figure S1: ¹³C NMR Spectrum of Compound **1** in DMSO-*d*₆.

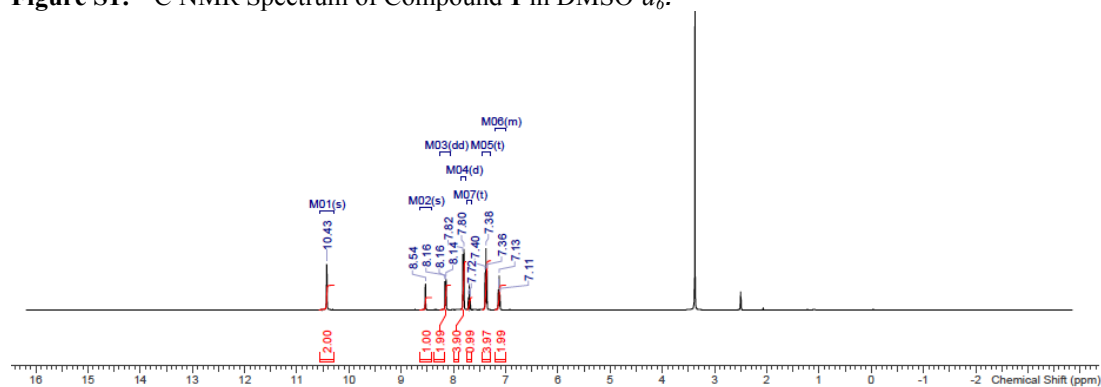


Figure S2: ¹H NMR Spectrum of Compound **1** in DMSO-*d*₆.

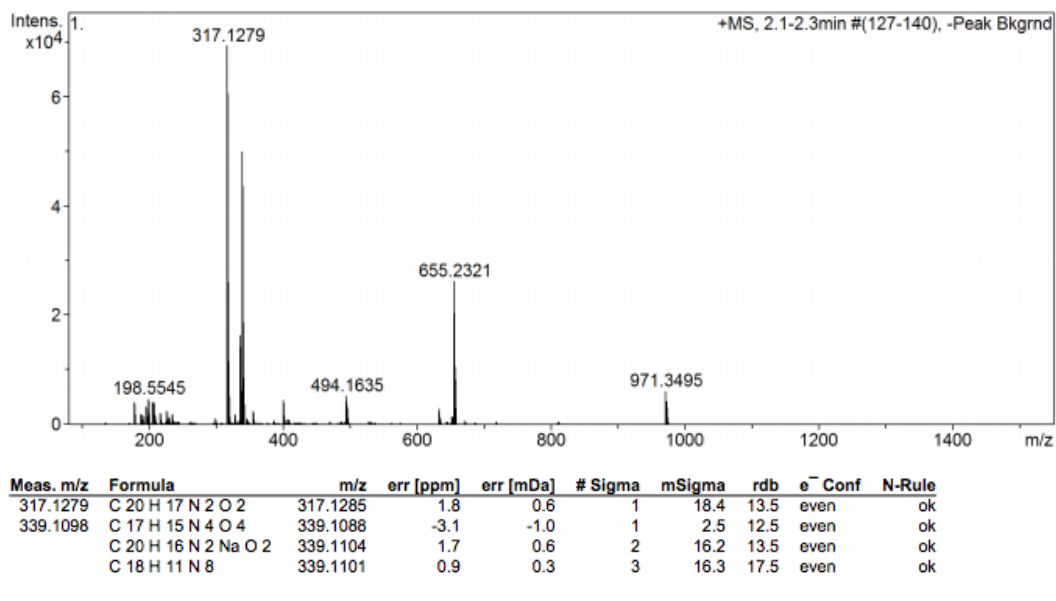


Figure S3: HRMS of receptor 1.

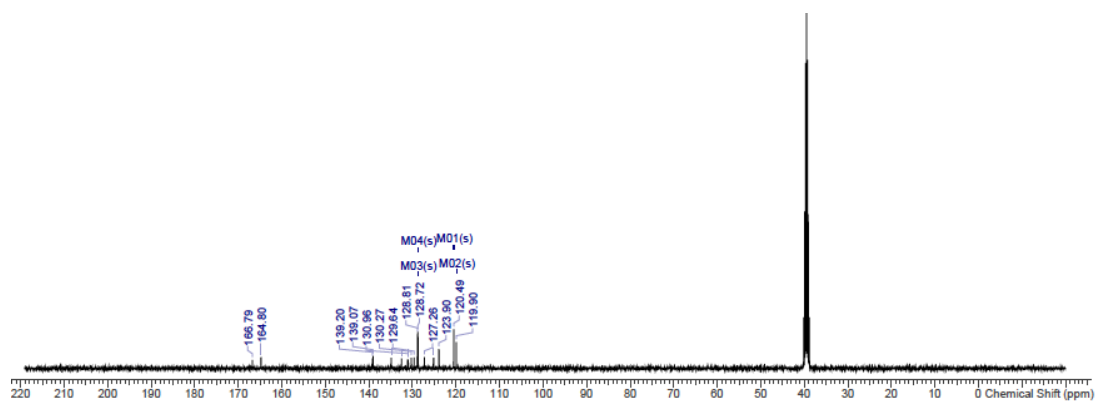


Figure S4: ¹³C NMR Spectrum of Compound 2 in DMSO-*d*₆.

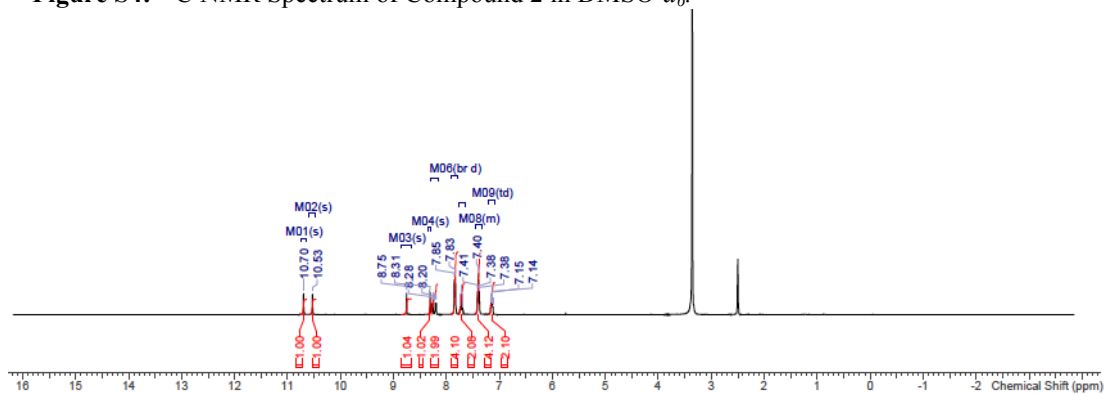
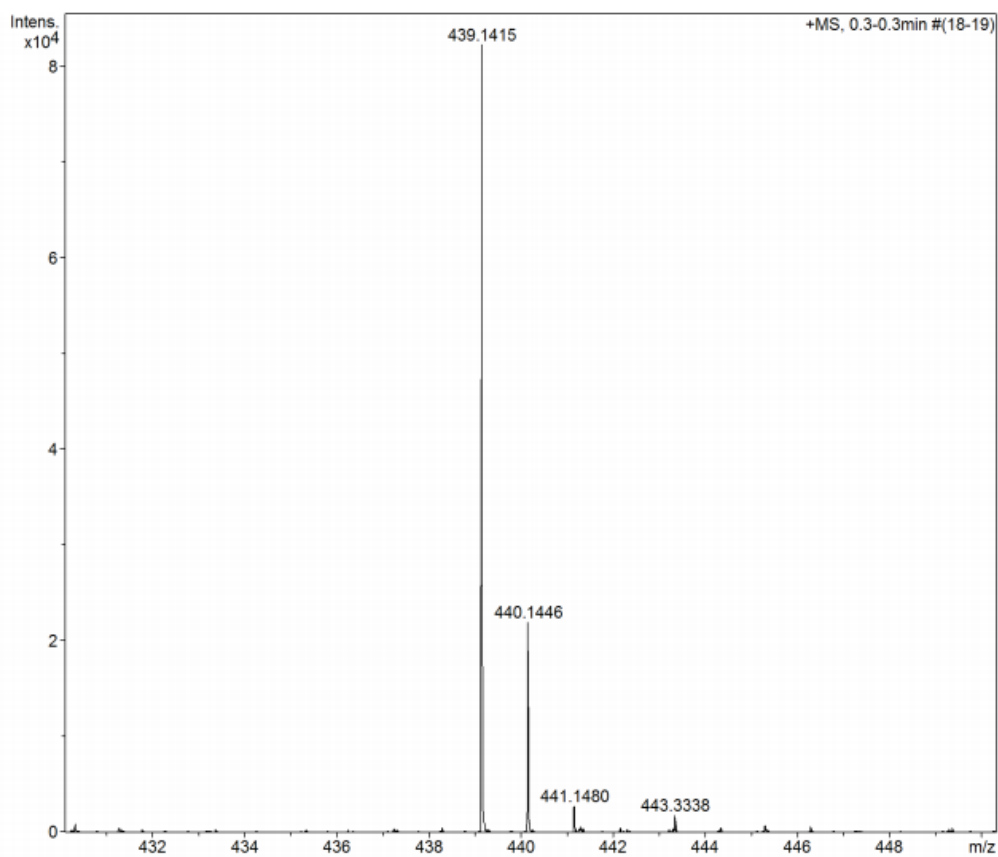


Figure S5: ¹H NMR Spectrum of Compound 2 in DMSO-*d*₆.



Meas. m/z	Formula	m/z	err [ppm]	err [mDa]	# Sigma	mSigma	rdb	e ⁻ Conf	N-Rule
439.1415	C 28 H 20 N 2 Na O 2	439.1417	0.4	0.2	1	23.6	19.5	even	ok
	C 26 H 15 N 8	439.1414	-0.2	-0.1	2	26.7	23.5	even	ok
	C 13 H 16 N 14 Na O 3	439.1422	1.6	0.7	3	43.3	12.5	even	ok
	C 11 H 11 N 20 O	439.1419	0.9	0.4	4	43.8	16.5	even	ok
	C 15 H 28 Na O 13	439.1422	1.6	0.7	5	49.9	1.5	even	ok
	C 13 H 23 N 6 O 11	439.1419	1.0	0.4	6	57.6	5.5	even	ok
	C 12 H 20 N 10 Na O 7	439.1409	-1.5	-0.6	7	57.8	7.5	even	ok

Figure S9: HRMS for receptor 3.

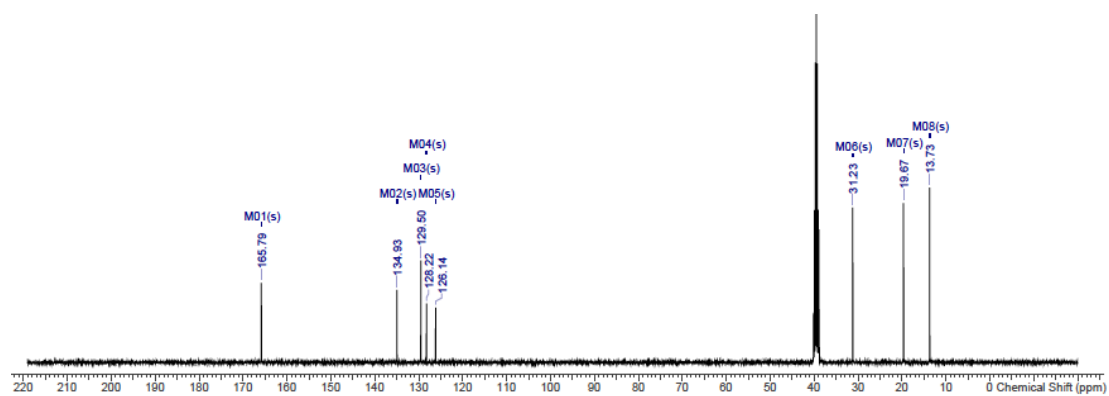


Figure S10: ¹³C NMR Spectrum of Compound 4 in DMSO-*d*₆.

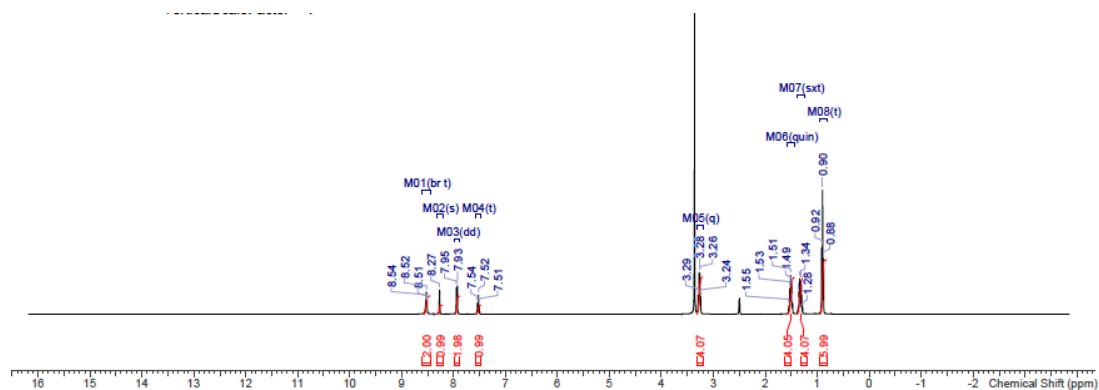
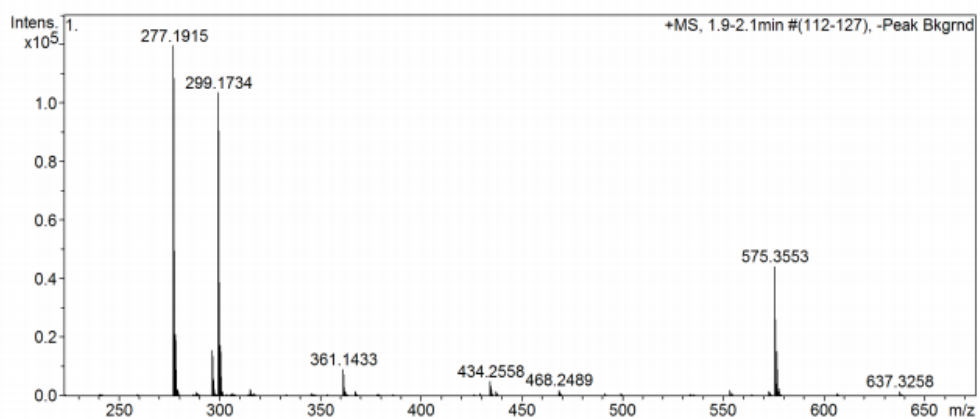


Figure S11: ^1H NMR Spectrum of Compound 4 in $\text{DMSO-}d_6$.



Meas. m/z	Formula	m/z	err [ppm]	err [mDa]	# Sigma	mSigma	rdb	e ⁻ Conf	N-Rule
277.1915	C 16 H 25 N 2 O 2	277.1911	-1.5	-0.4	1	2.8	5.5	even	ok
	C 19 H 26 Na	277.1927	4.3	1.2	2	17.2	6.5	even	ok
299.1734	C 14 H 19 N 8	299.1727	-2.4	-0.7	1	8.7	9.5	even	ok
	C 16 H 24 N 2 Na O 2	299.1730	-1.5	-0.4	2	9.0	5.5	even	ok
	C 9 H 24 N 8 Na S	299.1737	0.8	0.3	3	31.0	1.5	even	ok
	C 10 H 27 N 4 O 4 S	299.1748	4.4	1.3	4	35.4	-0.5	even	ok

Figure S12: HRMS Spectrum of receptor 4.

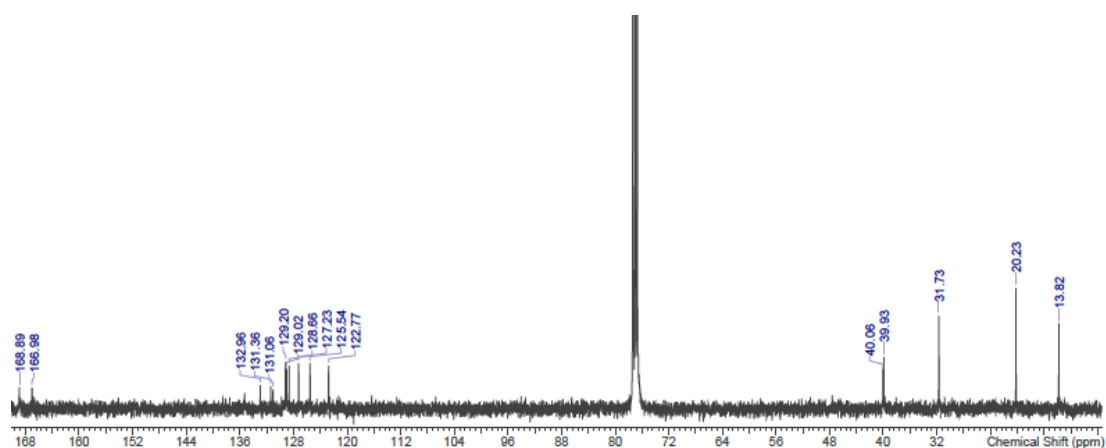


Figure S13: ^{13}C NMR Spectrum of Compound 5 in CDCl_3-d .

Figure S16: ^{13}C NMR Spectrum of Compound **6** in $\text{DMSO-}d_6$.

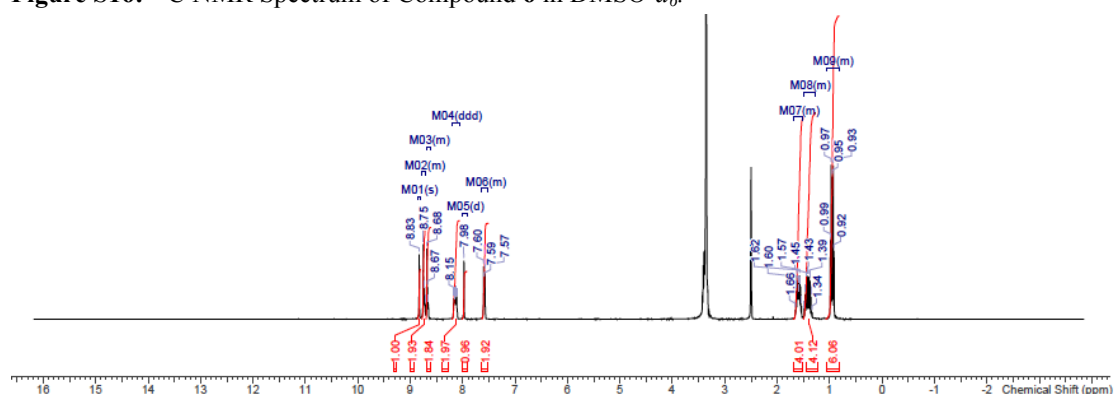
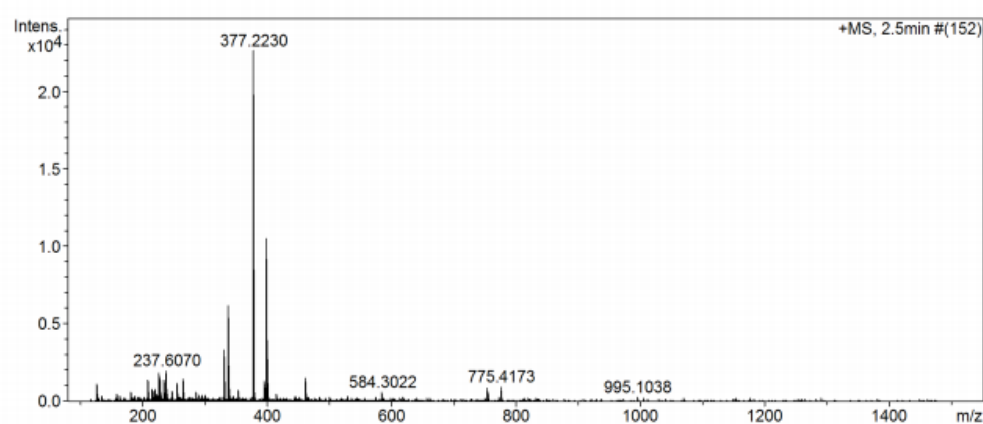


Figure S17: ^1H NMR Spectrum of Compound **6** in $\text{DMSO-}d_6$.



Meas. m/z	Formula	m/z	err [ppm]	err [mDa]	# Sigma	mSigma	rdb	e ⁻ Conf	N-Rule
377.2230	C 24 H 29 N 2 O 2	377.2224	-1.8	-0.7	1	25.8	11.5	even	ok
	C 17 H 29 N 8 S	377.2230	0.1	0.0	2	34.5	7.5	even	ok
	C 19 H 34 N 2 Na O 2 S	377.2233	0.8	0.3	3	37.1	3.5	even	ok
399.2049	C 24 H 28 N 2 Na O 2	399.2043	-1.4	-0.6	1	16.7	11.5	even	ok

Figure S18: HRMS of receptor **6**.

Anion Transport Studies

POPC was supplied by Avanti Polar Lipids. Vesicles used in these studies were prepared by literature methods.⁵ Intra-vesicular and extra-vesicular solutions were prepared to be isotonic to prevent vesicle membranes from bursting.

Preparation of unilamellar POPC vesicles: POPC was dissolved in chloroform (~29 mg/mL). A thin film of lipid was produced by transferring a known quantity of POPC solution to a RBF and removing the solvent *in vacuo*. The film was then dried on a

high vacuum line for a minimum of 4 hrs. The lipid was then suspended in the same volume of internal solution as the initial chloroform solution used using a lab dancer. Next, 9 freeze-thaw cycles were completed by alternating the lipid between liquid nitrogen and room temperature water. The lipid was then left to stand for 30 minutes. The formed vesicles were then extruded through 200nm polycarbonate membranes 25 times before being placed in dialysis tubing and then into the desired external solution a minimum of 2 hours. This removed any unencapsulated internal salts. Finally, the lipid was diluted to 1mM using the required external solution.

$\text{Cl}^-/\text{NO}_3^-$ Antiport Tests: Unilamellar POPC vesicles were prepared containing aqueous internal solution with 489 mM NaCl buffered to pH 7.2 with 5 mM sodium phosphate salts. The vesicles were dispersed in an aqueous external solution containing 489 mM NaNO_3 buffered to pH 7.2 with 5 mM sodium phosphate salts. The receptor was loaded at an appropriate molar percentage relative to the moles of lipid as a DMSO solution at 0 s. After 300 s, octaethylene glycol monododecyl ether detergent was added to lyse the vesicles (2.32 mM in 7:1 $\text{H}_2\text{O}:\text{DMSO}$ v/v) and calibrate the chloride selective electrode to 100% chloride efflux at 420 s. All endpoint values are taken as of 270 s. Chloride concentrations were monitored using an Accumet solid-state combination chloride selective electrode. The lipid concentration per sample was 1 mM. Each data point represents the average of 3 runs. For the blank runs (pure DMSO) there is a minimum of 1 repeat and a maximum of 3. Error bars are shown where appropriate.

Electrode Calibration

The Accumet Chloride Combination Ion Selective Electrodes used in this study were calibrated before each set of vesicle runs. The calibration was performed as follows: The potential of known concentrations of sodium chloride solutions were recorded by placing the electrode in the stirred solution for five minutes to allow the value to become stable. A plot of sodium chloride concentration (M) versus electrode potential (mV) was then produced and fitted to equation 1 below using Origin 9.1.

$$y = (P_1 \log_{10} x) + P_2$$

Equation 1: A simplified version of the Nernst equation where P_1 and P_2 are the parameters to be determined.

Equation 1 is a simplified version of the Nernst equation where P_1 and P_2 are the parameters to be determined. These therefore allow chloride concentration to be converted into chloride ion activity.

Although the electrodes used in this study are compatible with all the ions studied as stated in the manual, to test for interference with the electrode from other ions, the calibration was repeated using sodium chloride solutions also containing 489 mM NaNO_3 buffered to pH 7.2 with 5mM sodium phosphate salts or 167 mM Na_2SO_4 buffered to pH 7.2 with 20 mM sodium phosphate salts. While we obtained slightly different P_1 and P_2 values for the different calibration solutions, when a graph was plotted with a sample of data, the true difference between calibration solutions was negligible. This led us to infer that the other, non-chloride ions used in this study did not interfere with the chloride selective electrode. The results of these calibration tests are shown below.

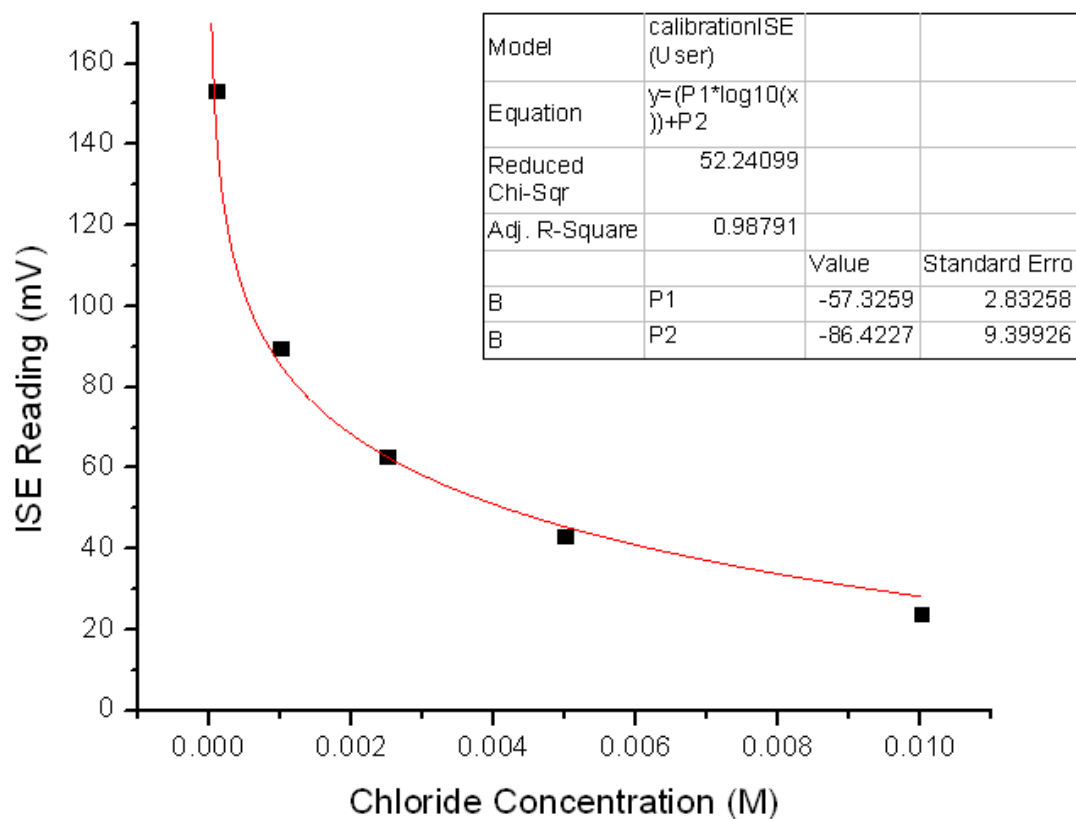


Figure S19: Chloride ISE calibration curve for various concentrations of aqueous NaCl solutions. The curve was fitted to equation 1 using Origin 9.1 to obtain P_1 and P_2 values.

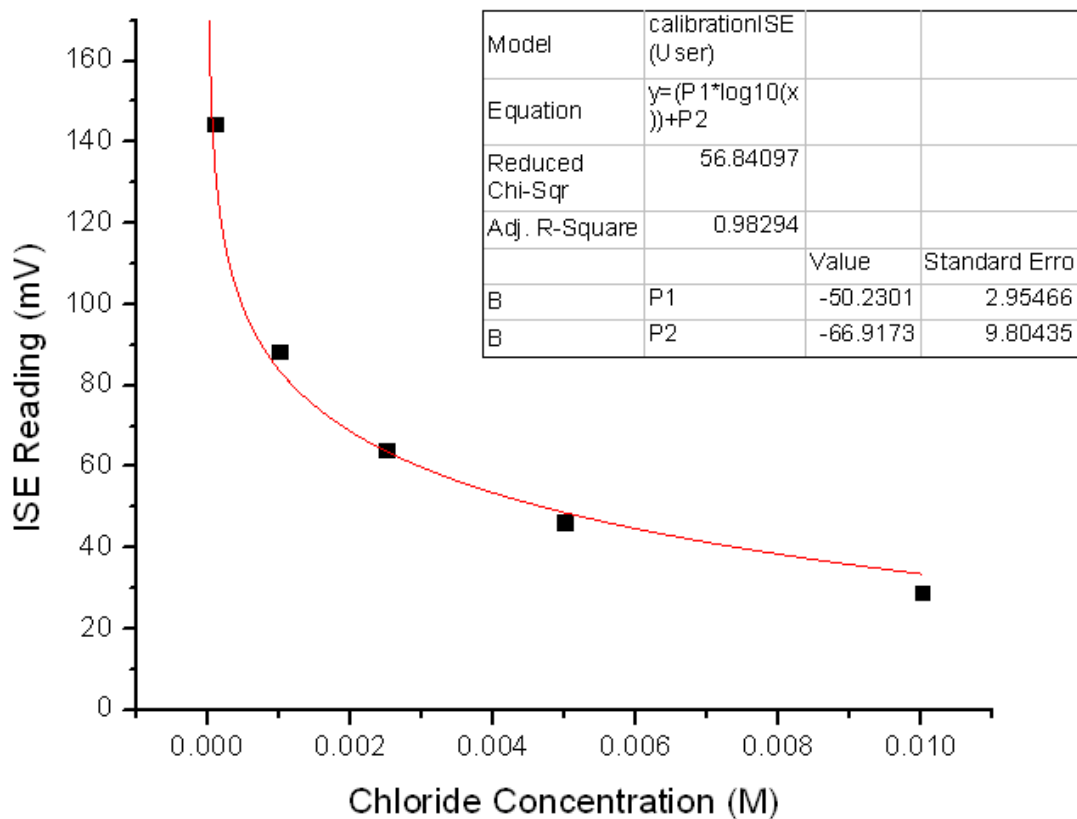


Figure S20: Chloride ISE calibration curve for various concentrations of aqueous NaCl solution containing 489 mM NaNO₃ buffered to pH 7.2 with 5 mM sodium phosphate salts. The curve was fitted to equation 1 using Origin 9.1 to obtain P₁ and P₂ values.

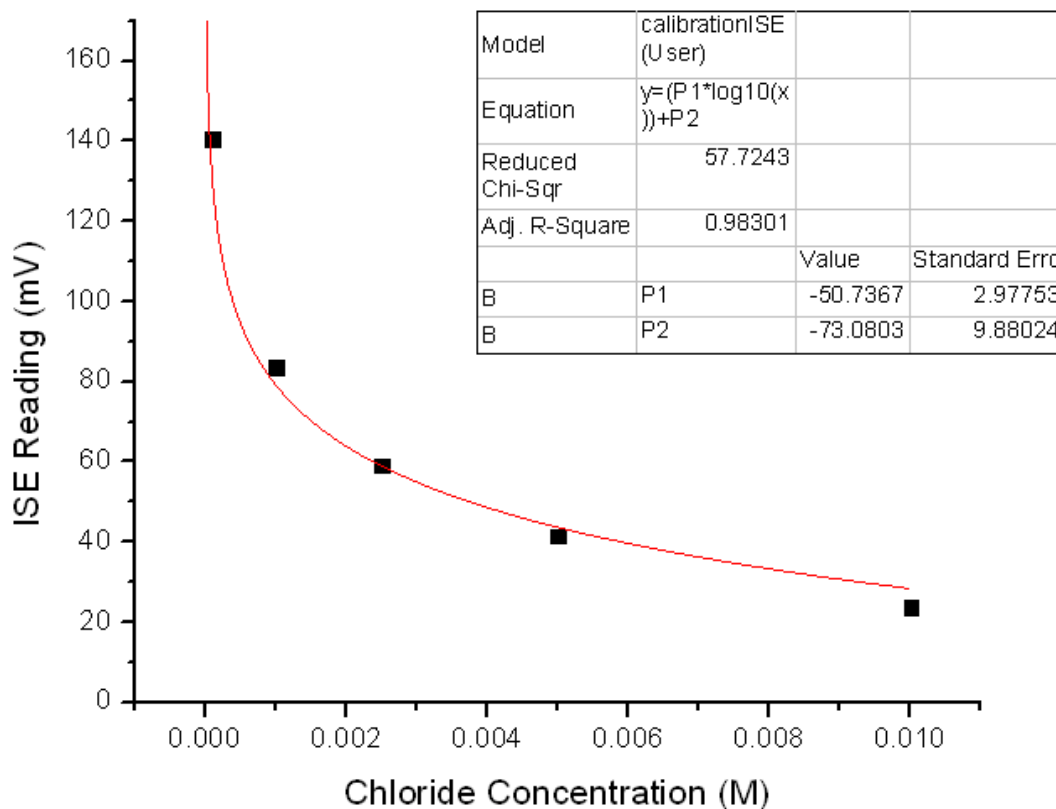


Figure S21: Chloride ISE calibration curve for various concentrations of aqueous NaCl solutions containing 167 mM Na₂SO₄ buffered to pH 7.2 with 20 mM sodium phosphate salts. The curve was fitted to equation 1 using Origin 9.1 to obtain P₁ and P₂ values.

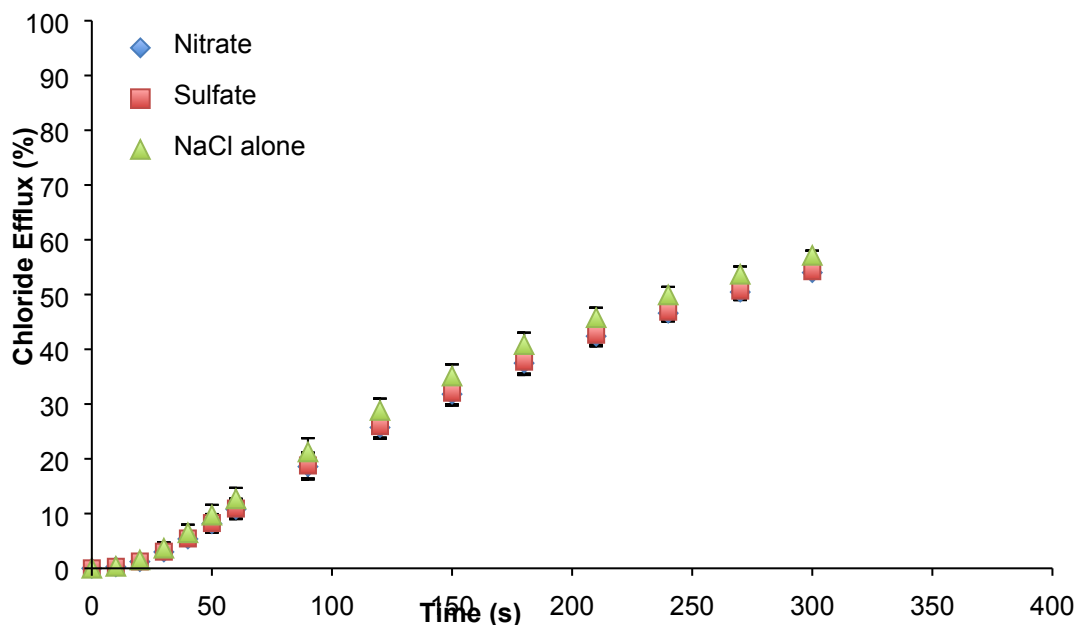


Figure S22: Representative data plot. Chloride efflux as a function of time, promoted by the addition of receptor **6** (2mol % loading), from unilamellar POPC vesicles containing 489 mM NaCl with 5 mM sodium phosphate salts. The vesicles were suspended in 489 mM NaNO₃ buffered to pH 7.2 with 5 mM sodium phosphate salts. The receptor was loaded as a DMSO solution at 0 s. The vesicles were lysed at the end of the experiment to calibrate 100% chloride efflux. Points are conducted using the calibration parameters calculated from **figures S19-S21** (calibration conducted in either NaCl solution alone (NaCl alone), or NaCl solution containing NaNO₃ (Nitrate), or NaCl solution containing Na₂SO₄ (Sulfate)). The negligible discrepancies between the three curves suggest there is no interference between the non-chloride ions used in this study and the chloride selective electrode.

Conversion of Raw Potentiometric Data to Percentage Chloride Efflux

The raw potentiometric data was converted into percentage chloride efflux as follows:

Using the calibration constants P_1 and P_2 obtained from the ISE calibration, the potentiometric data was plugged back into equation 1. Solving for x gives the concentration of chloride released from the vesicles at any given time point in mol/dm³. Next, the initial chloride concentration (concentration at $t = 0$ s) was subtracted from the chloride concentration at that given time to give the total concentration of chloride released from the vesicles by the receptor at that time point. Finally, as the vesicles were lysed with detergent at the end of the experiment to give the total chloride concentration in the solution, the percentage of chloride released from the vesicles at that given time point was calculated.

Cl⁻/NO₃⁻ Transport Studies

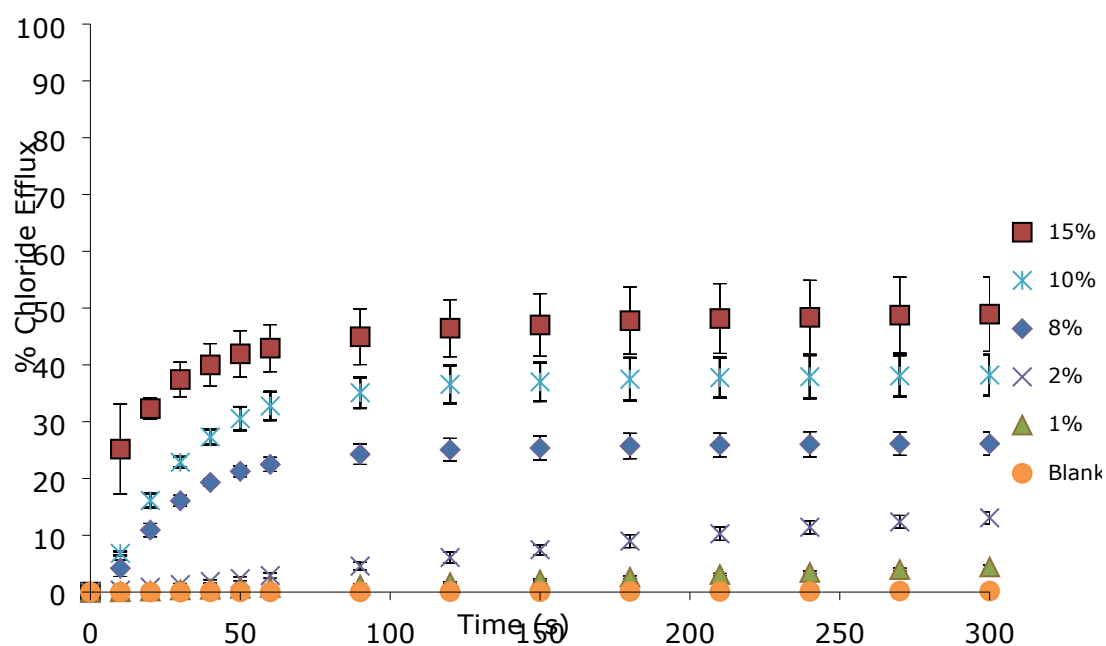


Figure S23: Chloride efflux as a function of time, promoted by the addition of various concentrations of receptor 1, from unilamellar POPC vesicles containing 489 mM NaCl with 5 mM sodium phosphate salts. The vesicles were suspended in 489 mM NaNO₃ buffered to pH 7.2 with 5 mM sodium phosphate salts. The receptor was loaded as a DMSO solution at 0 s. The vesicles were lysed at the end of the experiment to calibrate 100% chloride efflux.

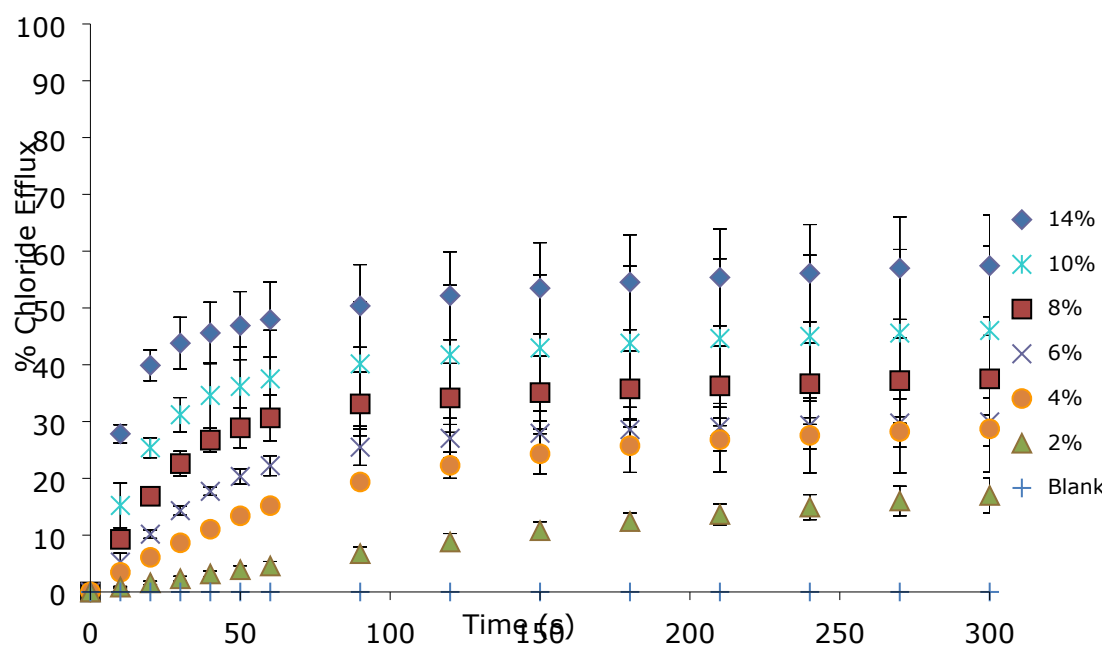


Figure S24: Chloride efflux as a function of time, promoted by the addition of various concentrations of receptor 1, from unilamellar POPC vesicles containing 489 mM NaCl with 5 mM sodium phosphate salts. The vesicles were suspended in 489 mM NaNO₃ buffered to pH 7.2 with 5 mM sodium phosphate salts. The receptor was loaded as a DMSO solution at 0 s. The vesicles were lysed at the end of the experiment to calibrate 100% chloride efflux.

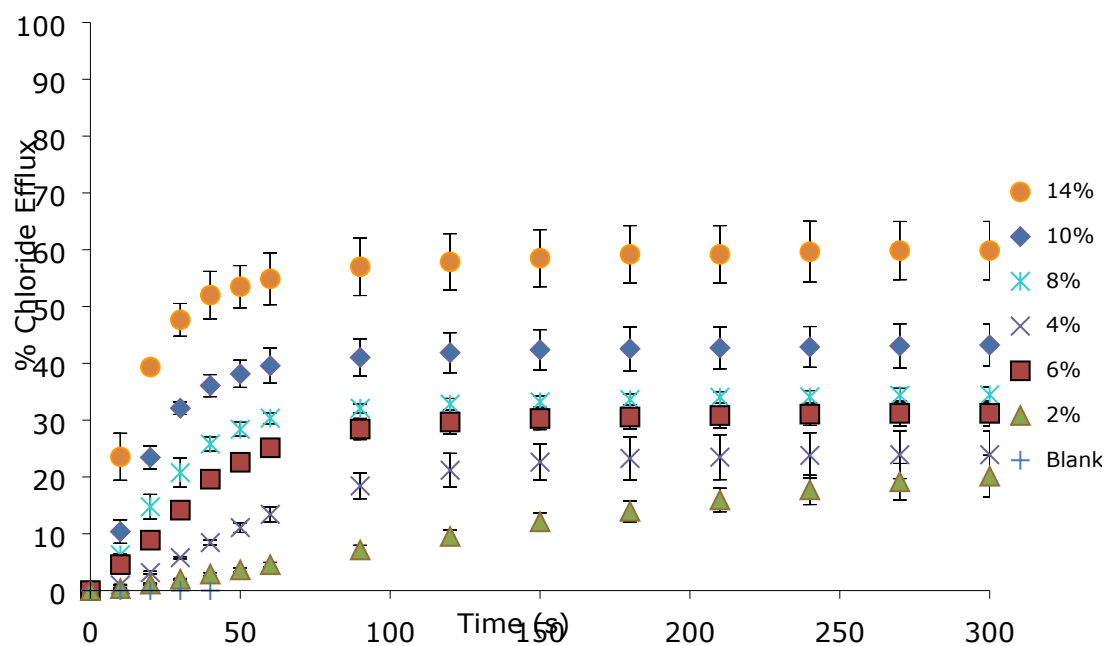


Figure S25: Chloride efflux as a function of time, promoted by the addition of various concentrations of receptor 1, from unilamellar POPC vesicles containing 489 mM NaCl with 5 mM sodium phosphate salts. The vesicles were suspended in 489 mM NaNO₃ buffered to pH 7.2 with 5 mM sodium phosphate salts. The receptor was loaded as a DMSO solution at 0 s. The vesicles were lysed at the end of the experiment to calibrate 100% chloride efflux.

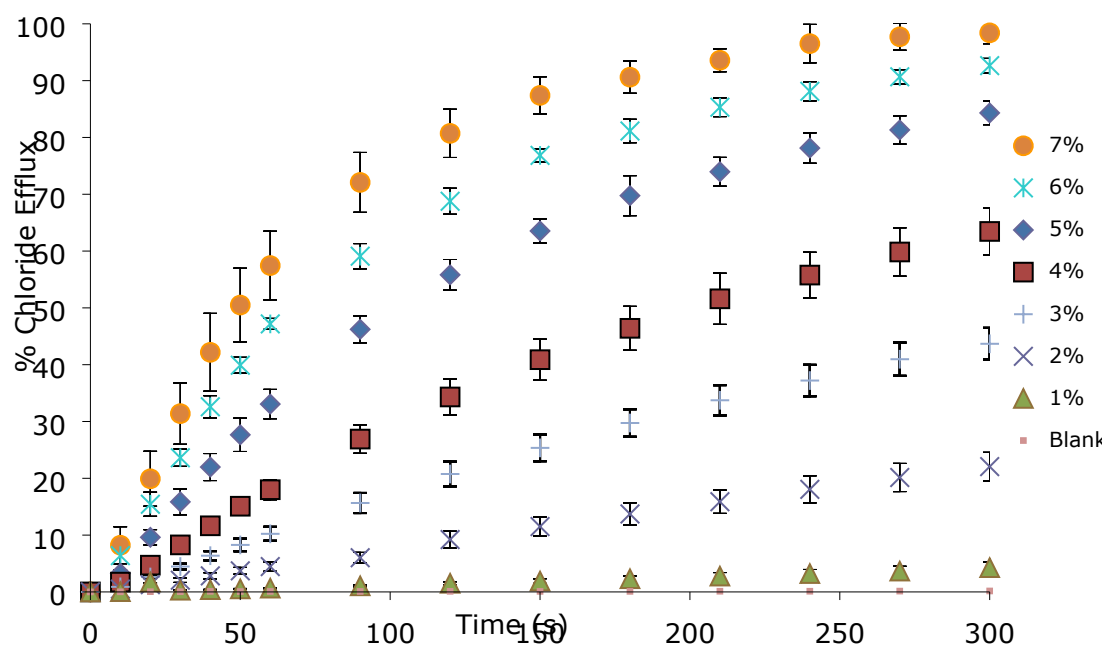


Figure S26: Chloride efflux as a function of time, promoted by the addition of various concentrations of receptor 2, from unilamellar POPC vesicles containing 489 mM NaCl with 5 mM sodium phosphate salts. The vesicles were suspended in 489 mM NaNO₃ buffered to pH 7.2 with 5 mM sodium phosphate salts. The receptor was loaded as a DMSO solution at 0 s. The vesicles were lysed at the end of the experiment to calibrate 100% chloride efflux.

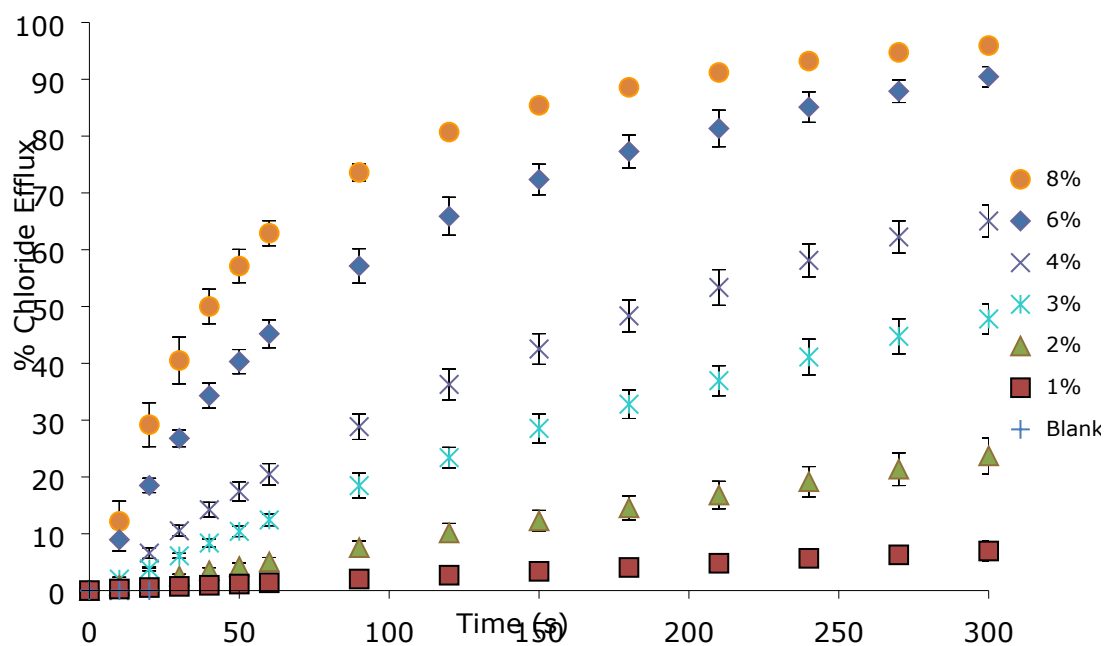


Figure S27: Chloride efflux as a function of time, promoted by the addition of various concentrations of receptor 2, from unilamellar POPC vesicles containing 489 mM NaCl with 5 mM sodium phosphate salts. The vesicles were suspended in 489 mM NaNO₃ buffered to pH 7.2 with 5 mM sodium phosphate salts. The receptor was loaded as a DMSO solution at 0 s. The vesicles were lysed at the end of the experiment to calibrate 100% chloride efflux.

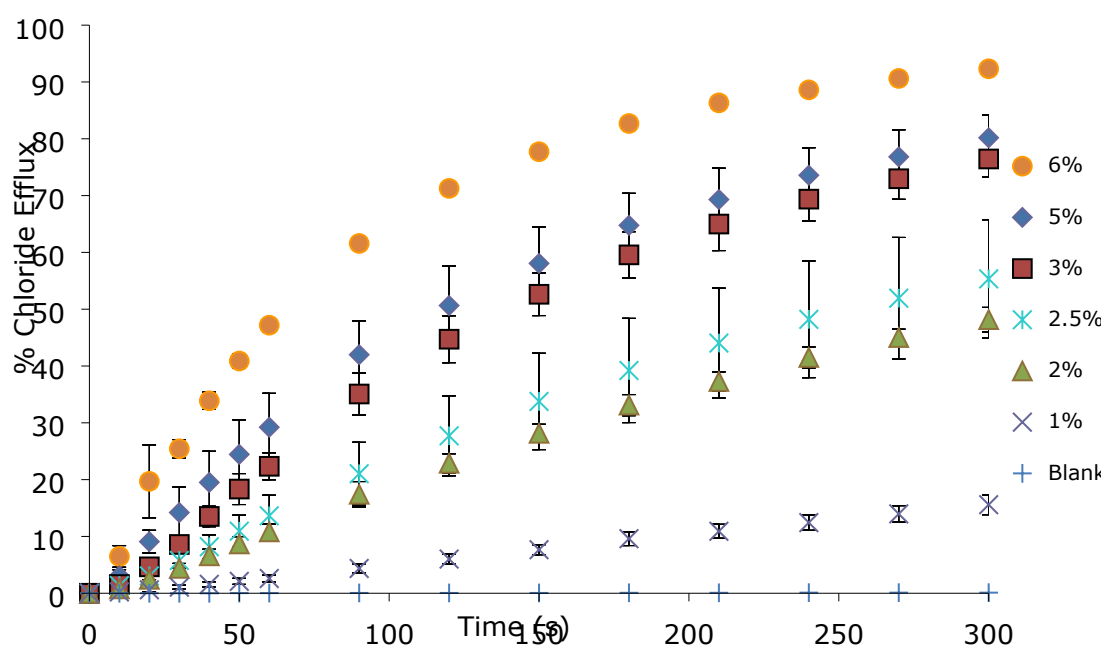


Figure S28: Chloride efflux as a function of time, promoted by the addition of various concentrations of receptor 2, from unilamellar POPC vesicles containing 489 mM NaCl with 5 mM sodium phosphate salts. The vesicles were suspended in 489 mM NaNO₃ buffered to pH 7.2 with 5 mM sodium phosphate salts. The receptor was loaded as a DMSO solution at 0 s. The vesicles were lysed at the end of the experiment to calibrate 100% chloride efflux.

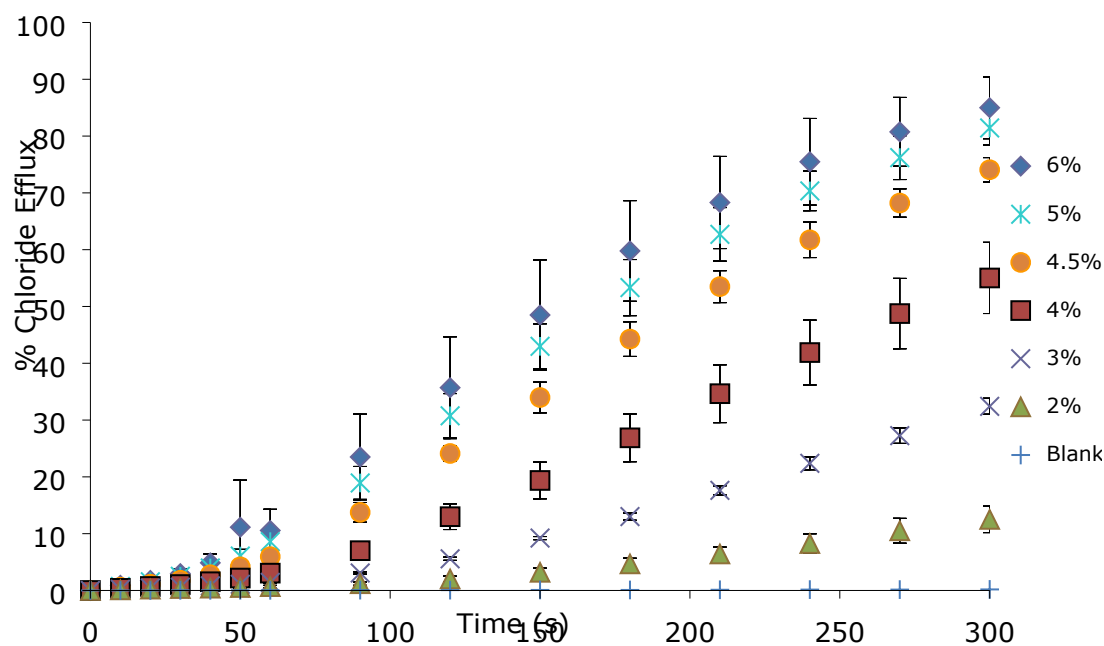


Figure S29: Chloride efflux as a function of time, promoted by the addition of various concentrations of receptor **3**, from unilamellar POPC vesicles containing 489 mM NaCl with 5 mM sodium phosphate salts. The vesicles were suspended in 489 mM NaNO₃ buffered to pH 7.2 with 5 mM sodium phosphate salts. The receptor was loaded as a DMSO solution at 0 s. The vesicles were lysed at the end of the experiment to calibrate 100% chloride efflux.

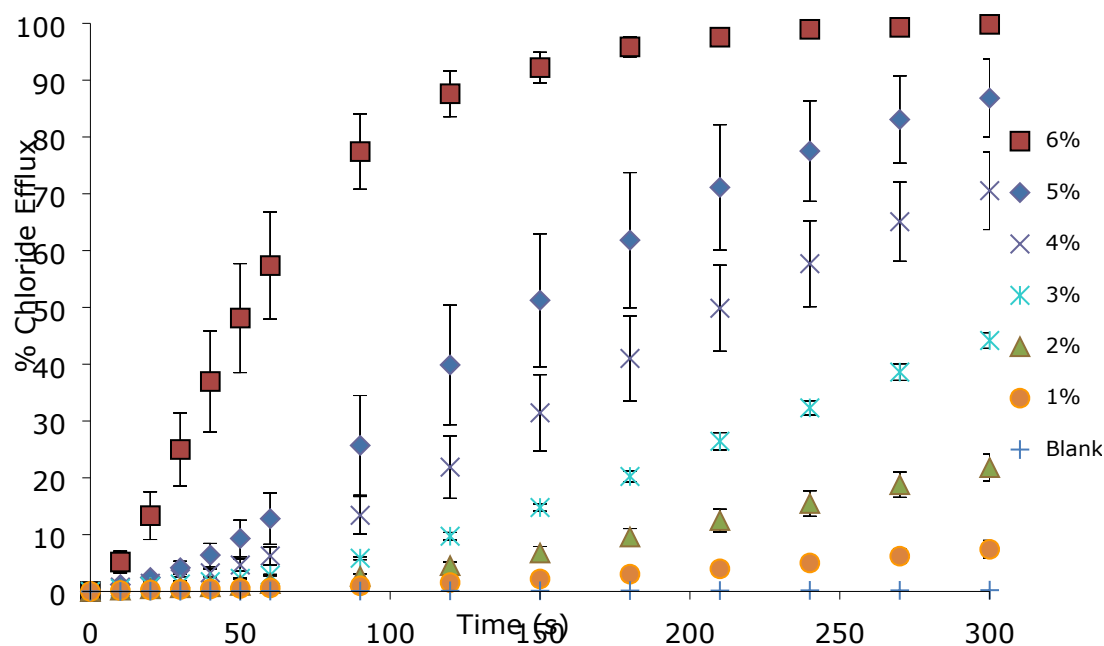


Figure S30: Chloride efflux as a function of time, promoted by the addition of various concentrations of receptor **3**, from unilamellar POPC vesicles containing 489 mM NaCl with 5 mM sodium phosphate salts. The vesicles were suspended in 489 mM NaNO₃ buffered to pH 7.2 with 5 mM sodium phosphate salts. The receptor was loaded as a DMSO solution at 0 s. The vesicles were lysed at the end of the experiment to calibrate 100% chloride efflux.

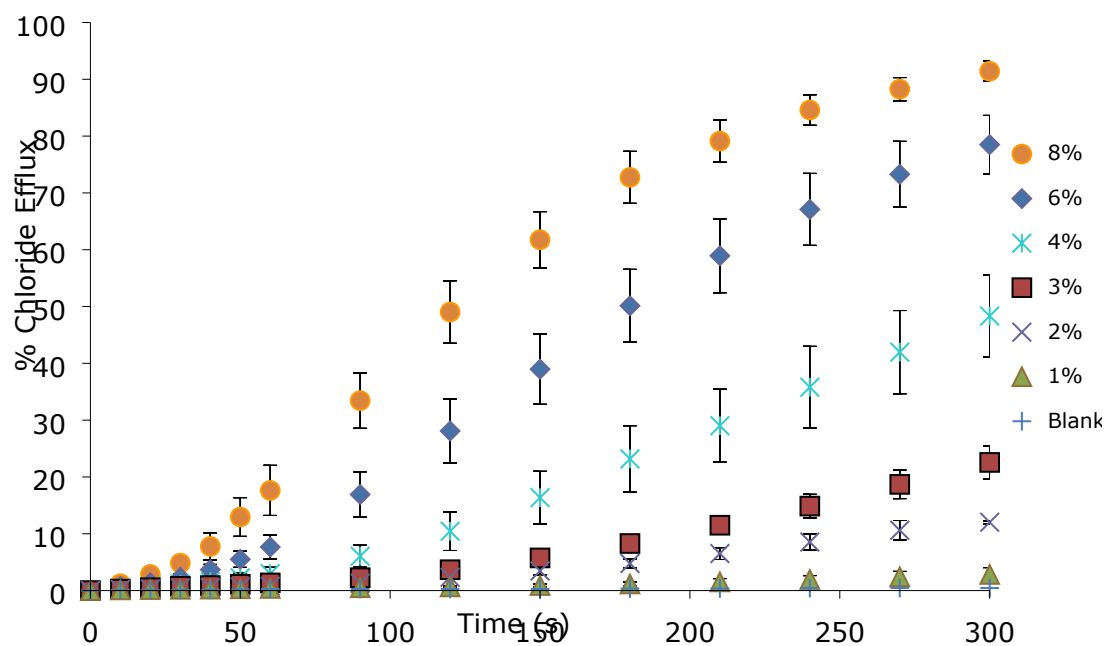


Figure S31: Chloride efflux as a function of time, promoted by the addition of various concentrations of receptor 3, from unilamellar POPC vesicles containing 489 mM NaCl with 5 mM sodium phosphate salts. The vesicles were suspended in 489 mM NaNO₃ buffered to pH 7.2 with 5 mM sodium phosphate salts. The receptor was loaded as a DMSO solution at 0 s. The vesicles were lysed at the end of the experiment to calibrate 100% chloride efflux.

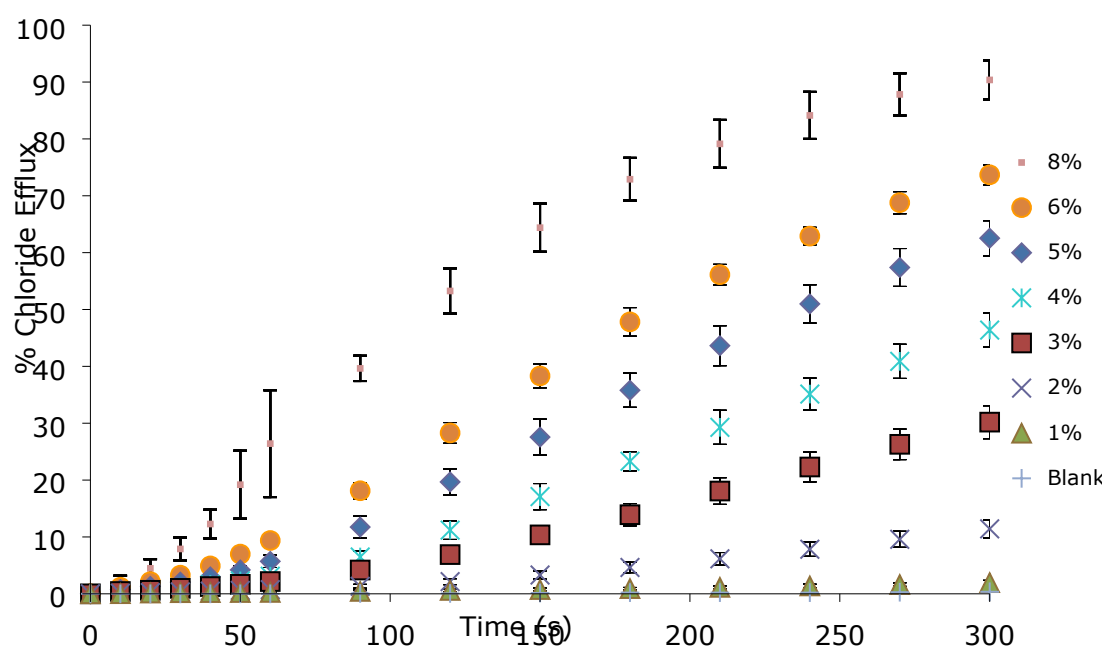


Figure S32: Chloride efflux as a function of time, promoted by the addition of various concentrations of receptor 3, from unilamellar POPC vesicles containing 489 mM NaCl with 5 mM sodium phosphate salts. The vesicles were suspended in 489 mM NaNO₃ buffered to pH 7.2 with 5 mM sodium phosphate salts. The receptor was loaded as a DMSO solution at 0 s. The vesicles were lysed at the end of the experiment to calibrate 100% chloride efflux.

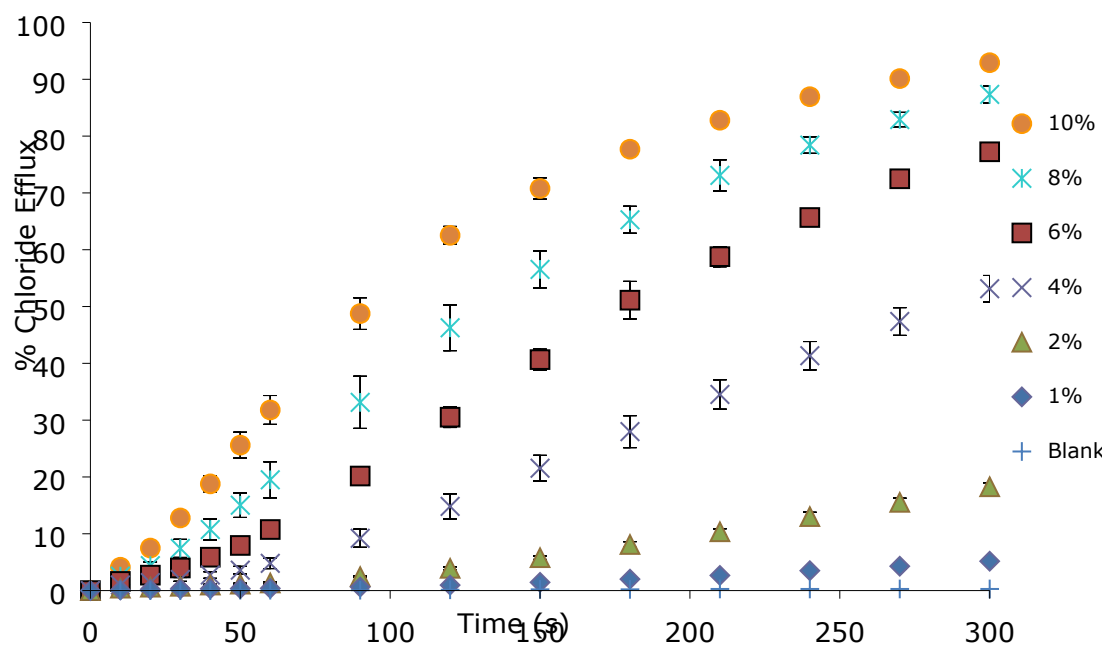


Figure S33: Chloride efflux as a function of time, promoted by the addition of various concentrations of receptor 3, from unilamellar POPC vesicles containing 489 mM NaCl with 5 mM sodium phosphate salts. The vesicles were suspended in 489 mM NaNO₃ buffered to pH 7.2 with 5 mM sodium phosphate salts. The receptor was loaded as a DMSO solution at 0 s. The vesicles were lysed at the end of the experiment to calibrate 100% chloride efflux.

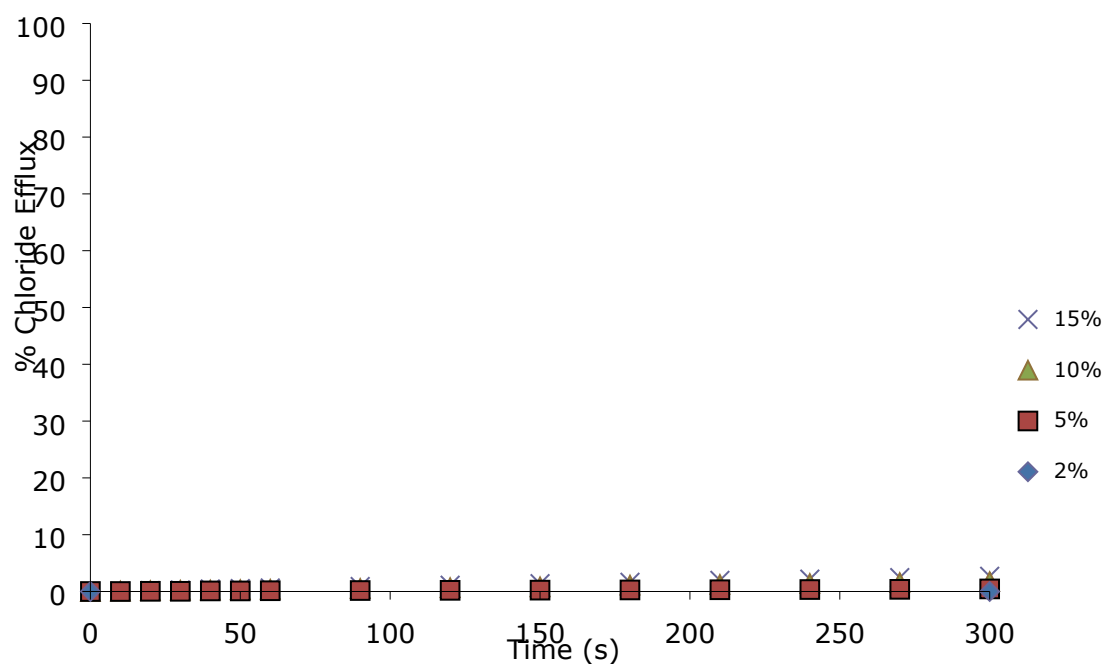


Figure S34: Chloride efflux as a function of time, promoted by the addition of various concentrations of receptor 4, from unilamellar POPC vesicles containing 489 mM NaCl with 5 mM sodium phosphate salts. The vesicles were suspended in 489 mM NaNO₃ buffered to pH 7.2 with 5 mM sodium phosphate salts. The receptor was loaded as a DMSO solution at 0 s. The vesicles were lysed at the end of the experiment to calibrate 100% chloride efflux. Figure shows lack of activity by receptor 4 even at the high concentration of 15 mol%.

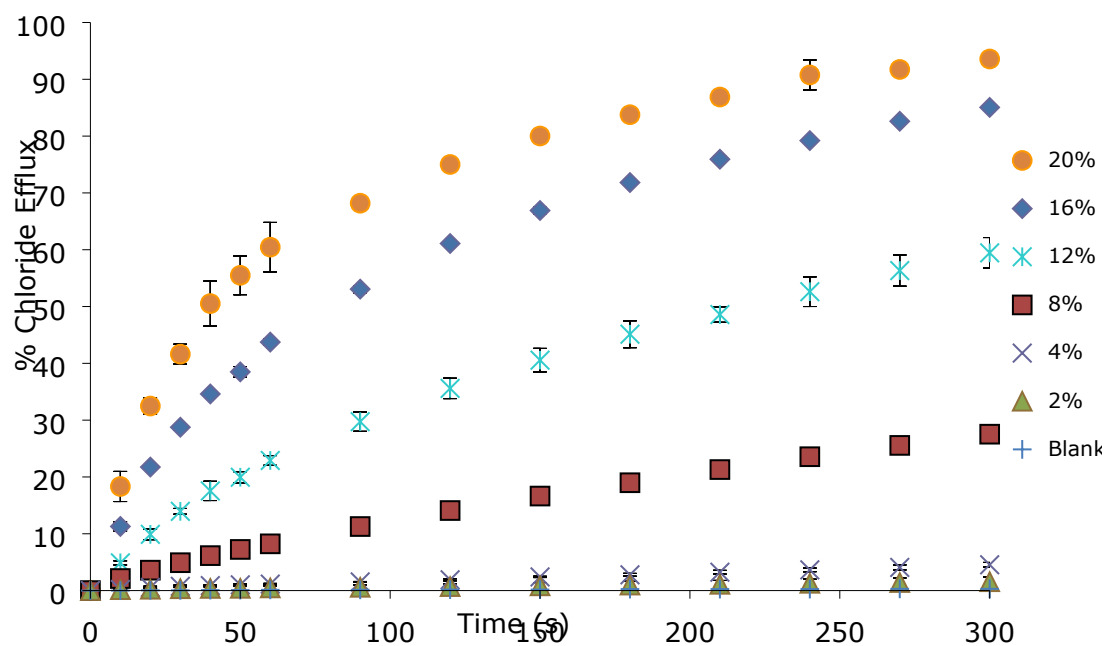


Figure S35: Chloride efflux as a function of time, promoted by the addition of various concentrations of receptor 5, from unilamellar POPC vesicles containing 489 mM NaCl with 5 mM sodium phosphate salts. The vesicles were suspended in 489 mM NaNO₃ buffered to pH 7.2 with 5 mM sodium phosphate salts. The receptor was loaded as a DMSO solution at 0 s. The vesicles were lysed at the end of the experiment to calibrate 100% chloride efflux.

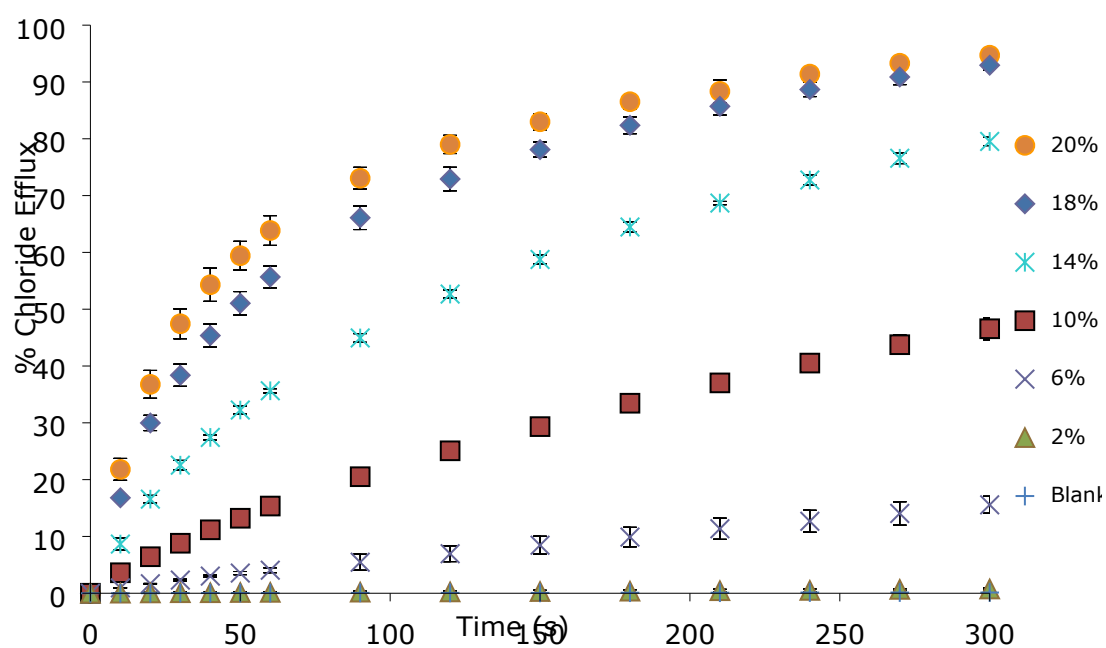


Figure S36: Chloride efflux as a function of time, promoted by the addition of various concentrations of receptor 5, from unilamellar POPC vesicles containing 489 mM NaCl with 5 mM sodium phosphate salts. The vesicles were suspended in 489 mM NaNO₃ buffered to pH 7.2 with 5 mM sodium phosphate salts. The receptor was loaded as a DMSO solution at 0 s. The vesicles were lysed at the end of the experiment to calibrate 100% chloride efflux.

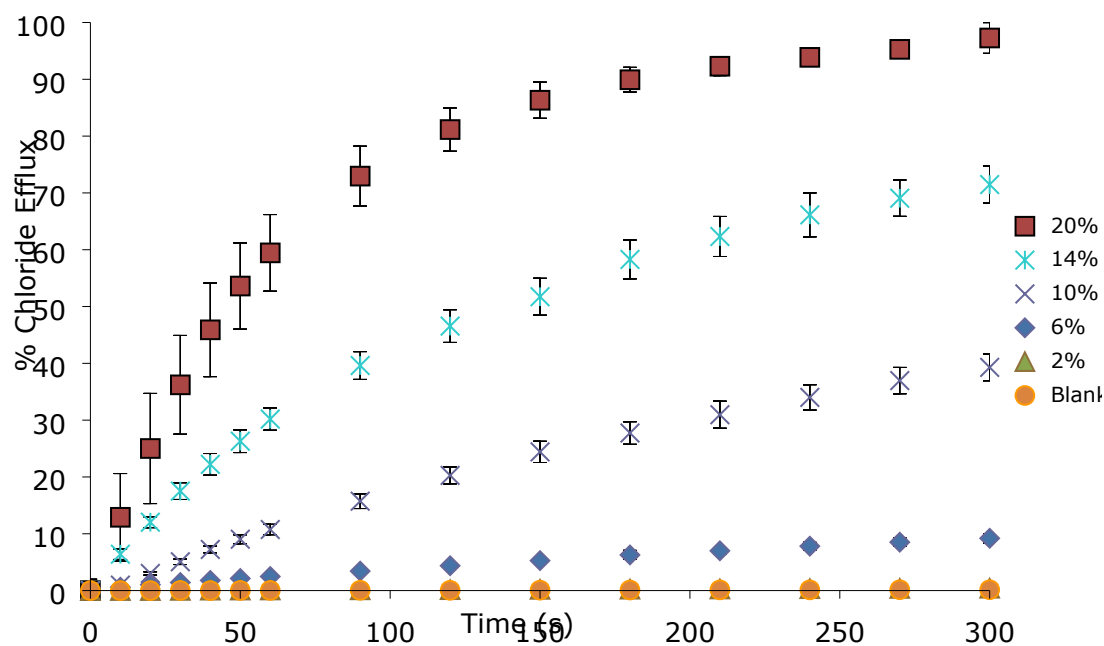


Figure S37: Chloride efflux as a function of time, promoted by the addition of various concentrations of receptor 5, from unilamellar POPC vesicles containing 489 mM NaCl with 5 mM sodium phosphate salts. The vesicles were suspended in 489 mM NaNO₃ buffered to pH 7.2 with 5 mM sodium phosphate salts. The receptor was loaded as a DMSO solution at 0 s. The vesicles were lysed at the end of the experiment to calibrate 100% chloride efflux.

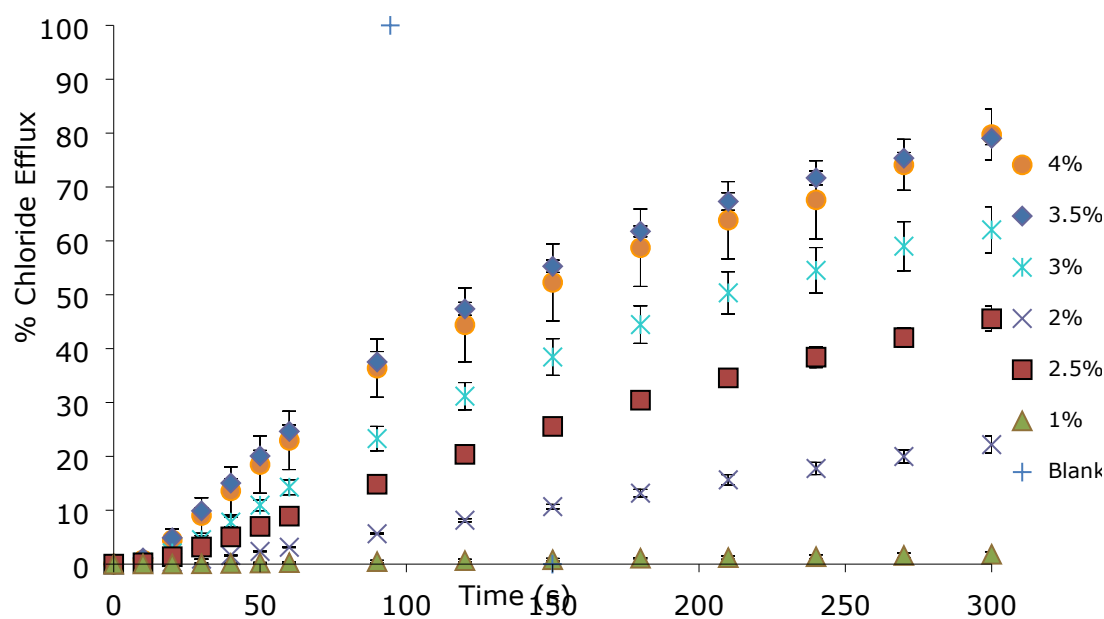


Figure S38: Chloride efflux as a function of time, promoted by the addition of various concentrations of receptor 6, from unilamellar POPC vesicles containing 489 mM NaCl with 5 mM sodium phosphate salts. The vesicles were suspended in 489 mM NaNO₃ buffered to pH 7.2 with 5 mM sodium phosphate salts. The receptor was loaded as a DMSO solution at 0 s. The vesicles were lysed at the end of the experiment to calibrate 100% chloride efflux.

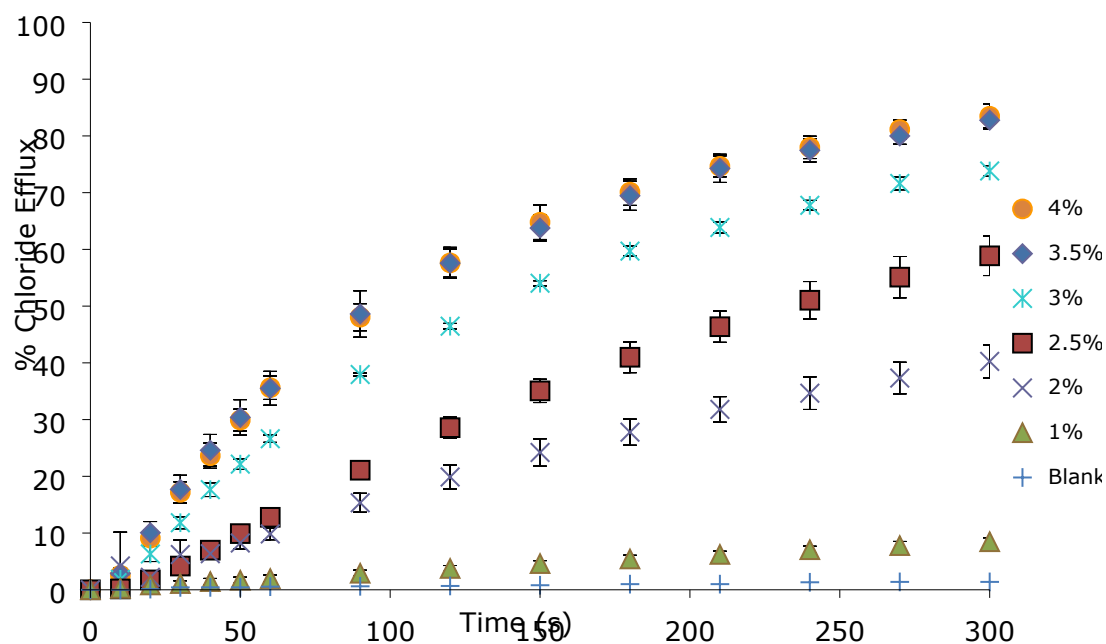


Figure S39: Chloride efflux as a function of time, promoted by the addition of various concentrations of receptor **6**, from unilamellar POPC vesicles containing 489 mM NaCl with 5 mM sodium phosphate salts. The vesicles were suspended in 489 mM NaNO₃ buffered to pH 7.2 with 5 mM sodium phosphate salts. The receptor was loaded as a DMSO solution at 0 s. The vesicles were lysed at the end of the experiment to calibrate 100% chloride efflux.

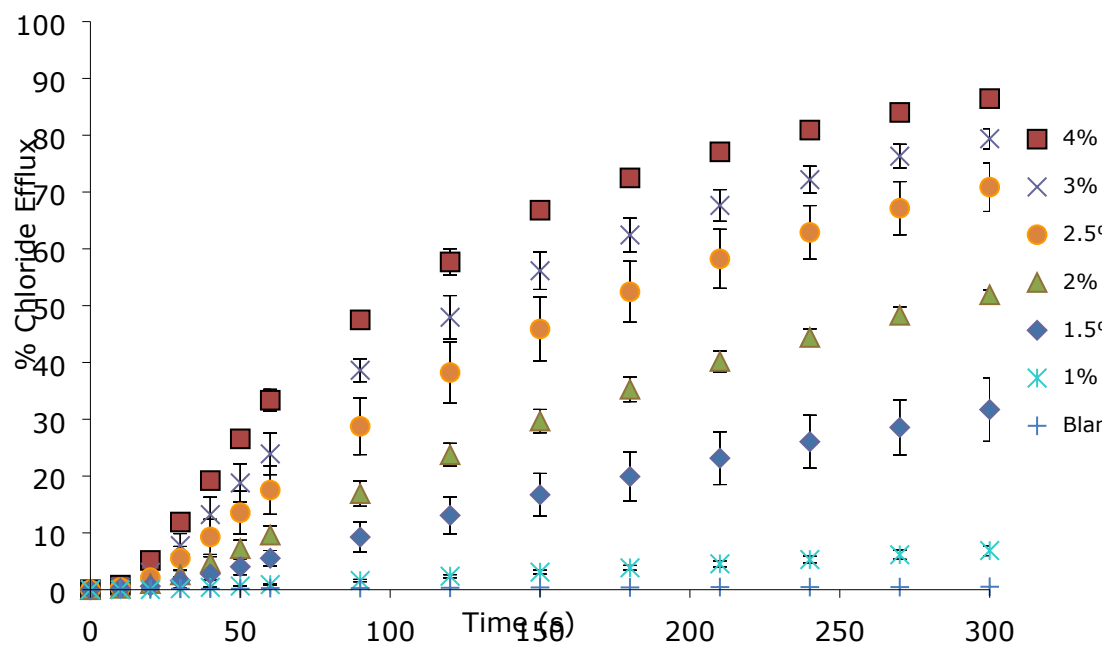


Figure S40: Chloride efflux as a function of time, promoted by the addition of various concentrations of receptor **6**, from unilamellar POPC vesicles containing 489 mM NaCl with 5 mM sodium phosphate salts. The vesicles were suspended in 489 mM NaNO₃ buffered to pH 7.2 with 5 mM sodium phosphate salts. The receptor was loaded as a DMSO solution at 0 s. The vesicles were lysed at the end of the experiment to calibrate 100% chloride efflux.

Hill Plots

During the Hill plots the Cl⁻/NO₃⁻ transport assays were performed for various concentrations of receptor. The percentage of chloride efflux 270 seconds after addition of carrier was plotted as a function of receptor concentration. Data points were fitted using the Hill equation using Origin 9.1:

$$y = V_{max} \frac{x^n}{k^n + x^n} = 100\% \frac{x^n}{(EC_{50})^n + x^n}$$

This is where y is the chloride efflux at 270 s (%) and x is the receptor concentration (mol % with respect to lipid concentration). V_{max}, k and n are the parameters to be determined. V_{max} is the maximum efflux possible (fixed to 100%, as this is physically the maximum chloride efflux possible), n is the Hill coefficient and k is the carrier concentration needed to reach V_{max}/2 (when V_{max} is fixed to 100%, k is the EC₅₀ value). To ensure repeatability, each Hill plot was repeated a minimum of 3 times with a newly prepared set of vesicles. Within each Hill plot repeat, the chloride efflux for every concentration was monitored a further 3 times to ensure stability if the data during that repeat.

In certain cases where the compound is particularly inactive, chloride efflux does not reach 100%. This is due to solubility reasons as the compound begins to precipitate out of solution at high receptor loadings. Where this is the case, the Hill plot was fitted with V_{max} set to the highest receptor concentration at which efflux occurred and then fitted to the Hill equation.

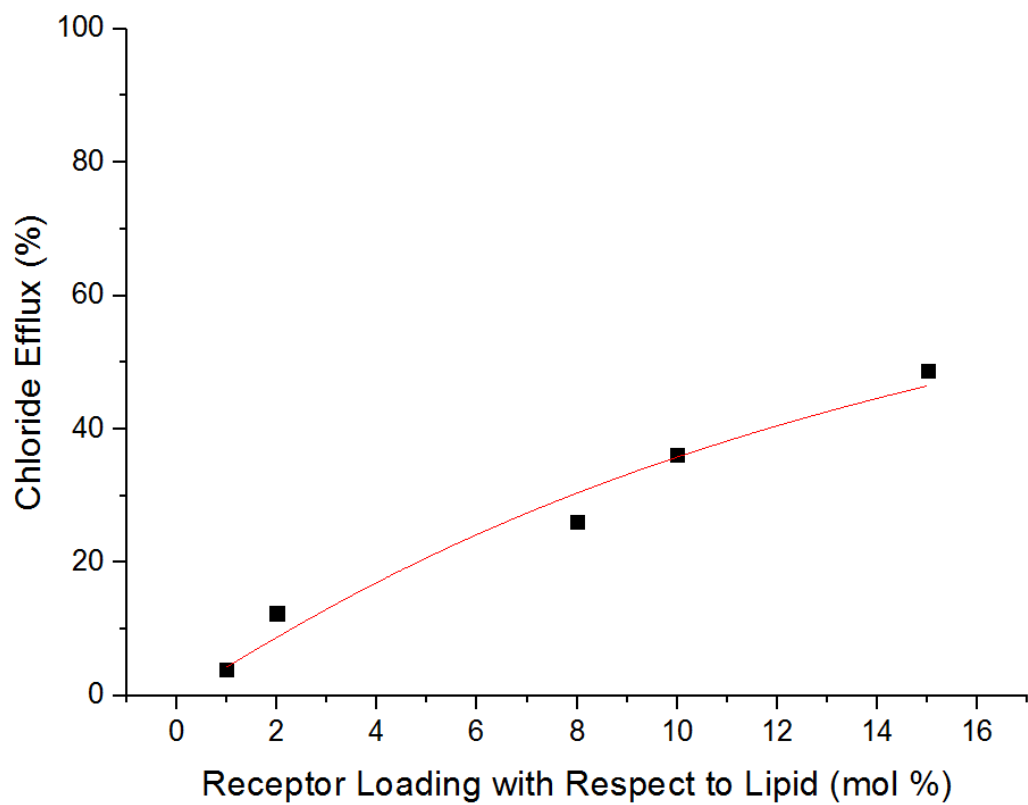


Figure S41: Hill analysis for $\text{Cl}^-/\text{NO}_3^-$ antiport mediated by **1**. Data was fitted to the Hill equation using Origin 9.1. $R^2 = 0.96208$, $\text{EC}_{50} = 17.066$, $n = 1.0934 \pm 0.17959$.

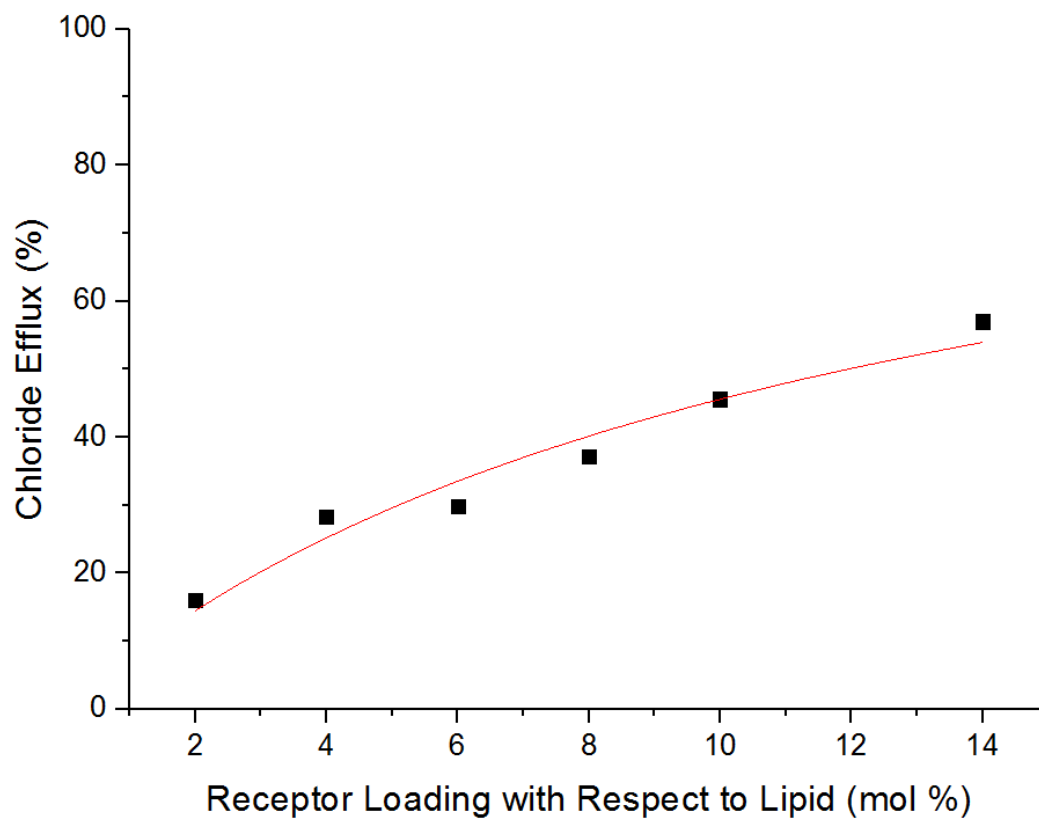


Figure S42: Hill analysis for $\text{Cl}^-/\text{NO}_3^-$ antiport mediated by **1**. Data was fitted to the Hill equation using Origin 9.1. $R^2 = 0.94673$, $\text{EC}_{50} = 11.954$, $n = 0.9949 \pm 0.12324$.

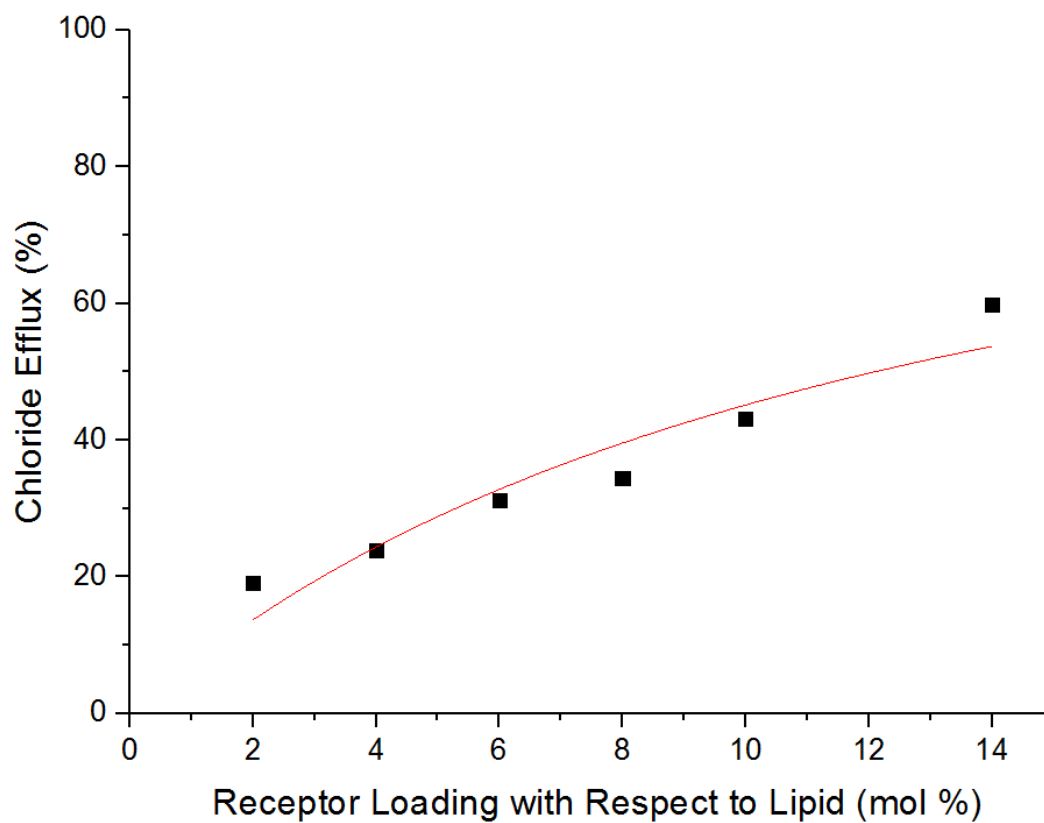


Figure S43: Hill analysis for $\text{Cl}^-/\text{NO}_3^-$ antiport mediated by **1**. Data was fitted to the Hill equation using Origin 9.1. $R^2 = 0.88167$, $\text{EC}_{50} = 12.1067$, $n = 1.02363 \pm 0.19139$.

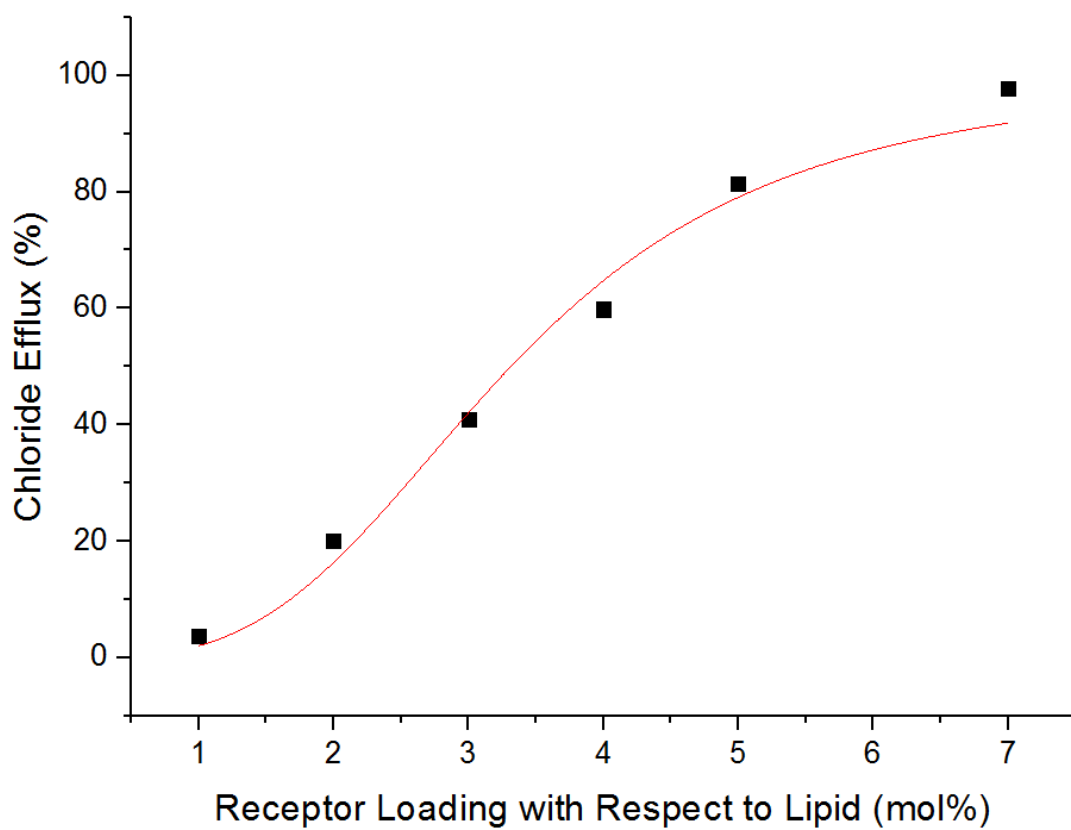


Figure S44: Hill analysis for $\text{Cl}^-/\text{NO}_3^-$ antiport mediated by **2**. Data was fitted to the Hill equation using Origin 9.1. $R^2 = 0.98412$, $\text{EC}_{50} = 3.3148$, $n = 3.23232 \pm 0.36991$.

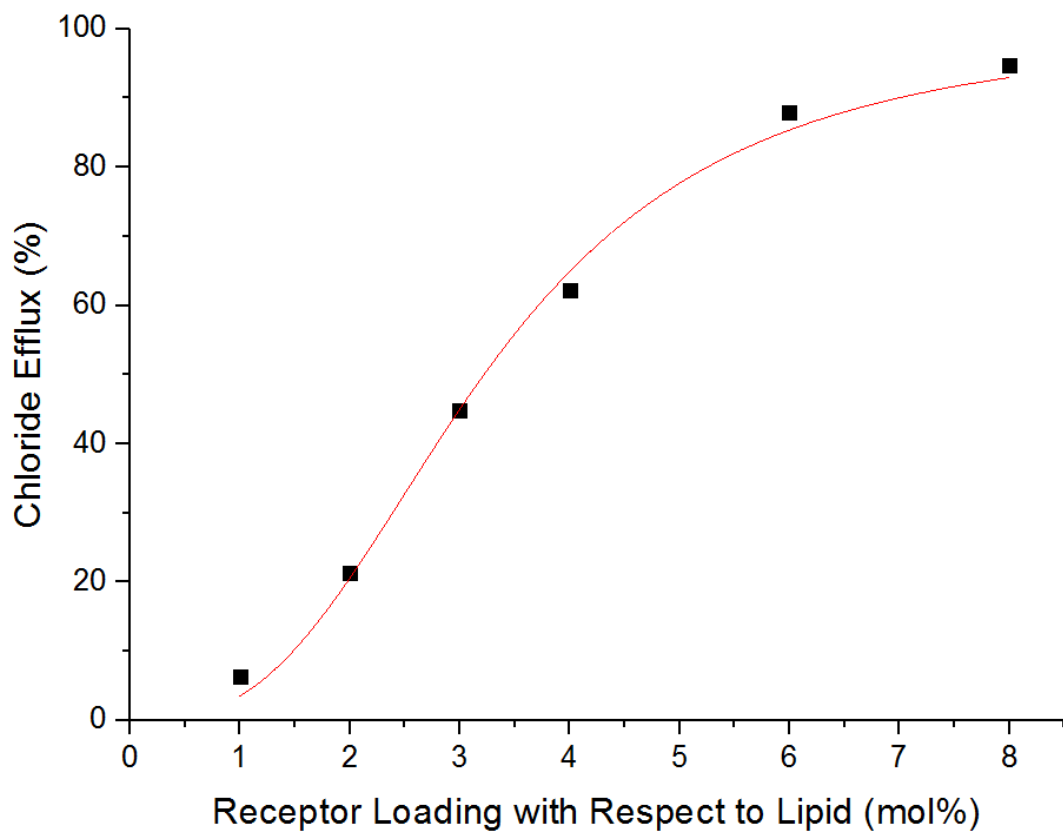


Figure S45: Hill analysis for $\text{Cl}^-/\text{NO}_3^-$ antiport mediated by **2**. Data was fitted to the Hill equation using Origin 9.1. $R^2 = 0.99503$, $\text{EC}_{50} = 3.2210$, $n = 2.84374 \pm 0.17844$.

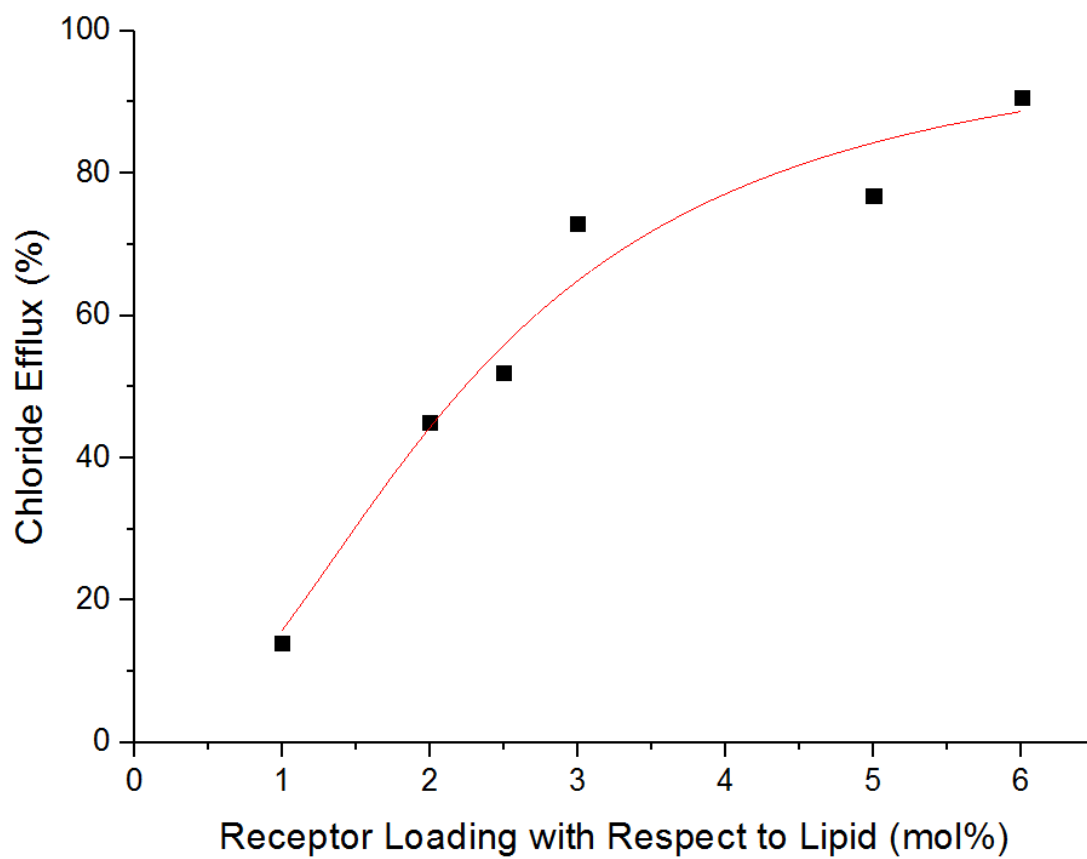


Figure S46: Hill analysis for Cl⁻/NO₃⁻ antiport mediated by **2**. Data was fitted to the Hill equation using Origin 9.1. $R^2 = 0.95262$, $EC_{50} = 2.2324$, $n = 2.0837 \pm 0.3168$.

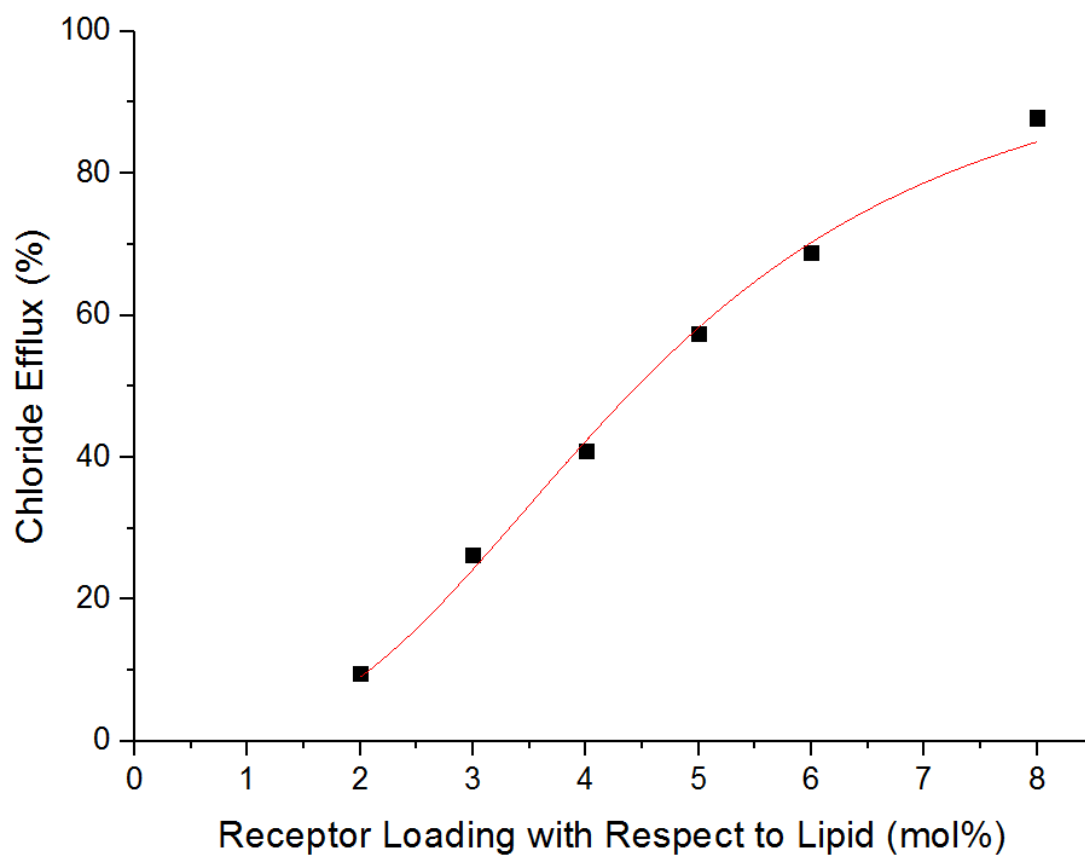


Figure S47: Hill analysis for $\text{Cl}^-/\text{NO}_3^-$ antiport mediated by **3**. Data was fitted to the Hill equation using Origin 9.1. $R^2 = 0.99361$, $\text{EC}_{50} = 4.4543$, $n = 2.8874 \pm 0.15921$.

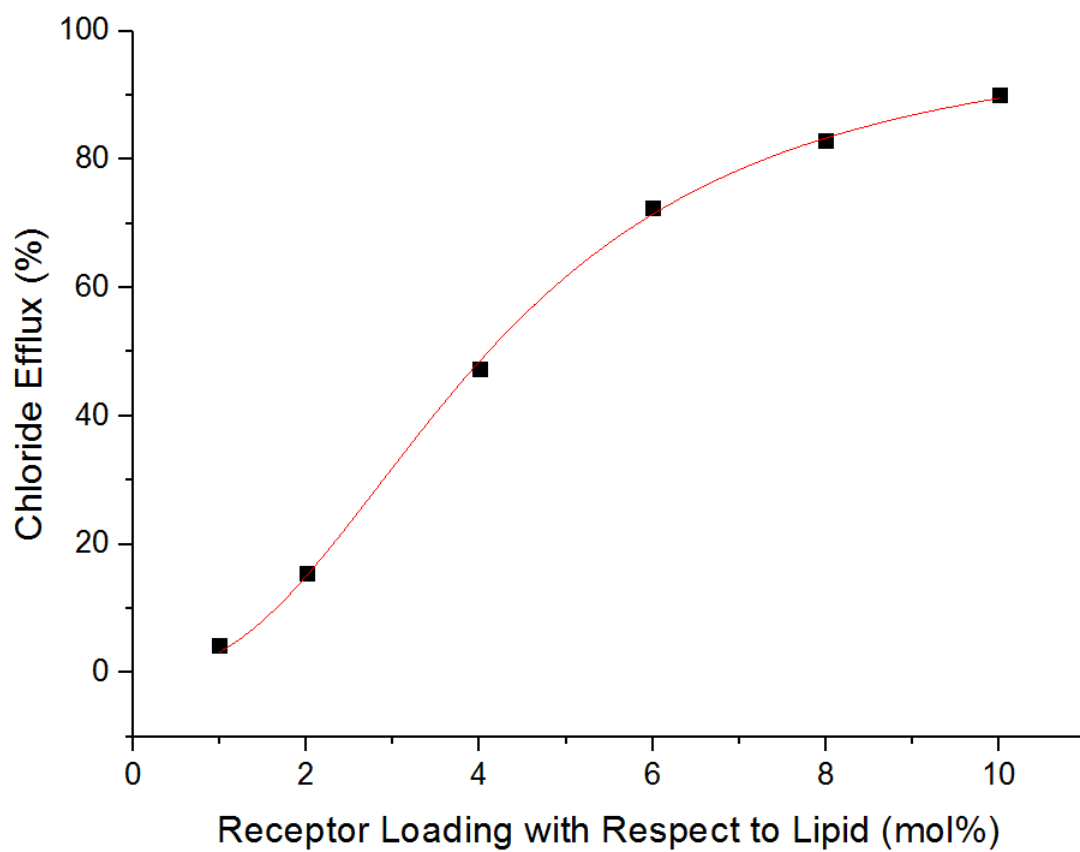


Figure S48: Hill analysis for $\text{Cl}^-/\text{NO}_3^-$ antiport mediated by **3**. Data was fitted to the Hill equation using Origin 9.1. $R^2 = 0.99918$, $\text{EC}_{50} = 4.0992$, $n = 2.4110 \pm 0.06076$.

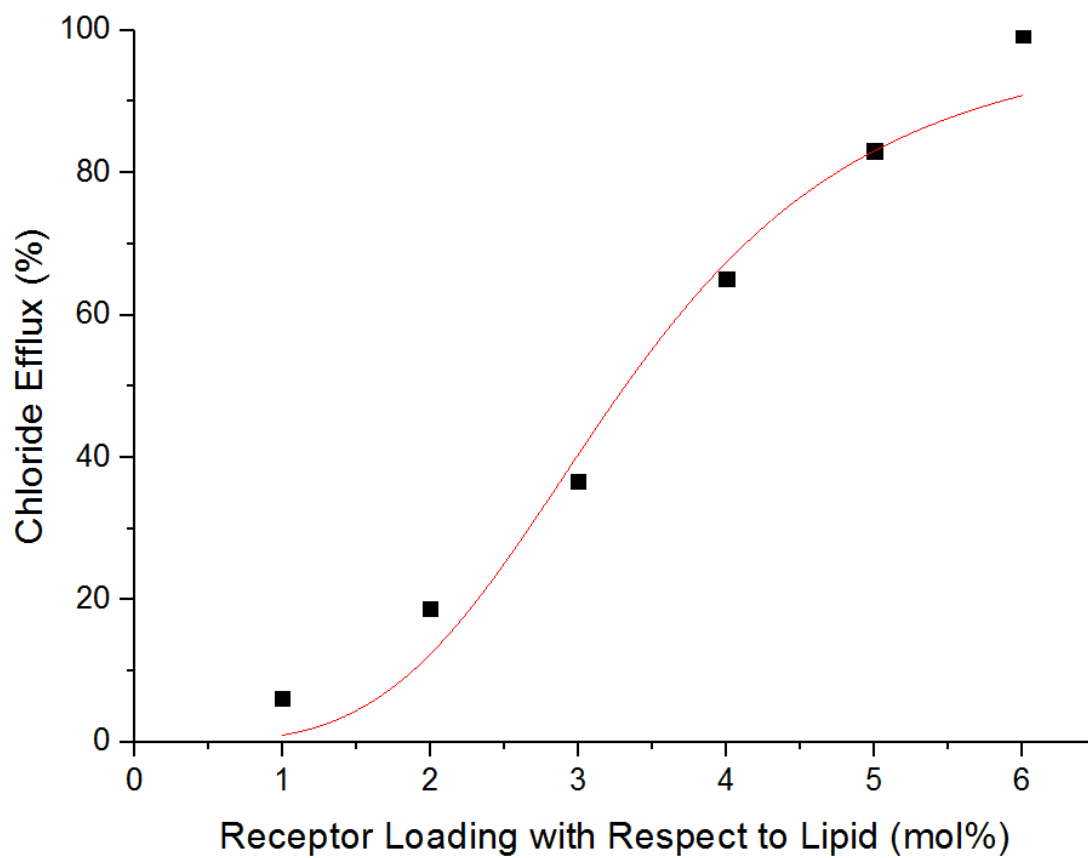


Figure S49: Hill analysis for $\text{Cl}^-/\text{NO}_3^-$ antiport mediated by **3**. Data was fitted to the Hill equation using Origin 9.1. $R^2 = 0.97065$, $\text{EC}_{50} = 3.3146$, $n = 3.8718 \pm 0.61508$.

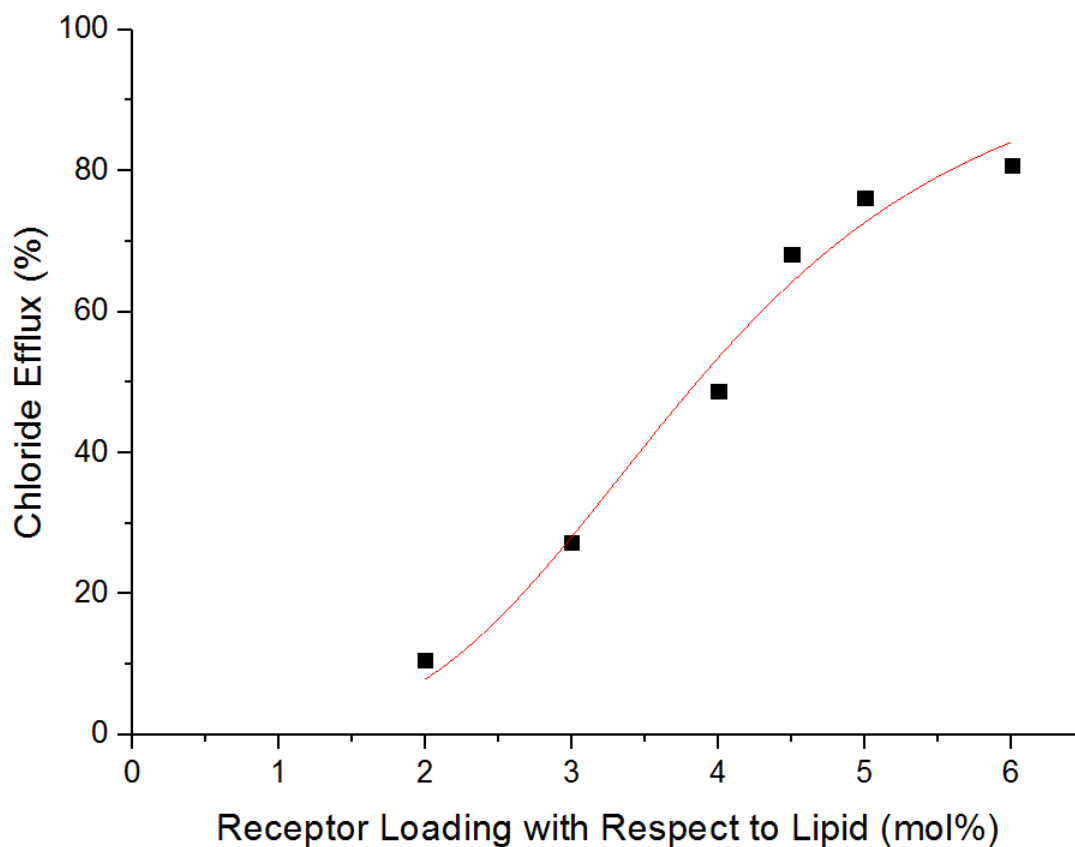


Figure S50: Hill analysis for $\text{Cl}^-/\text{NO}_3^-$ antiport mediated by **3**. Data was fitted to the Hill equation using Origin 9.1. $R^2 = 0.97818$, $\text{EC}_{50} = 3.8519$, $n = 3.7551 \pm 0.39366$.

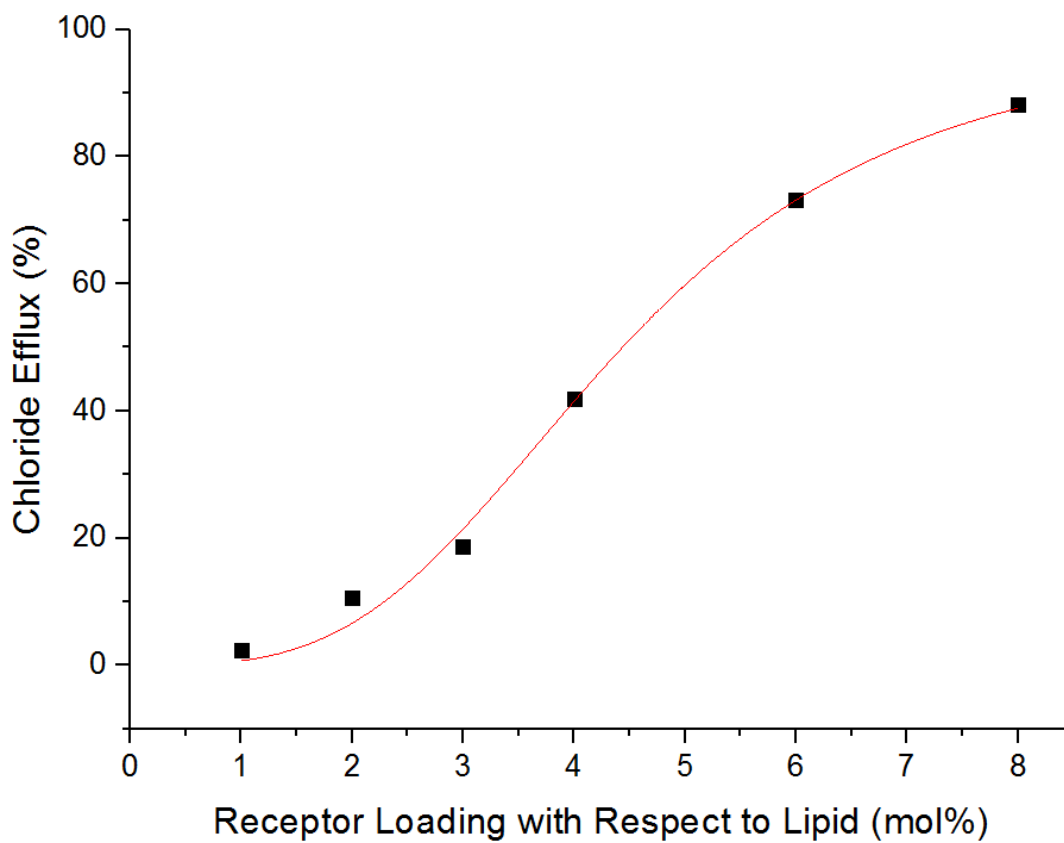


Figure S51: Hill analysis for $\text{Cl}^-/\text{NO}_3^-$ antiport mediated by **3**. Data was fitted to the Hill equation using Origin 9.1. $R^2 = 0.99452$, $\text{EC}_{50} = 4.4355$, $n = 3.3216 \pm 0.2117$.

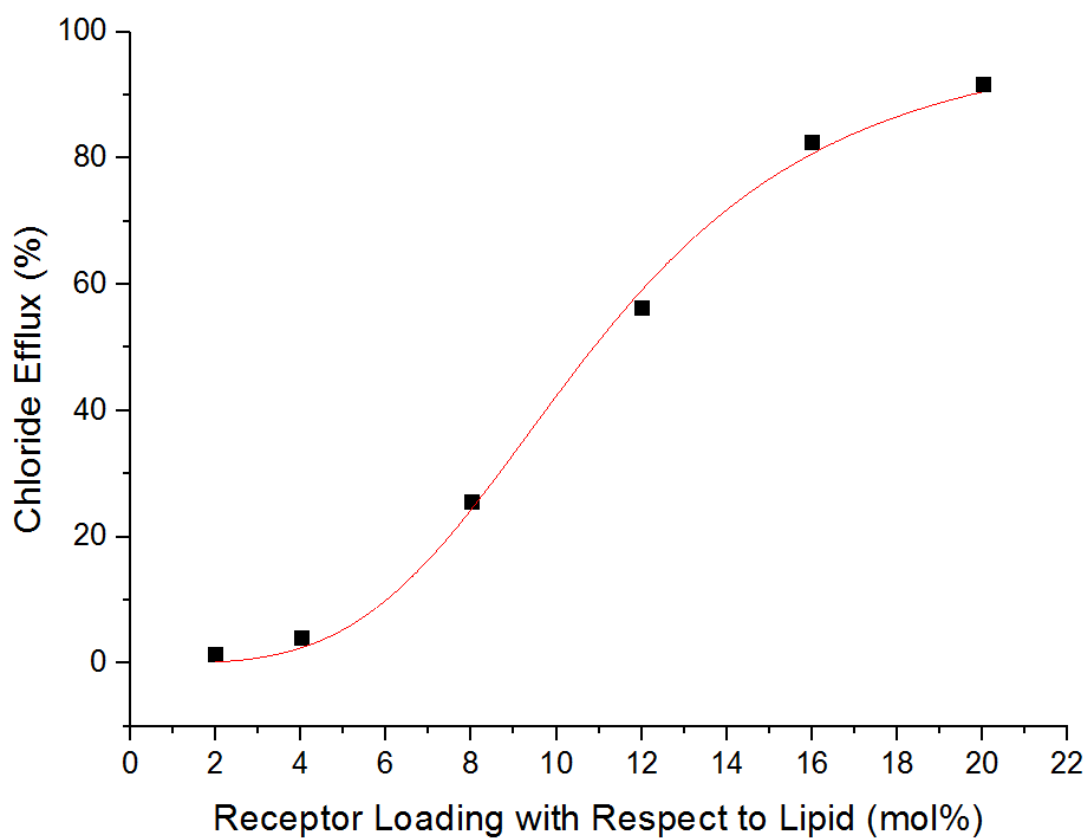


Figure S52: Hill analysis for $\text{Cl}^-/\text{NO}_3^-$ antiport mediated by **5**. Data was fitted to the Hill equation using Origin 9.1. $R^2 = 0.99702$, $\text{EC}_{50} = 10.867$, $n = 3.7014 \pm 0.21304$.

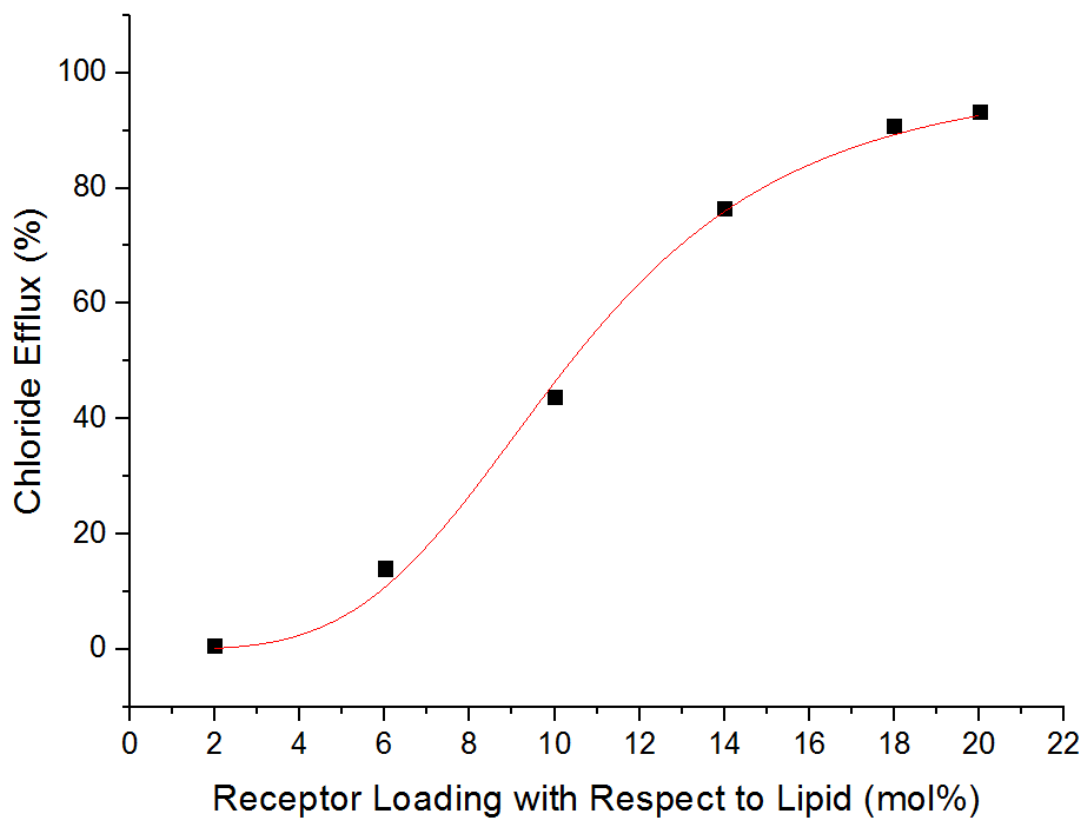


Figure S53: Hill analysis for $\text{Cl}^-/\text{NO}_3^-$ antiport mediated by **5**. Data was fitted to the Hill equation using Origin 9.1. $R^2 = 0.99666$, $\text{EC}_{50} = 10.390$, $n = 3.8554 \pm 0.23425$.

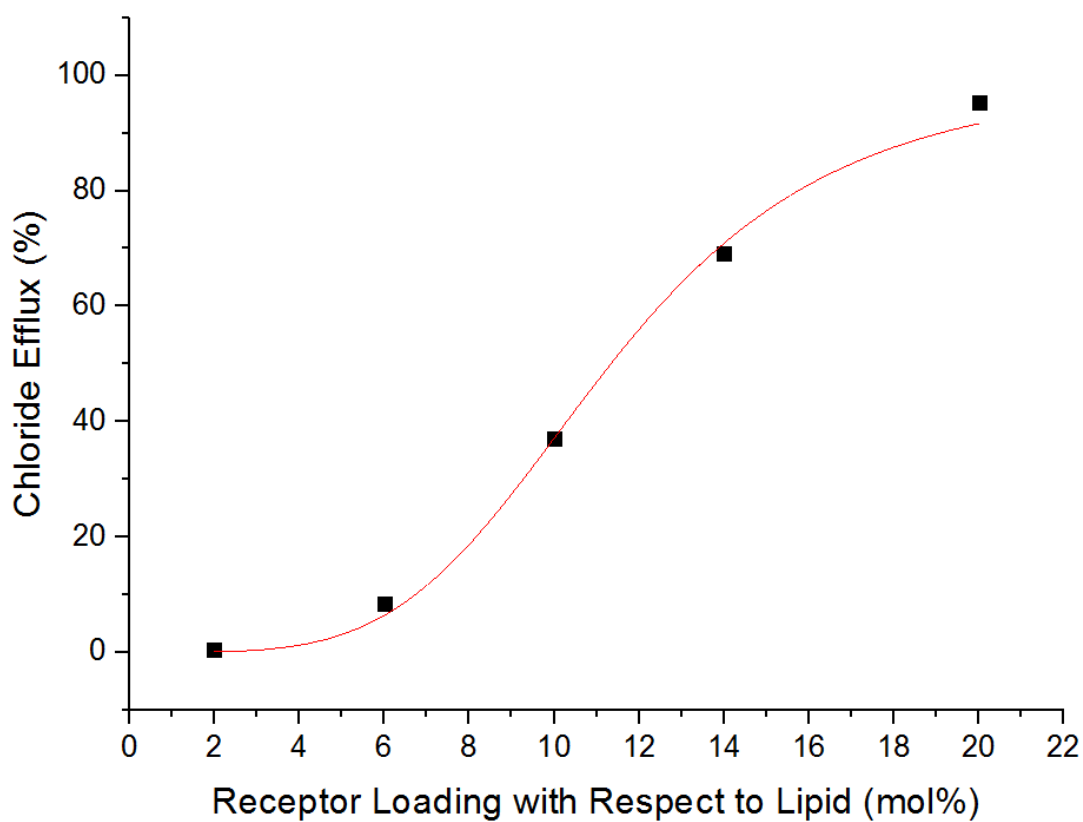


Figure S54: Hill analysis for $\text{Cl}^-/\text{NO}_3^-$ antiport mediated by **5**. Data was fitted to the Hill equation using Origin 9.1. $R^2 = 0.99564$, $\text{EC}_{50} = 11.335$, $n = 4.2182 \pm 0.34247$.

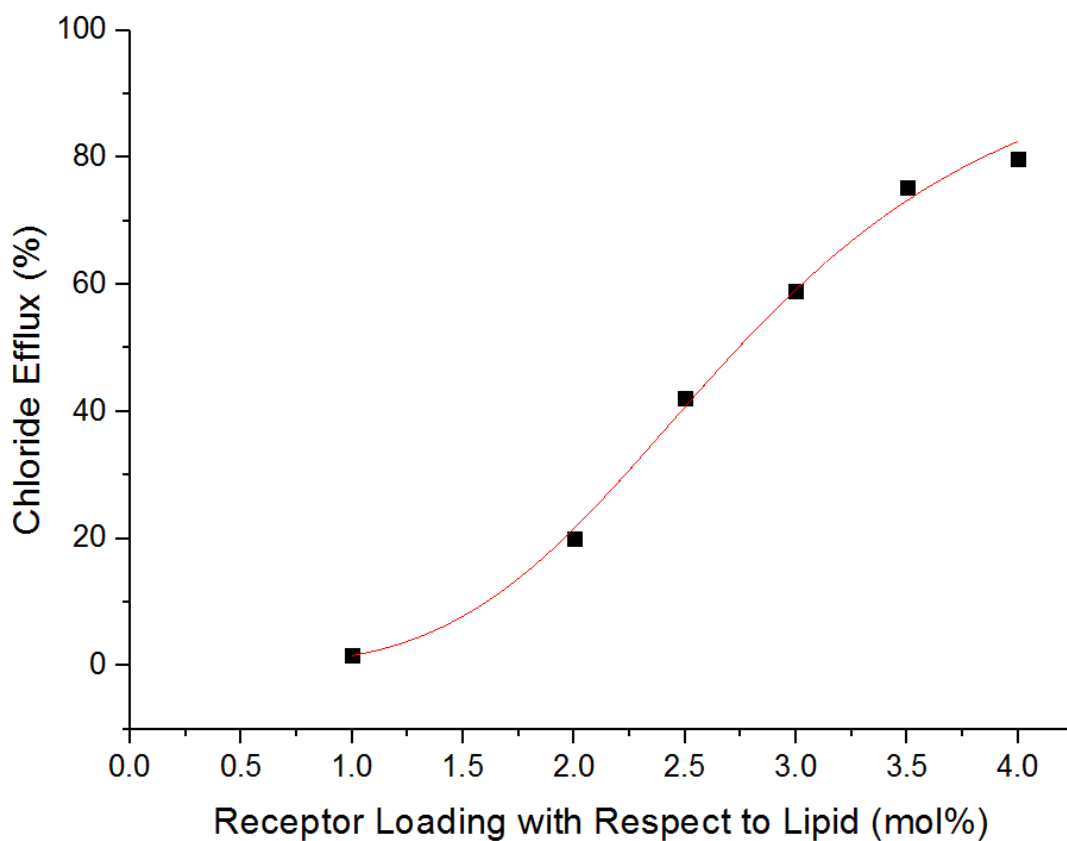


Figure S55: Hill analysis for $\text{Cl}^-/\text{NO}_3^-$ antiport mediated by **6**. Data was fitted to the Hill equation using Origin 9.1. $R^2 = 0.99566$, $\text{EC}_{50} = 2.7389$, $n = 4.1034 \pm 0.21571$.

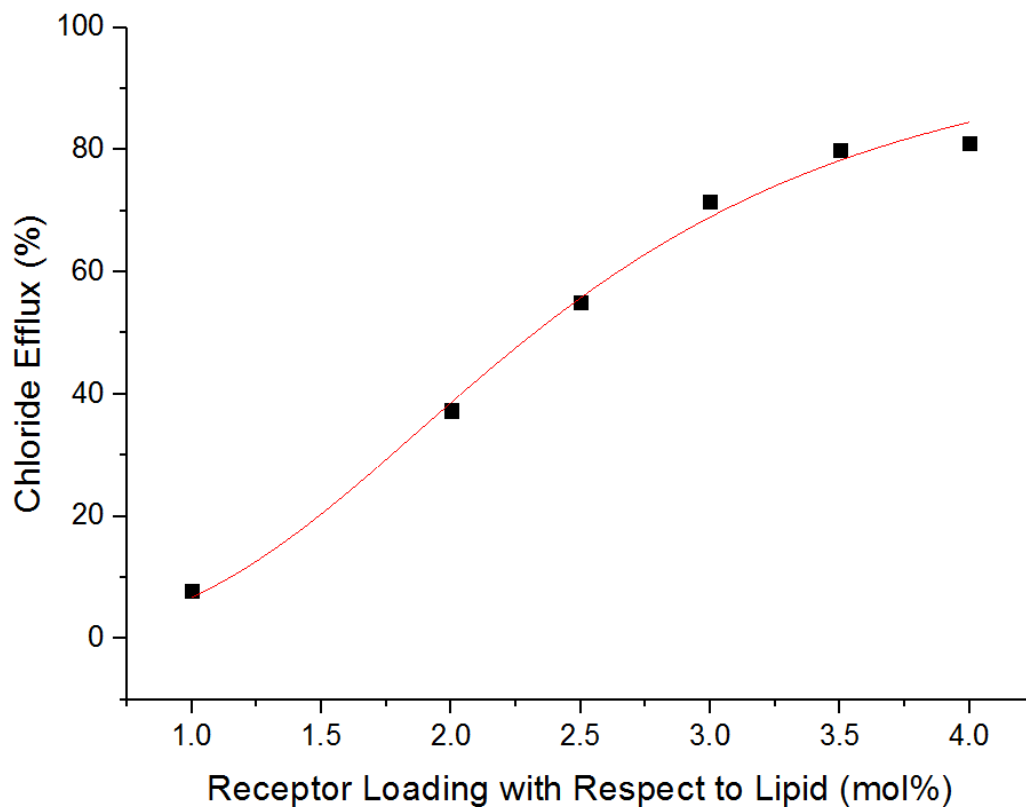


Figure S56: Hill analysis for $\text{Cl}^-/\text{NO}_3^-$ antiport mediated by **6**. Data was fitted to the Hill equation using Origin 9.1. $R^2 = 0.99259$, $\text{EC}_{50} = 2.3206$, $n = 3.1186 \pm 0.20716$.

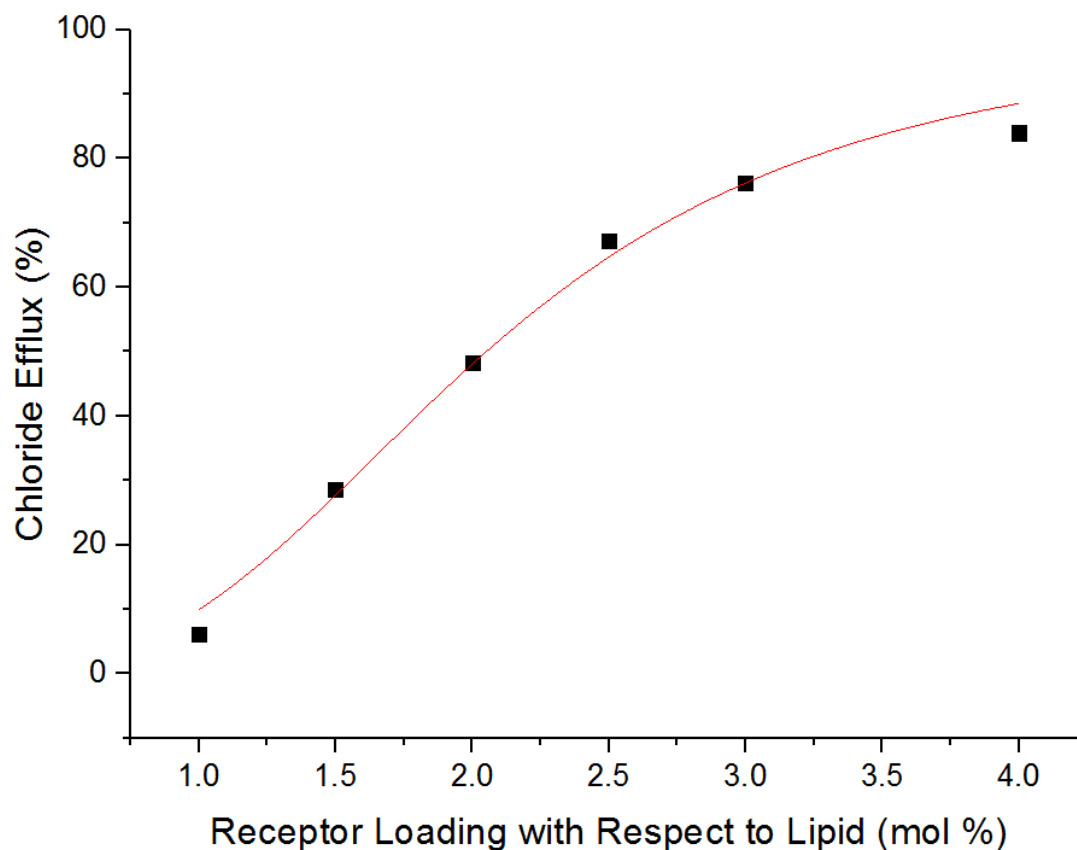


Figure S57: Hill analysis for $\text{Cl}^-/\text{NO}_3^-$ antiport mediated by **6**. Data was fitted to the Hill equation using Origin 9.1. $R^2 = 0.98837$, $\text{EC}_{50} = 2.0510$, $n = 3.0639 \pm 0.23479$.

Hill Analysis in POPC:Cholesterol Vesicles

To demonstrate that aggregation and therefore cooperativity is less prevalent in POPC:Cholesterol vesicles as opposed to pure POPC vesicles alone, we performed Hill analysis for compound **3** in POPC:Cholesterol vesicles (7:3 molar ratio) (**figure S54**). The Hill analysis performed was done in the same way as described previously.

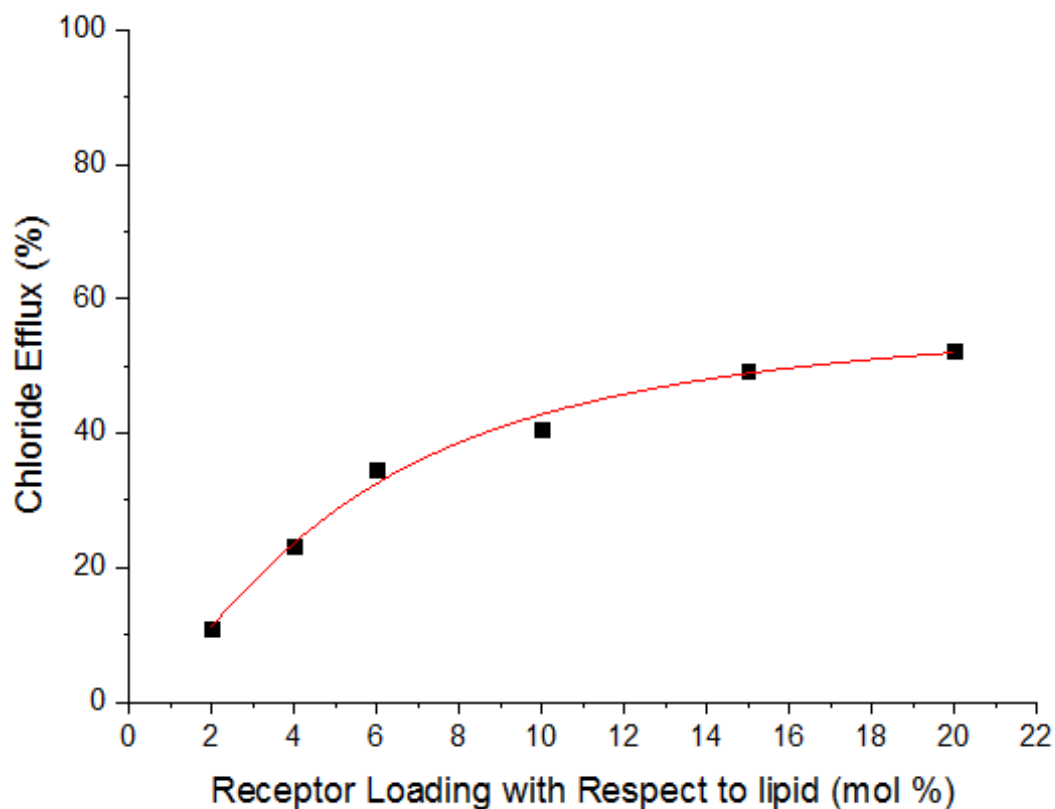


Figure S59: Hill analysis for $\text{Cl}^-/\text{NO}_3^-$ antiport mediated by **6**. Data was fitted to the Hill equation using Origin 9.1. $R^2 = 0.98720$, $\text{EC}_{50} = 16.4767$, $n = 1.5032 \pm 0.2$.

Evidence for Antiport

Symport vs Antiport: Cation exchange tests.

i) KCl vesicles

To test for Na^+/Cl^- symport as opposed to $\text{Cl}^-/\text{NO}_3^-$ antiport, the vesicle experiments were repeated with KCl encapsulated vesicles as opposed to NaCl. The following figures show that there is little difference (within error) between chloride efflux observed in the case of KCl and NaCl. This suggests an antiport process.

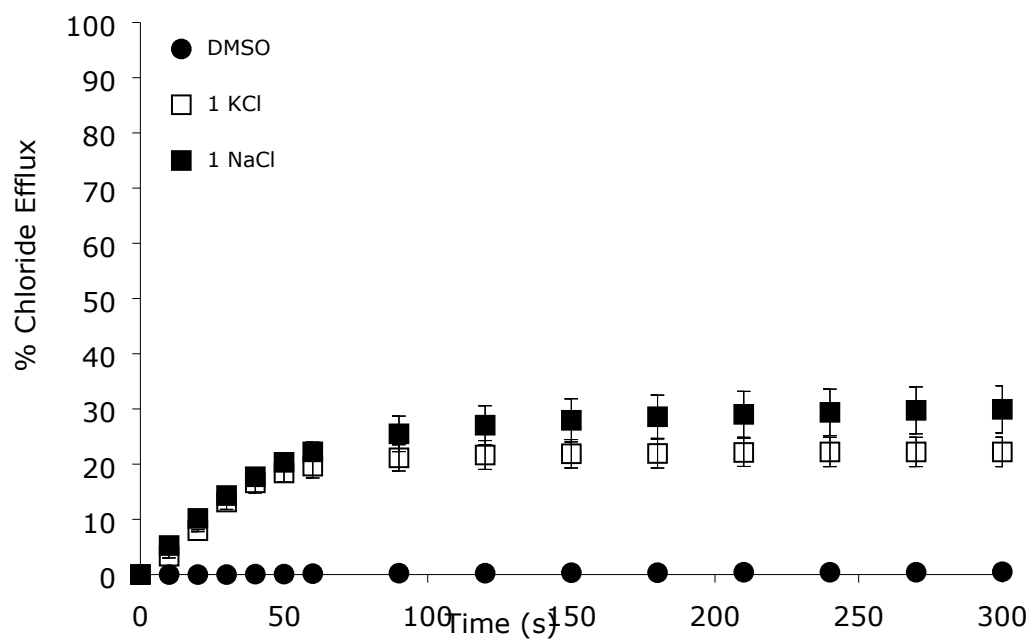


Figure S60: Chloride efflux promoted by **1** (6 mol% carrier to lipid concentration) from (■) unilamellar POPC vesicles loaded with 489 mM NaCl buffered to pH 7.2 with 5 mM phosphate salts and (□) unilamellar POPC vesicles loaded with 489 mM KCl buffered to pH 7.2 with 5 mM phosphate salts. The vesicles were dispersed in 489 mM NaNO₃ buffered to pH 7.2 with 5 mM sodium phosphate salts. At the end of the experiment, the vesicles were lysed with detergent to calibrate the electrode to 100% efflux. Each point represents the average of three trials; error bars are ± standard deviation about the mean.

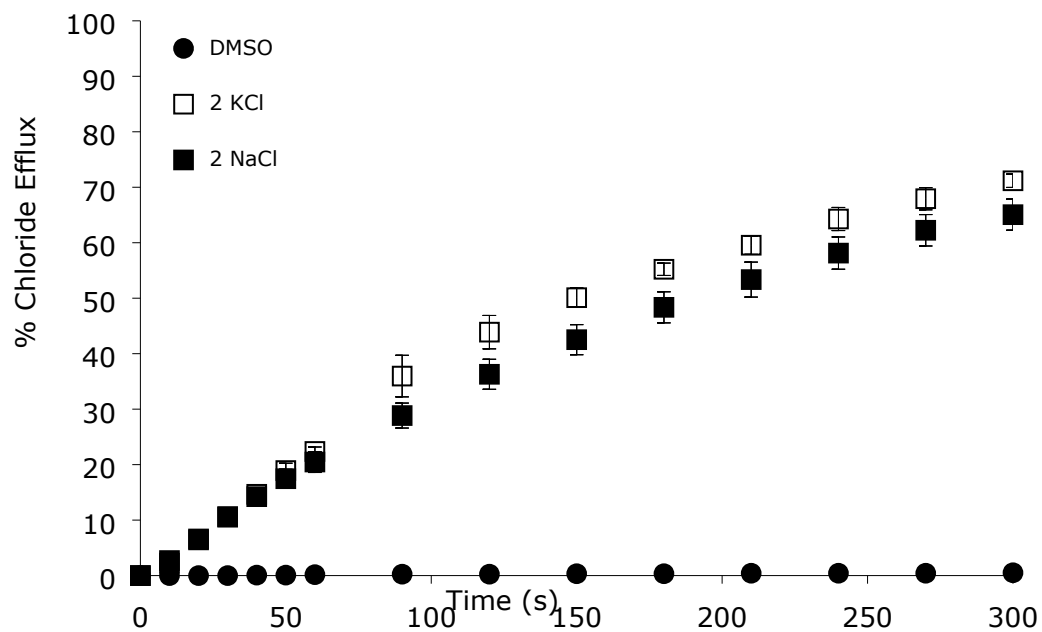


Figure S61: Chloride efflux promoted by **2** (4 mol% carrier to lipid concentration) from (■) unilamellar POPC vesicles loaded with 489 mM NaCl buffered to pH 7.2 with 5 mM phosphate salts and (□) unilamellar POPC vesicles loaded with 489 mM KCl buffered to pH 7.2 with 5 mM phosphate salts. The vesicles were dispersed in 489 mM NaNO₃ buffered to pH 7.2 with 5 mM sodium phosphate salts. At the end of the experiment, the vesicles were lysed with detergent to calibrate the electrode to 100% efflux. Each point represents the average of three trials; error bars are ± standard deviation about the mean.

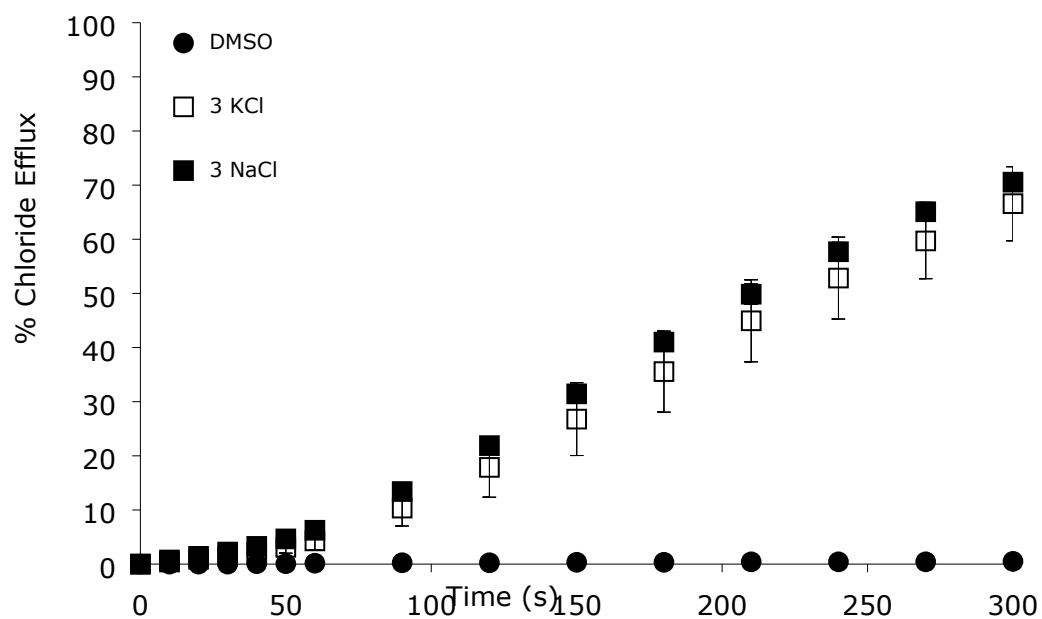


Figure S62: Chloride efflux promoted by **3** (4 mol% carrier to lipid concentration) from (■) unilamellar POPC vesicles loaded with 489 mM NaCl buffered to pH 7.2 with 5 mM phosphate salts and (□) unilamellar POPC vesicles loaded with 489 mM KCl buffered to pH 7.2 with 5 mM phosphate salts. The vesicles were dispersed in 489 mM NaNO₃ buffered to pH 7.2 with 5 mM sodium phosphate salts. At the end of the experiment, the vesicles were lysed with detergent to calibrate the electrode to 100% efflux. Each point represents the average of three trials; error bars are ± standard deviation about the mean.

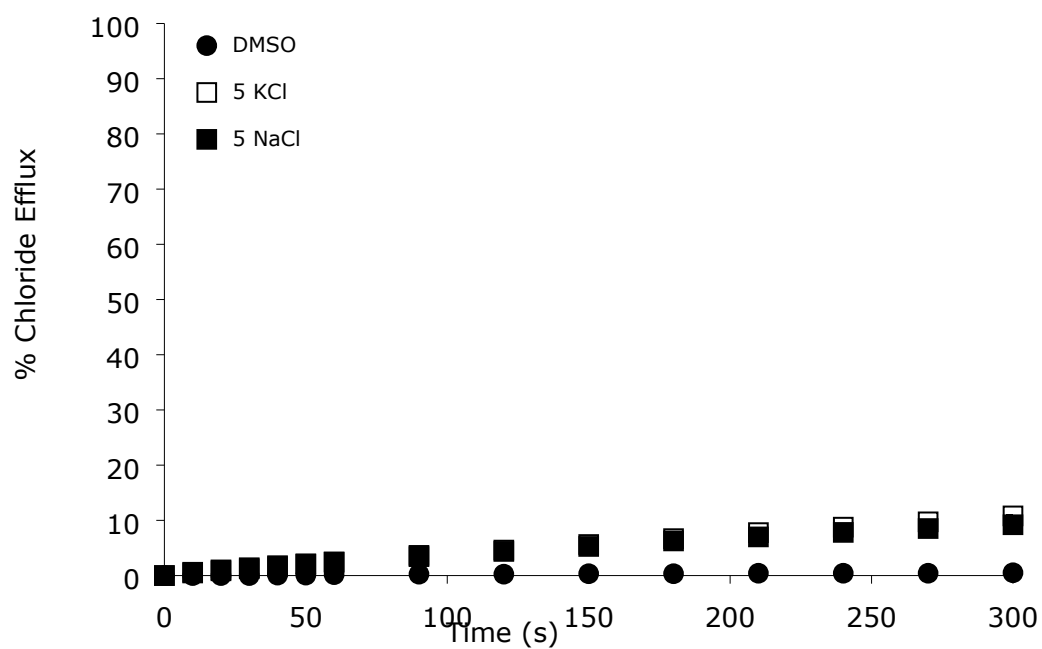


Figure S63: Chloride efflux promoted by **5** (6 mol% carrier to lipid concentration) from (■) unilamellar POPC vesicles loaded with 489 mM NaCl buffered to pH 7.2 with 5 mM phosphate salts and (□) unilamellar POPC vesicles loaded with 489 mM KCl buffered to pH 7.2 with 5 mM phosphate salts. The vesicles were dispersed in 489 mM NaNO₃ buffered to pH 7.2 with 5 mM sodium phosphate salts. At the end of the experiment, the vesicles were lysed with detergent to calibrate the electrode to 100% efflux. Each point represents the average of three trials; error bars are ± standard deviation about the mean.

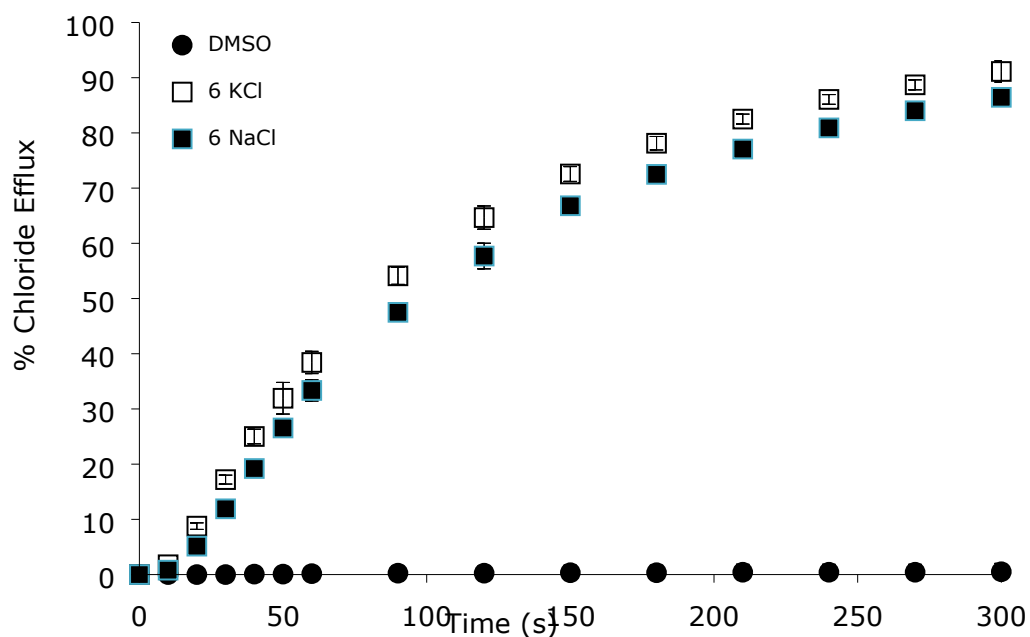


Figure S64: Chloride efflux promoted by **6** (4 mol% carrier to lipid concentration) from (■) unilamellar POPC vesicles loaded with 489 mM NaCl buffered to pH 7.2 with 5 mM phosphate salts and (□) unilamellar POPC vesicles loaded with 489 mM KCl buffered to pH 7.2 with 5 mM phosphate salts. The vesicles were dispersed in 489 mM NaNO₃ buffered to pH 7.2 with 5 mM sodium phosphate salts. At the end of the experiment, the vesicles were lysed with detergent to calibrate the electrode to 100% efflux. Each point represents the average of three trials; error bars are ± standard deviation about the mean.

ii) CsCl vesicles:

We performed our standard run for 2Cl⁻/SO₄²⁻ exchange, however we used vesicles encapsulating NaCl and CsCl. The following figures show that there is little difference (within error) between chloride efflux observed in the case of CsCl and NaCl. This suggests that any chloride efflux detected is due to 2Cl⁻/SO₄²⁻ antiport.

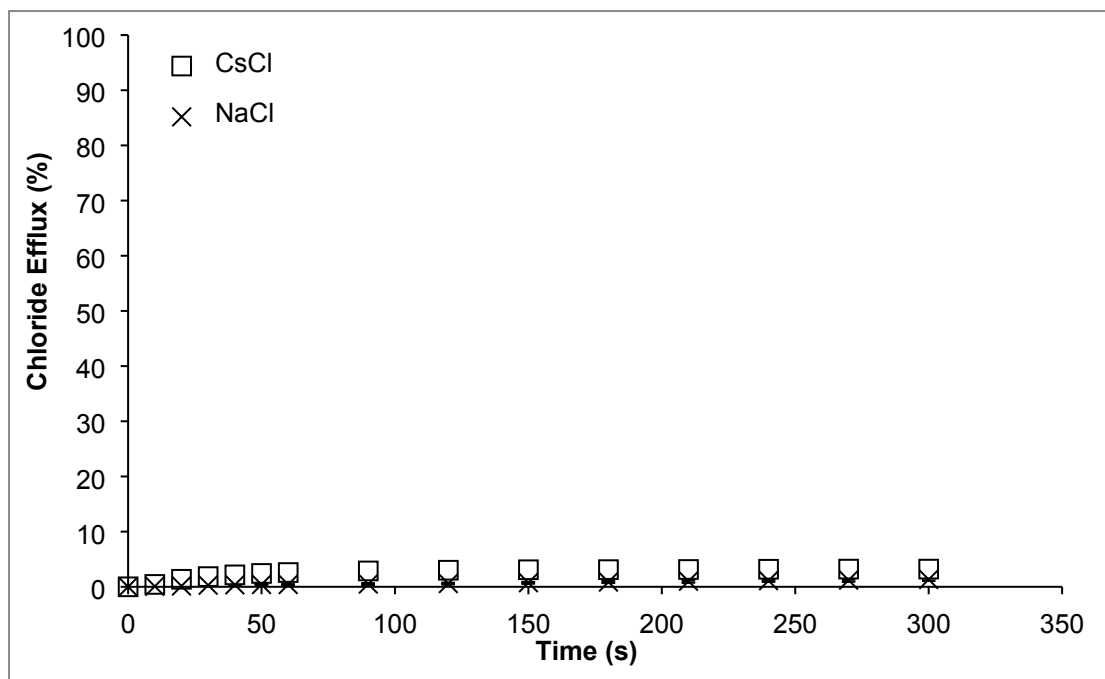


Figure S65: Chloride efflux promoted by a DMSO solution of compound **1** (8 mol% receptor concentration versus lipid) from ■ unilamellar POPC vesicles loaded with 451 mM NaCl buffered to pH 7.2 with 20 mM sodium phosphate salts and □ unilamellar POPC vesicles loaded with 451 mM CsCl buffered to pH 7.2 with 20 mM sodium phosphate salts. The vesicles were suspended in an external solution of 162 mM Na₂SO₄ buffered to pH 7.2 with phosphate salts. At the end of the experiment, the vesicles were lysed to calibrate the electrode to 100% efflux. Each point is an average of 3 repeated runs, error bars are ± standard deviation about the mean.

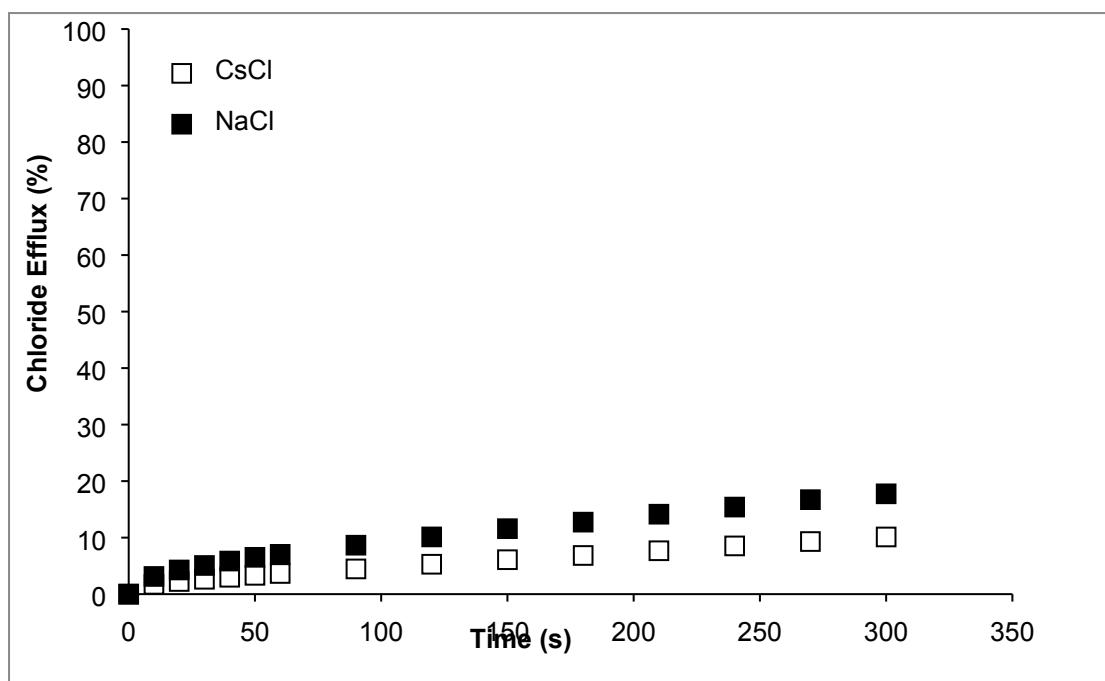


Figure S66: Chloride efflux promoted by a DMSO solution of compound **2** (5 mol% receptor concentration versus lipid) from ■ unilamellar POPC vesicles loaded with 451 mM NaCl buffered to pH 7.2 with 20 mM sodium phosphate salts and □ unilamellar POPC vesicles loaded with 451 mM CsCl buffered to pH 7.2 with 20 mM sodium phosphate salts. The vesicles were suspended in an external solution of 162 mM Na₂SO₄ buffered to pH 7.2 with phosphate salts. At the end of the experiment, the vesicles were lysed to calibrate the electrode to 100% efflux. Each point is an average of 3 repeated runs, error bars are ± standard deviation about the mean.

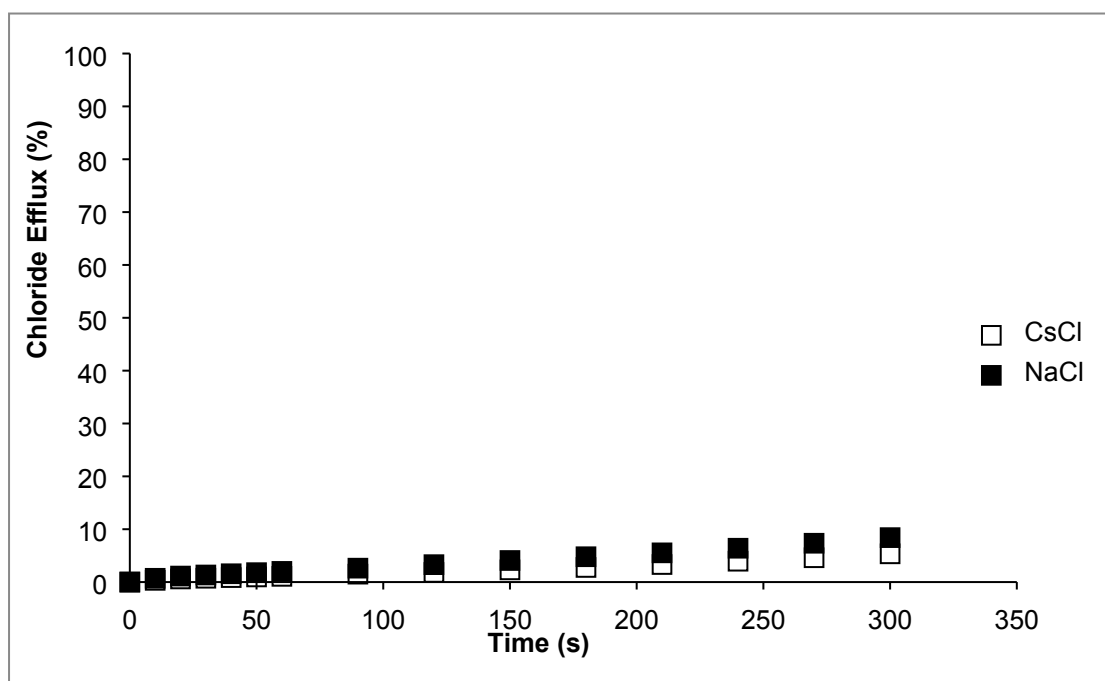


Figure S67: Chloride efflux promoted by a DMSO solution of compound **3** (5 mol% receptor concentration versus lipid) from ■ unilamellar POPC vesicles loaded with 451 mM NaCl buffered to pH 7.2 with 20 mM sodium phosphate salts and □ unilamellar POPC vesicles loaded with 451 mM CsCl buffered to pH 7.2 with 20 mM sodium phosphate salts. The vesicles were suspended in an external solution of 162 mM Na₂SO₄ buffered to pH 7.2 with phosphate salts. At the end of the experiment, the vesicles were lysed to calibrate the electrode to 100% efflux. Each point is an average of 3 repeated runs, error bars are ± standard deviation about the mean.

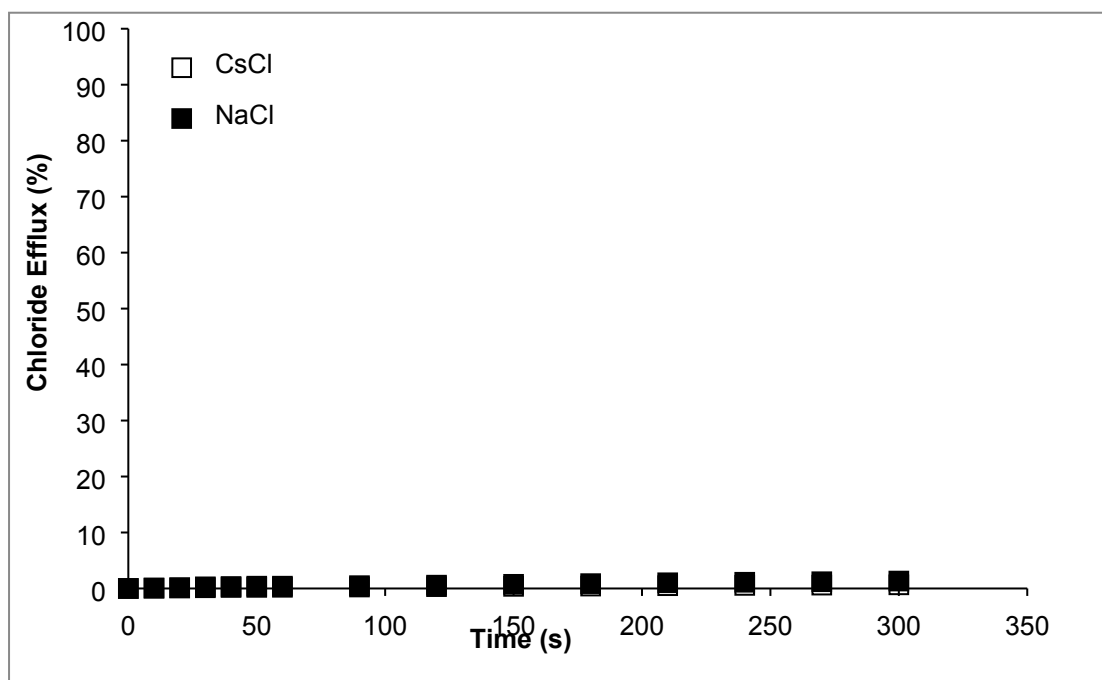


Figure S68: Chloride efflux promoted by a DMSO solution of compound **4** (8 mol% receptor concentration versus lipid) from ■ unilamellar POPC vesicles loaded with 451 mM NaCl buffered to pH 7.2 with 20 mM sodium phosphate salts and □ unilamellar POPC vesicles loaded with 451 mM CsCl buffered to pH 7.2 with 20 mM sodium phosphate salts. The vesicles were suspended in an external solution of 162 mM Na₂SO₄ buffered to pH 7.2 with phosphate salts. At the end of the experiment, the vesicles were lysed to calibrate the electrode to 100% efflux. Each point is an average of 3 repeated runs, error bars are ± standard deviation about the mean.

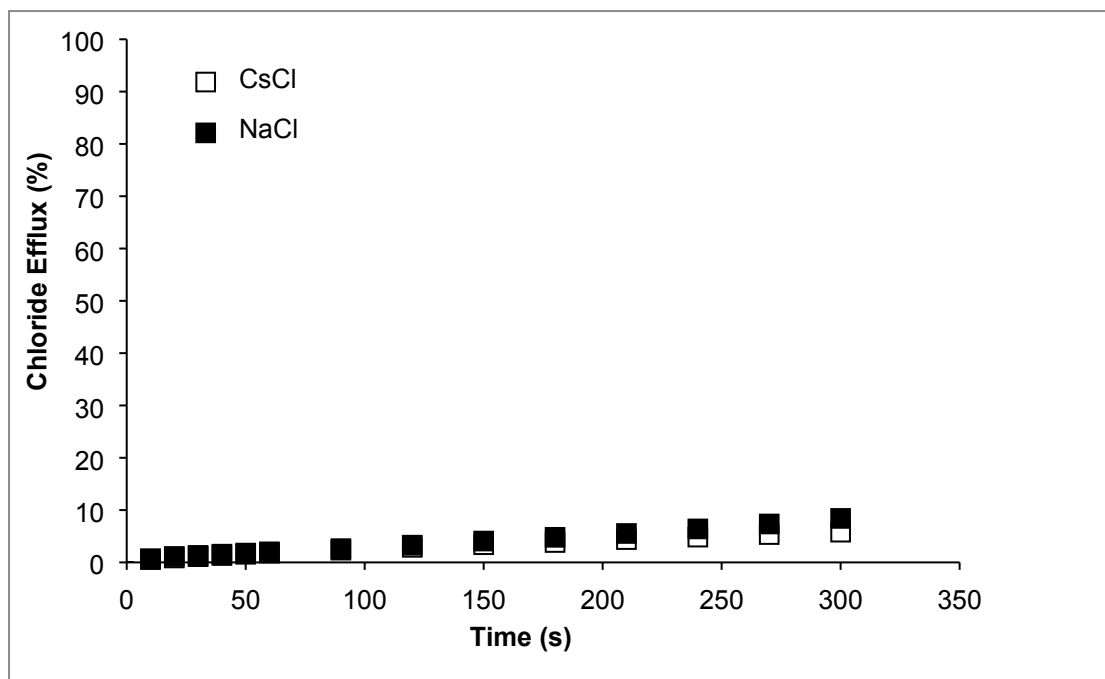


Figure S69: Chloride efflux promoted by a DMSO solution of compound **5** (5 mol% receptor concentration versus lipid) from ■ unilamellar POPC vesicles loaded with 451 mM NaCl buffered to pH 7.2 with 20 mM sodium phosphate salts and □ unilamellar POPC vesicles loaded with 451 mM CsCl buffered to pH 7.2 with 20 mM sodium phosphate salts. The vesicles were suspended in an external solution of 162 mM Na₂SO₄ buffered to pH 7.2 with phosphate salts. At the end of the experiment, the vesicles were lysed to calibrate the electrode to 100% efflux. Each point is an average of 3 repeated runs, error bars are ± standard deviation about the mean.

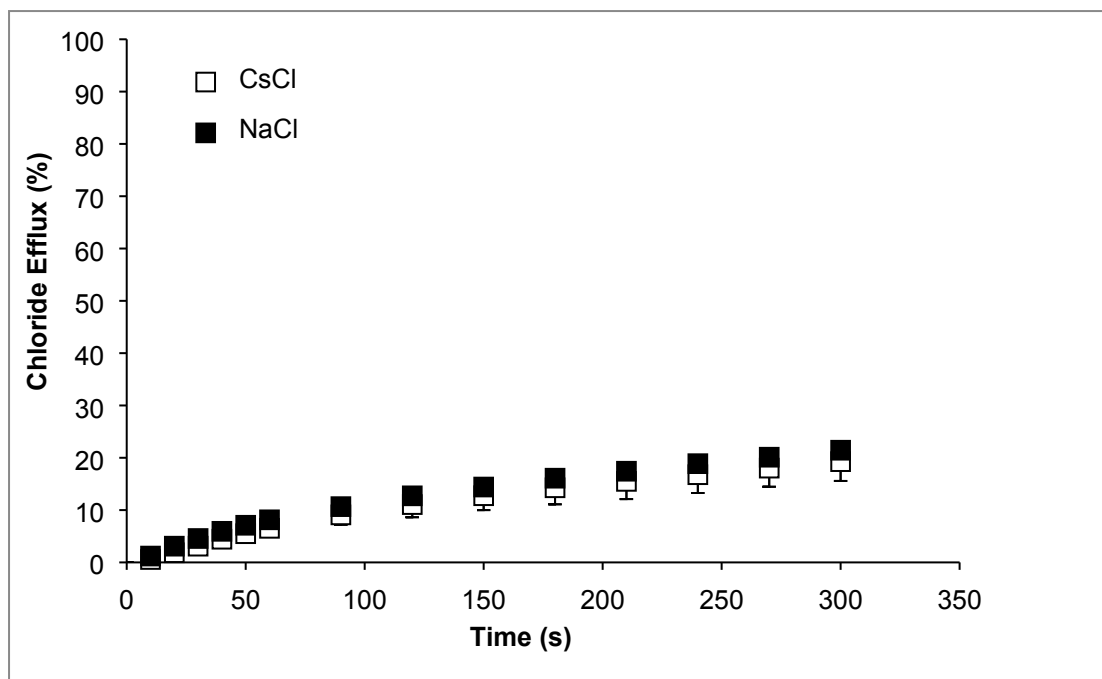


Figure S70: Chloride efflux promoted by a DMSO solution of compound **6** (5 mol% receptor concentration versus lipid) from ■ unilamellar POPC vesicles loaded with 451 mM NaCl buffered to pH 7.2 with 20 mM sodium phosphate salts and □ unilamellar POPC vesicles loaded with 451 mM CsCl buffered to pH 7.2 with 20 mM sodium phosphate salts. The vesicles were suspended in an external solution of 162 mM Na₂SO₄ buffered to pH 7.2 with phosphate salts. At the end of the experiment, the vesicles were lysed to calibrate the electrode to 100% efflux. Each point is an average of 3 repeated runs, error bars are ± standard deviation about the mean.

Symport vs Antiport - Cl⁻/HCO₃⁻ Exchange:

The plot of the bicarbonate exchange test shown in **Figure 2** (main text) with error bars is shown in **Figure S71** below.

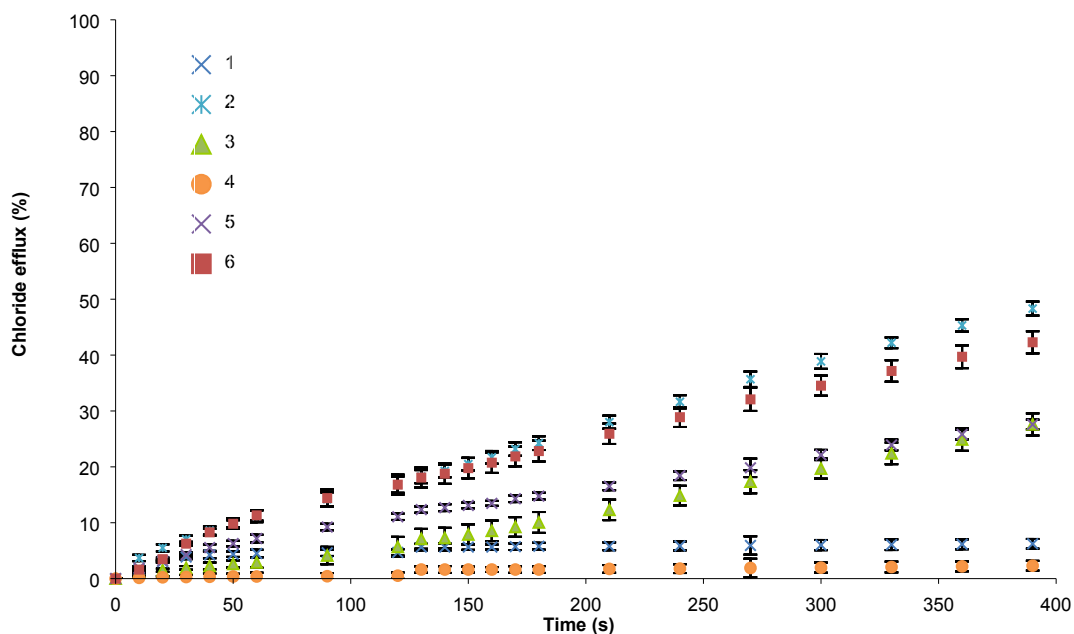


Figure S71: Chloride efflux promoted by a DMSO solution of compounds **1-6** (5 mol% receptor concentration versus lipid) from unilamellar POPC vesicles loaded with 451 mM NaCl buffered to pH 7.2 with 20 mM sodium phosphate salts. At $t = 120$ s a solution of sodium bicarbonate was added such that the external bicarbonate concentration was 40 mM. At the end of the experiment, the vesicles were lysed to calibrate the electrode to 100% efflux. Each point is an average of 3 repeated runs, error bars are \pm standard deviation about the mean.

Symport vs Antiport – Sulfate Exchange

A run of the $\text{Cl}^-/\text{HCO}_3^-$ exchange experiment was repeated without the bicarbonate spike is shown below.

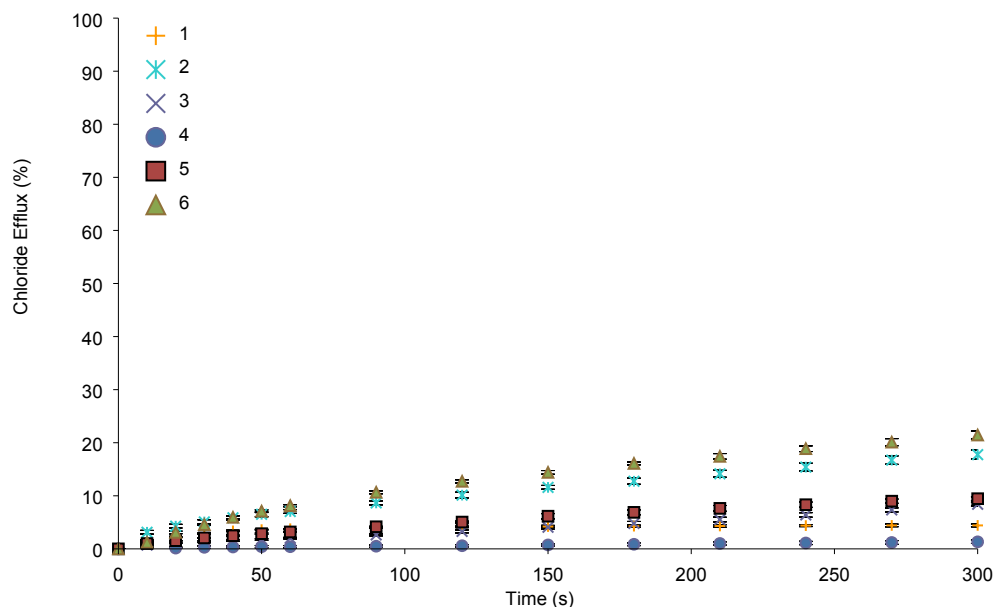


Figure S72: Chloride efflux promoted by a DMSO solution of compounds **1-6** (5 mol% receptor concentration versus lipid) from unilamellar POPC vesicles loaded with 451 mM NaCl buffered to pH 7.2 with 20 mM sodium phosphate salts. At the end of the experiment, the vesicles were lysed to calibrate the electrode to 100% efflux. Each point is an average of 3 repeated runs, error bars are \pm standard deviation about the mean.

Evidence for Aggregation

Cholesterol Tests:

To examine whether these transporters were acting as mobile carriers, channels or a mobile aggregate, the vesicle studies were repeated in a lipid mix containing 7:3 POPC:cholesterol. It is believed that cholesterol increases the viscosity of the membrane which affects partitioning of the compound into the lipid bilayer. It would therefore be expected that a transporter acting as a mobile carrier would show decreased activity in the mixed POPC:cholesterol vesicles than POPC alone whilst a compound acting as a membrane spanning channel would not expect to see this decrease in activity. With the exception of compound **2**, all of these receptors have

significantly reduced activity in the POPC:cholesterol vesicles than the POPC vesicles. This does not necessarily mean however that these receptors are acting as mobile carriers because one could argue that increasing the viscosity of the membrane would also affect the partitioning of individual monomers of an aggregate which, if these compounds were acting as a mobile aggregate would also therefore show reduced transport activity.

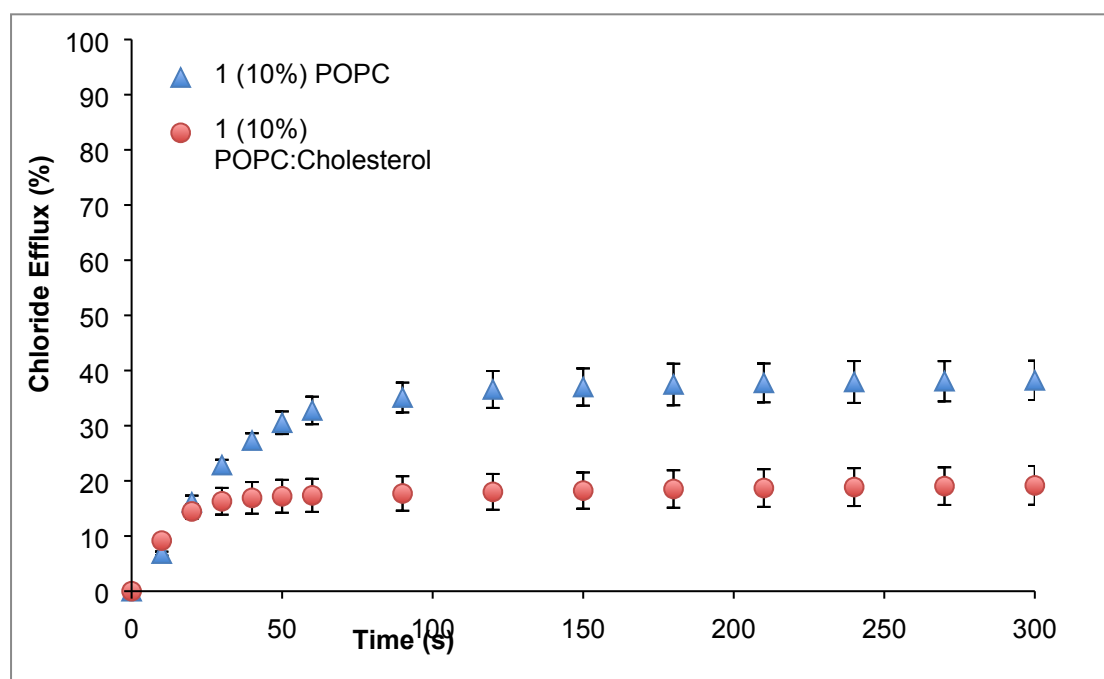


Figure S73: Chloride efflux promoted by **1** (10 mol% with respect to lipid concentration) from unilamellar POPC vesicles or unilamellar 7:3 POPC:cholesterol vesicles loaded with 489 mM NaCl buffered to pH 7.2 with 5 mM sodium phosphate salts. The vesicles were dispersed in 489 mM NaNO₃ buffered to pH 7.2 with 5 mM sodium phosphate salts. At the end of the experiment, detergent was added to lyse the vesicles and calibrate the ISE to 100% chloride efflux. Each point represents the average of 3 trials.

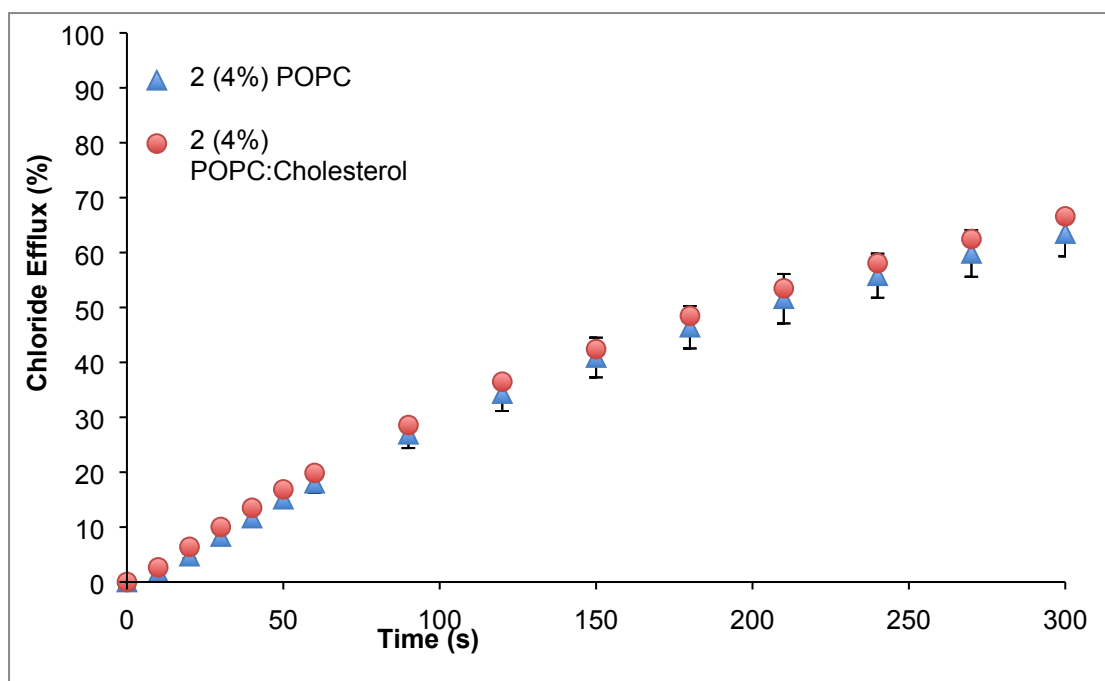


Figure S74: Chloride efflux promoted by **2** (4 mol% with respect to lipid concentration) from unilamellar POPC vesicles or unilamellar 7:3 POPC:cholesterol vesicles loaded with 489 mM NaCl buffered to pH 7.2 with 5 mM sodium phosphate salts. The vesicles were dispersed in 489 mM NaNO₃ buffered to pH 7.2 with 5 mM sodium phosphate salts. At the end of the experiment, detergent was added to lyse the vesicles and calibrate the ISE to 100% chloride efflux. Each point represents the average of 3 trials.

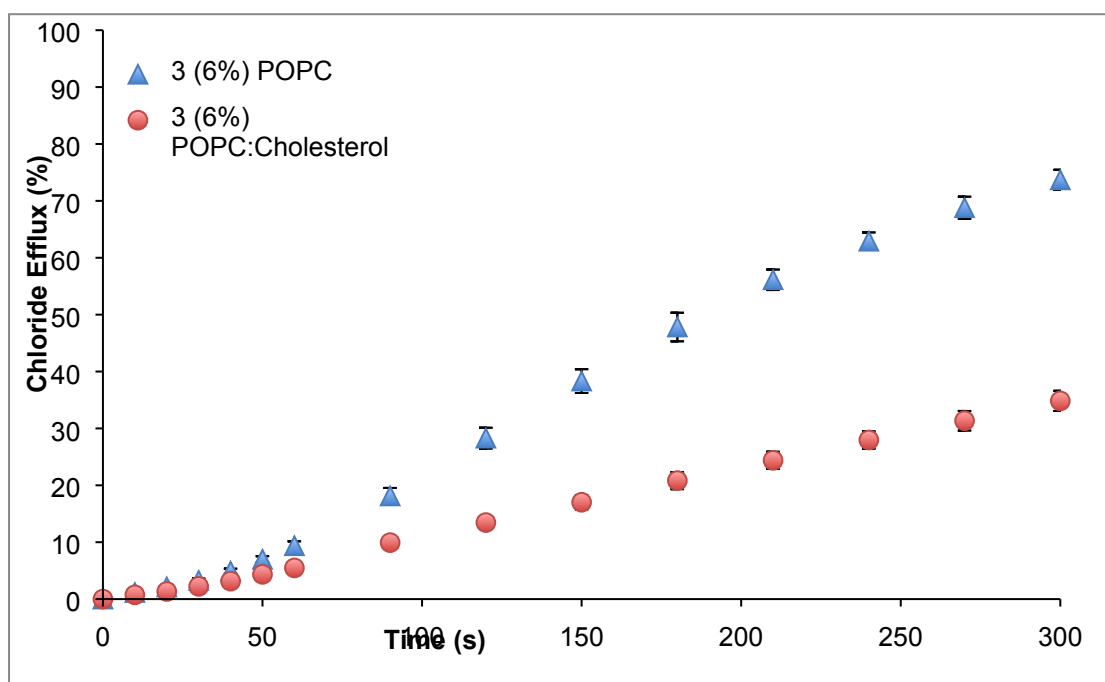


Figure S75: Chloride efflux promoted by **3** (6 mol% with respect to lipid concentration) from unilamellar POPC vesicles or unilamellar 7:3 POPC:cholesterol vesicles loaded with 489 mM NaCl buffered to pH 7.2 with 5 mM sodium phosphate salts. The vesicles were dispersed in 489 mM NaNO₃ buffered to pH 7.2 with 5 mM sodium phosphate salts. At the end of the experiment, detergent was added to lyse the vesicles and calibrate the ISE to 100% chloride efflux. Each point represents the average of 3 trials.

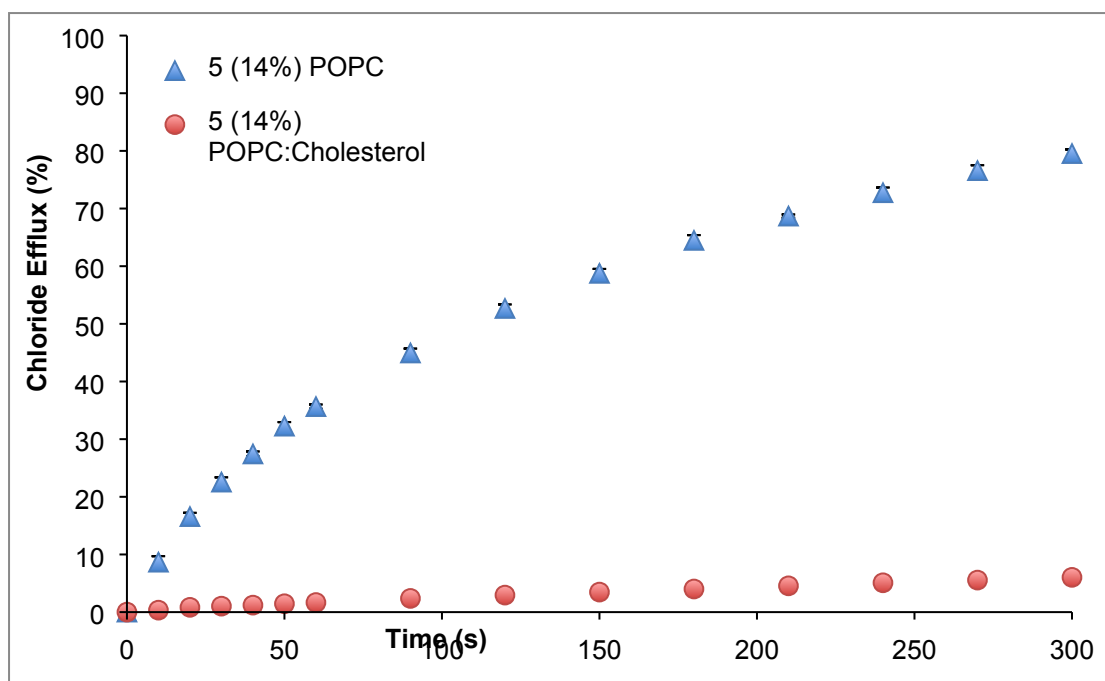


Figure S76: Chloride efflux promoted by **5** (14 mol% with respect to lipid concentration) from unilamellar POPC vesicles or unilamellar 7:3 POPC:cholesterol vesicles loaded with 489 mM NaCl buffered to pH 7.2 with 5 mM sodium phosphate salts. The vesicles were dispersed in 489 mM NaNO₃ buffered to pH 7.2 with 5 mM sodium phosphate salts. At the end of the experiment, detergent was added to lyse the vesicles and calibrate the ISE to 100% chloride efflux. Each point represents the average of 3 trials.

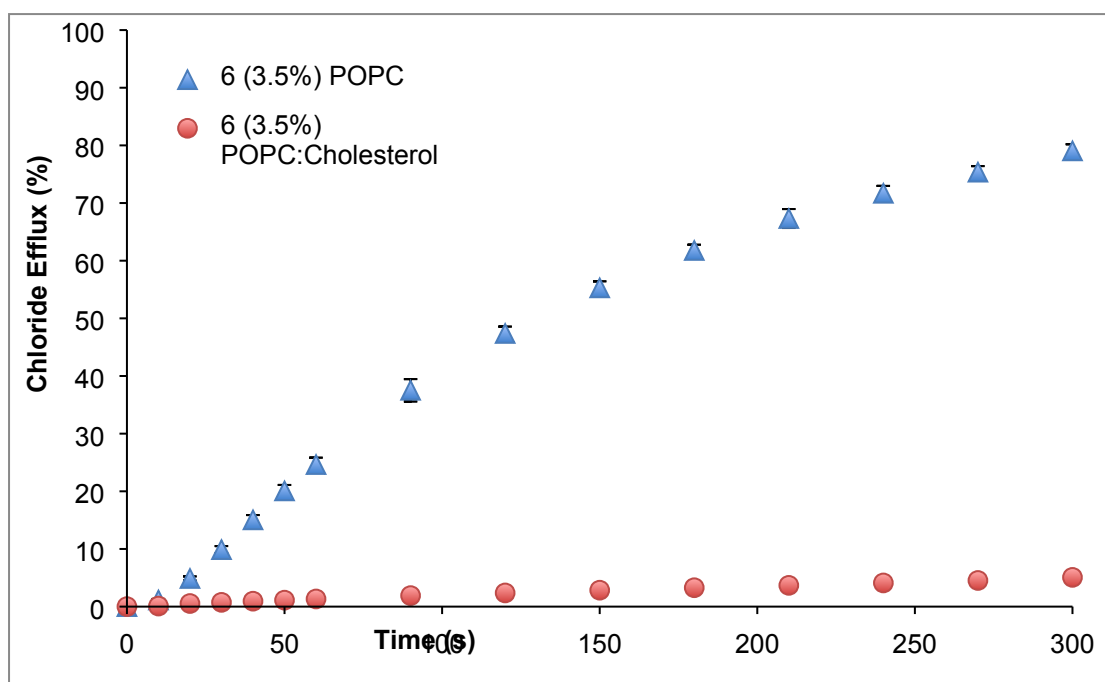


Figure S77: Chloride efflux promoted by **6** (3.5 mol% with respect to lipid concentration) from unilamellar POPC vesicles or unilamellar 7:3 POPC:cholesterol vesicles loaded with 489 mM NaCl buffered to pH 7.2 with 5 mM sodium phosphate salts. The vesicles were dispersed in 489 mM NaNO₃ buffered to pH 7.2 with 5 mM sodium phosphate salts. At the end of the experiment, detergent was added to lyse the vesicles and calibrate the ISE to 100% chloride efflux. Each point represents the average of 3 trials.

U-Tube Experiments:

In a U-Tube experiment, the lipid bilayer is substituted with a bulk organic phase. Under these conditions, ion channel formation is virtually impossible. The U-Tubes were set up with the following conditions:

Organic Phase: Nitrobenzene (15 mL) for solubility reasons, 1 mM carrier and 2 mM TBA⁺PF₆⁻ (to provide counterions during transport).

Aqueous Donating Phase: 489 mM NaCl buffered to pH 7.2 with 5 mM sodium phosphate salts.

Aqueous Receiving Phase: 489 mM NaNO₃ buffered to pH 7.2 with 5 mM sodium phosphate salts.

The change in chloride concentration of the receiving phase was monitored using a chloride selective ISE which was then calibrated at the end of the experiment to convert potential readings (mV) to chloride concentrations (mM). A blank experiment was run using neat nitrobenzene (no carrier) to act as a control measurement. **Figure S78** below shows a plot of chloride concentration in the receiving phase. It is evident that only compound **2** transports more chloride to the receiving phase than the blank control experiment. The small amount of chloride transported in the control experiment can be rationalised by ion pairings between the TBA⁺ counter ion and the Cl⁻. The fact that most of the compounds transport less chloride than the blank control supports the idea that these compounds act as a mobile aggregate in lipid bilayers. One could argue that the distance between the two aqueous phases is simply too far for compounds which transport chloride ions as self-assembled polymers to spontaneously assemble and transport the anion from one side of the U-tube to the other.

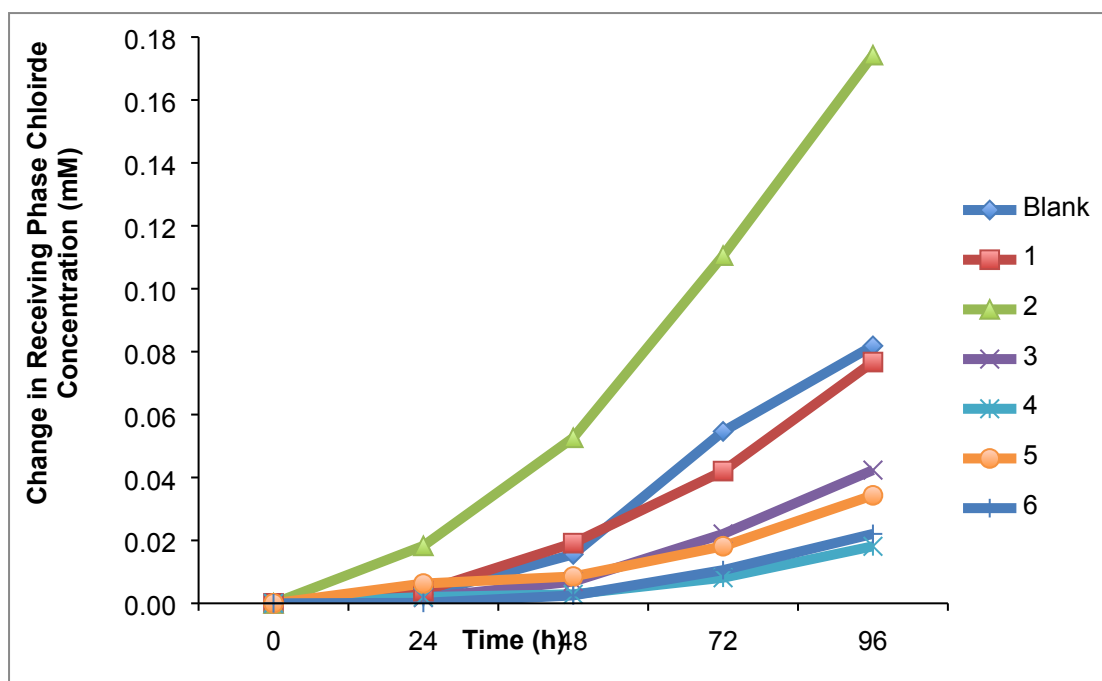
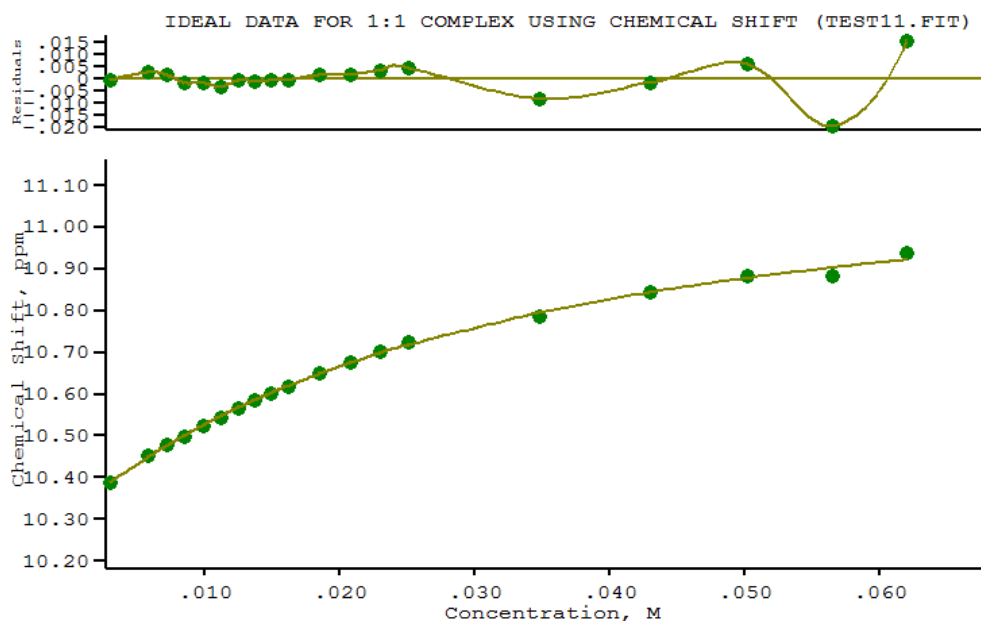


Figure S78: Graph showing change in chloride concentration of the receiving aqueous phase as a function of time for the compounds used in this study.

Anion Binding Studies

^1H NMR titrations were performed as follows: A 1.5 mL 0.01M DMSO- d_6 /0.5% H_2O solution of the receptor was prepared. Of this solution, 0.5 mL was added to an airtight sealed NMR tube. The remaining 1 mL of receptor solution was used to make a 0.15 M solution of a guest anion, which was added as the TBA salt (TEA salt in the case of HCO_3^-). The receptor/salt solution was titrated into the NMR tube in small aliquots and a ^1H NMR spectrum taken after each addition. This ensures the concentration of receptor stays the same whilst the concentration of titrated anion changes. Chemical shifts are reported in ppm and were referenced to residual solvent peaks. The data was fitted to a 1:1 receptor:anion binding isotherm using WinEQNMR2.⁶ DMSO- d_6 is highly hygroscopic and thus, by adding 0.5% water, it ensures no additional moisture from the environment is absorbed by the solvent, meaning the exact concentrations of receptor and receptor/anion solutions are known.



$$K_1 = 42 \text{ M}^{-1} \pm 7\%.$$

Figure S79: Binding curve generated from the ^1H NMR titration of **1** with TBACl in $\text{DMSO-d}_6/0.5\% \text{H}_2\text{O}$. The data was fitted to a 1:1 receptor:anion binding model using WinEQNMR2.

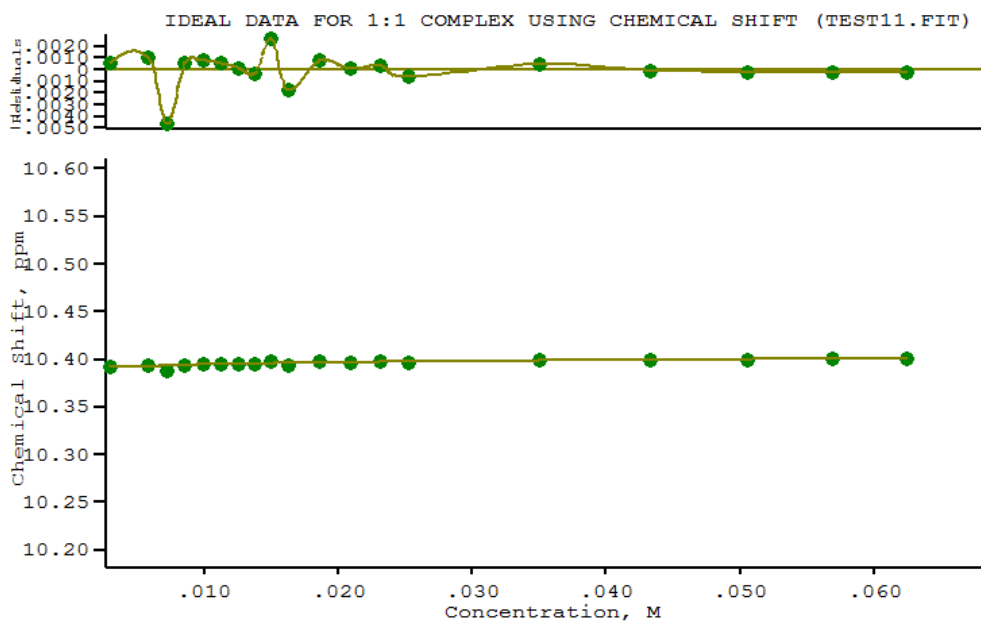
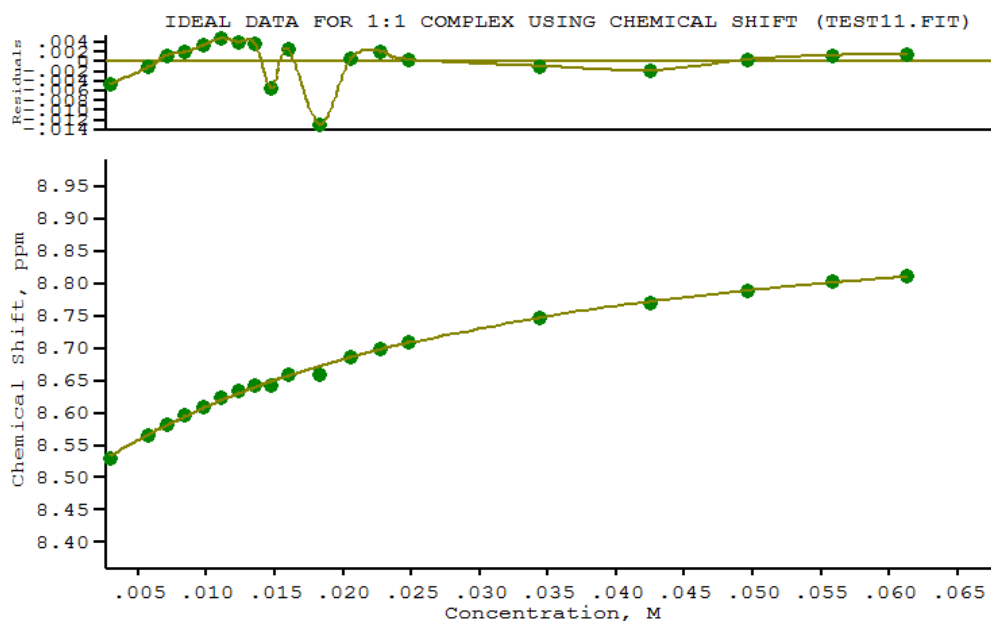
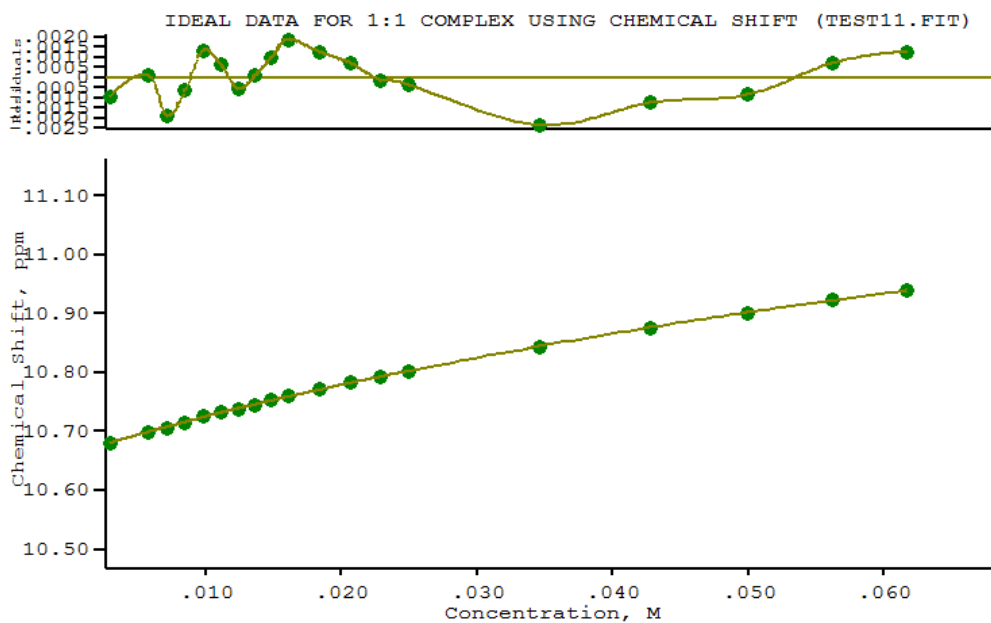


Figure S80: Binding curve generated from the ^1H NMR titration of **1** with TBANO_3 in $\text{DMSO-d}_6/0.5\% \text{H}_2\text{O}$. The data was fitted to a 1:1 receptor:anion binding model using WinEQNMR2. A binding constant could not be accurately obtained due to low changes in chemical shift.



$$K_1 = 47.6 \text{ M}^{-1} \pm 8\%$$

Figure S81: Binding curve generated from the ^1H NMR titration of **1** with TEAHCO_3 in $\text{DMSO-d}_6/0.5\% \text{H}_2\text{O}$. The data was fitted to a 1:1 receptor:anion binding model using WinEQNMR2.



$$K_1 = 9.6 \text{ M}^{-1} \pm 4\%$$

Figure S82: Binding curve generated from the ^1H NMR titration of **2** with TBACl in $\text{DMSO-d}_6/0.5\% \text{H}_2\text{O}$. The data was fitted to a 1:1 receptor:anion binding model using WinEQNMR2.

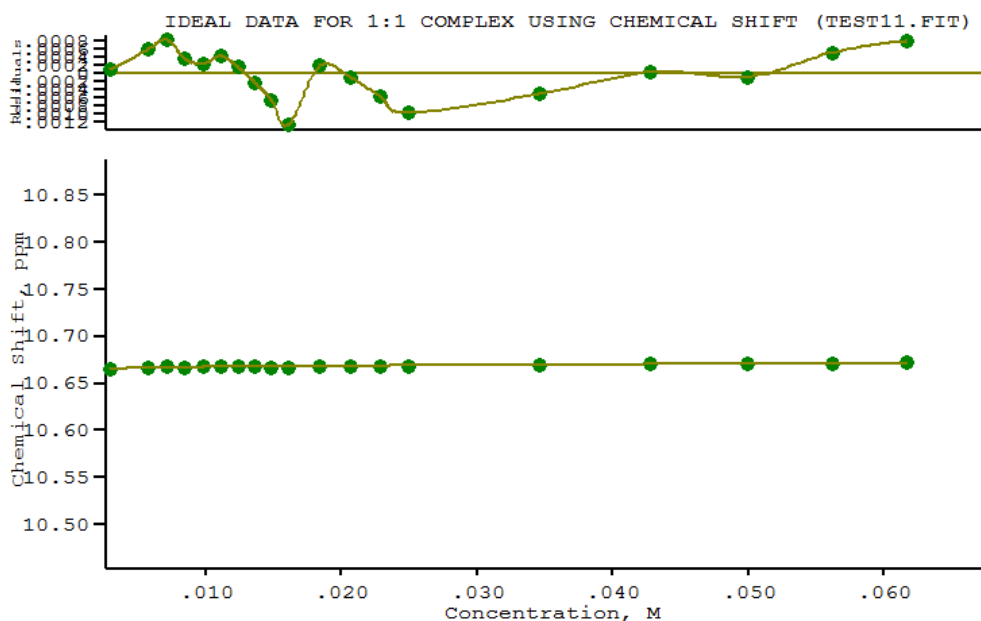
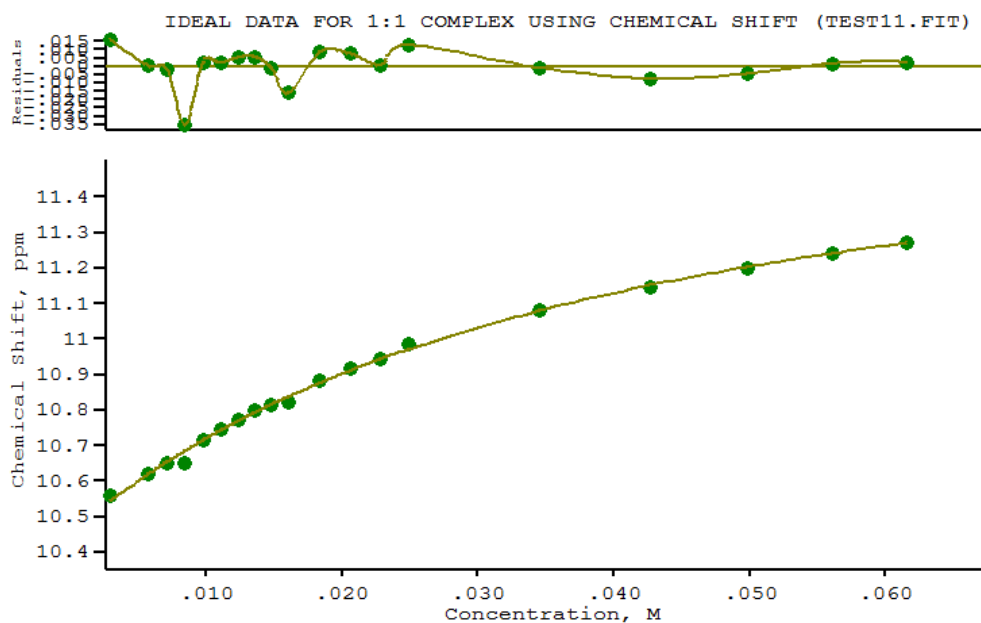
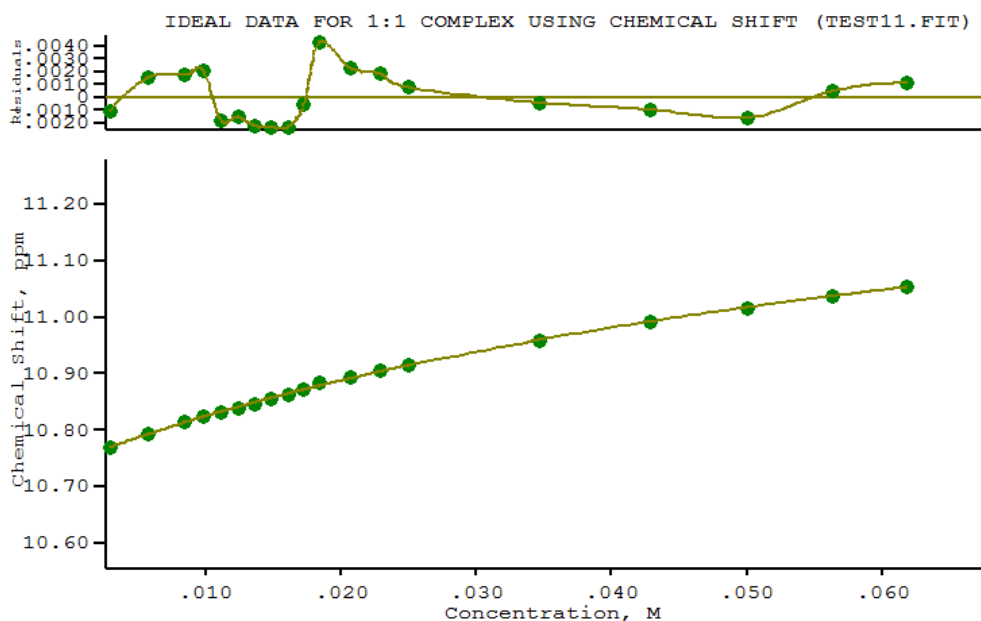


Figure S83: Binding curve generated from the ^1H NMR titration of **2** with TBANO_3 in $\text{DMSO-d}_6/0.5\% \text{H}_2\text{O}$. The data was fitted to a 1:1 receptor:anion binding model using WinEQNMR2. A binding constant could not be accurately obtained due to low change in chemical shift.



$$K_1 = 33.1 \text{ M}^{-1} \pm 9.6\%$$

Figure S84: Binding curve generated from the ^1H NMR titration of **2** with TEAHCO_3 in $\text{DMSO-d}_6/0.5\% \text{H}_2\text{O}$. The data was fitted to a 1:1 receptor:anion binding model using WinEQNMR2.



$$K_1 = 15.4 \text{ M}^{-1} \pm 5.4\%$$

Figure S85: Binding curve generated from the ^1H NMR titration of **3** with TBACl in $\text{DMSO-d}_6/0.5\% \text{H}_2\text{O}$. The data was fitted to a 1:1 receptor:anion binding model using WinEQNMR2.

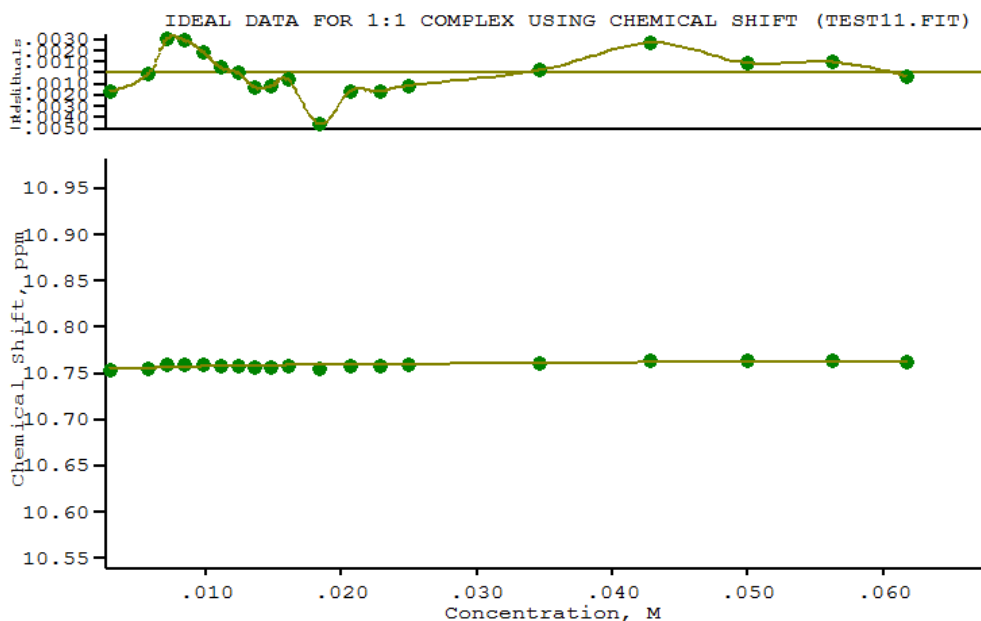
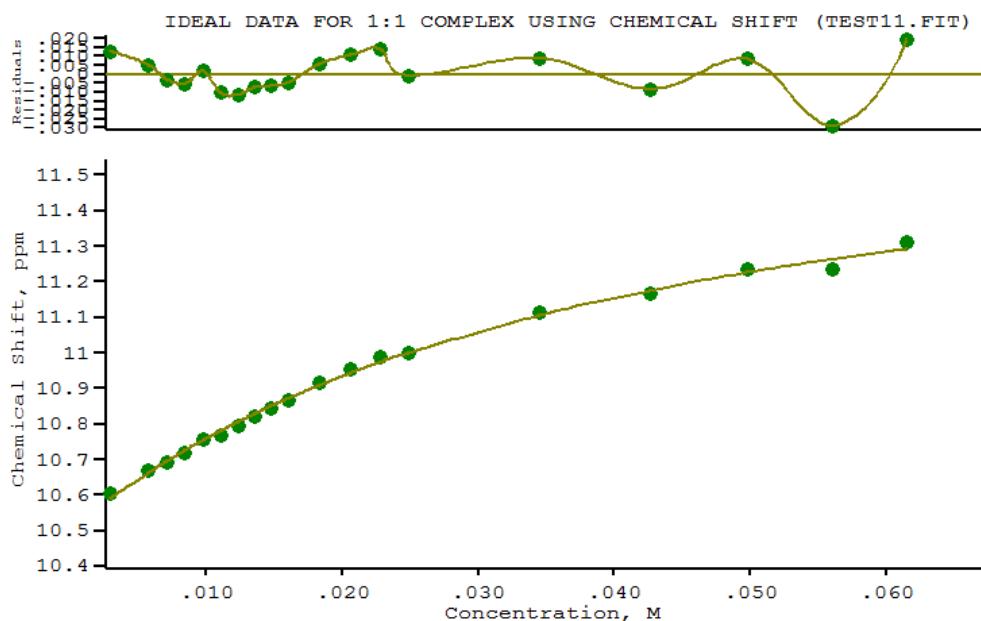


Figure S86: Binding curve generated from the ^1H NMR titration of **3** with TBANO_3 in $\text{DMSO-d}_6/0.5\% \text{H}_2\text{O}$. The data was fitted to a 1:1 receptor:anion binding model using WinEQNMR2. A binding constant could not be accurately obtained due to small change in chemical shift.



$$K_1 = 32.1 \text{ M}^{-1} \pm 10\%$$

Figure S87: Binding curve generated from the ^1H NMR titration of **3** with TEAHCO_3 in $\text{DMSO-d}_6/0.5\% \text{H}_2\text{O}$. The data was fitted to a 1:1 receptor:anion binding model using WinEQNMR2.

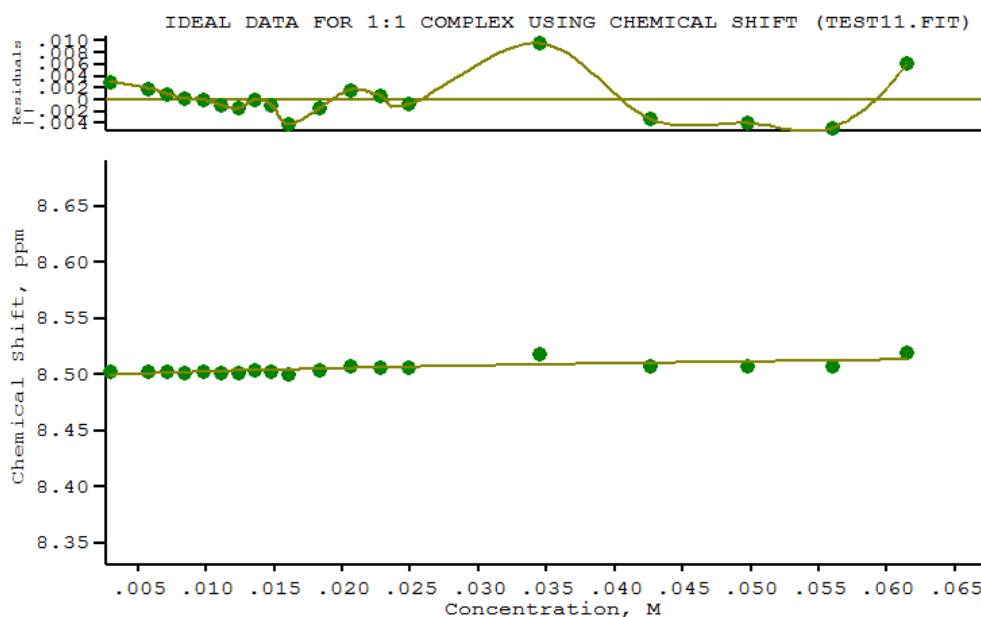
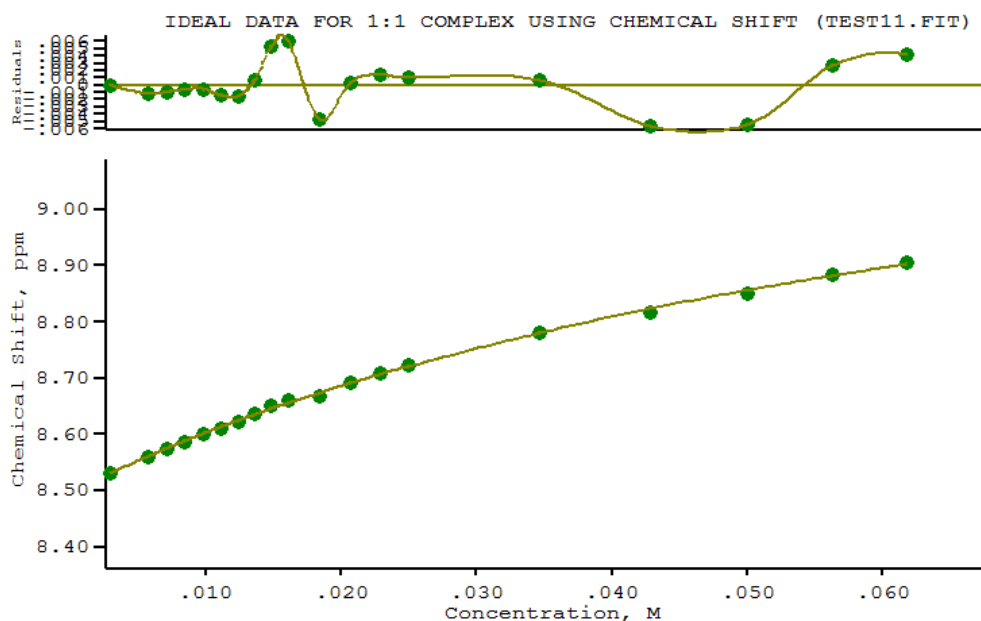
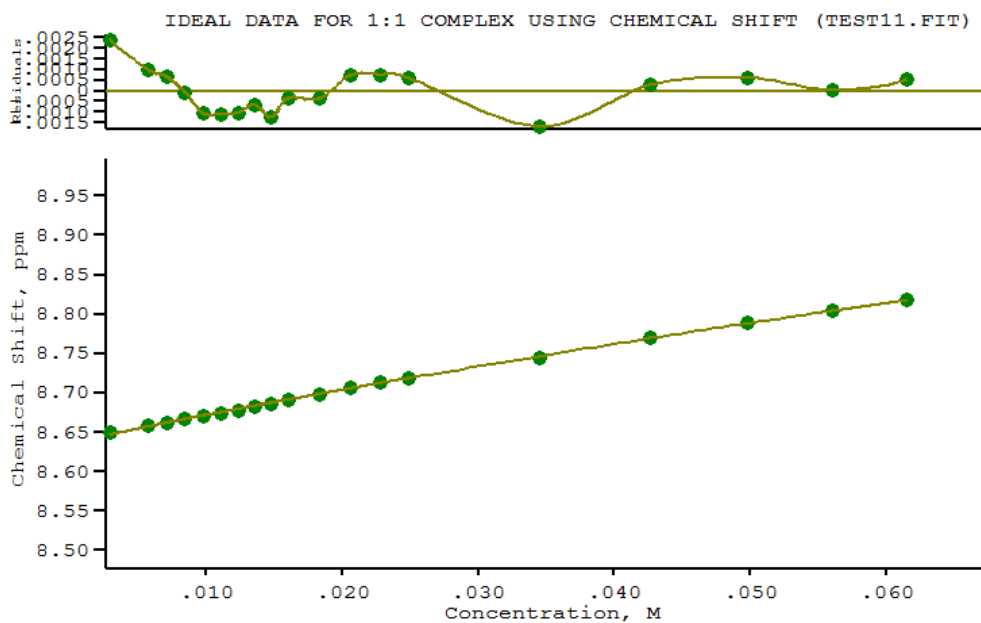


Figure S88: Binding curve generated from the ^1H NMR titration of **4** with TBANO_3 in $\text{DMSO-d}_6/0.5\% \text{H}_2\text{O}$. The data was fitted to a 1:1 receptor:anion binding model using WinEQNMR2. A binding constant could not be accurately obtained due to small change in chemical shift.



$$K_1 = 15.8 \text{ M}^{-1} \pm 5\%$$

Figure S89: Binding curve generated from the ^1H NMR titration of **4** with TEAHCO_3 in $\text{DMSO-d}_6/0.5\% \text{H}_2\text{O}$. The data was fitted to a 1:1 receptor:anion binding model using WinEQNMR2.



$$K_1 = 3.6 \text{ M}^{-1} \pm 10\%$$

Figure S90: Binding curve generated from the ^1H NMR titration of **5** with TBACl in $\text{DMSO-d}_6/0.5\% \text{H}_2\text{O}$. The data was fitted to a 1:1 receptor:anion binding model using WinEQNMR2.

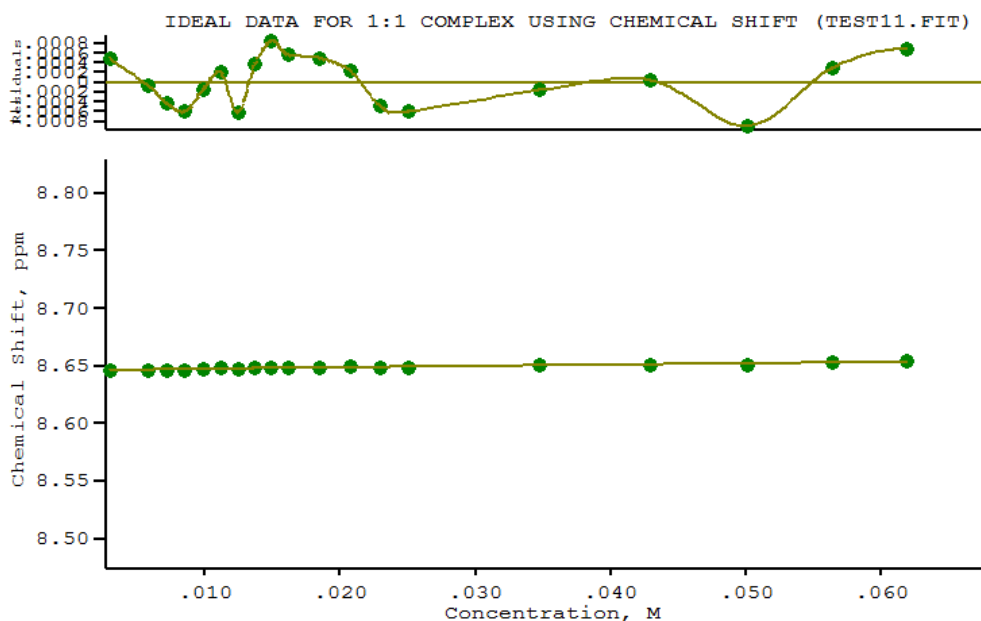
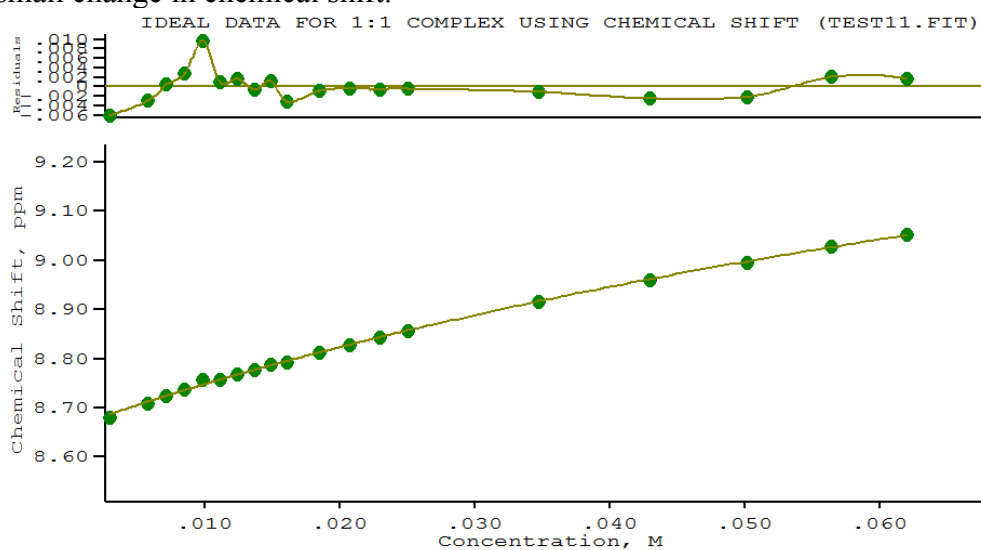
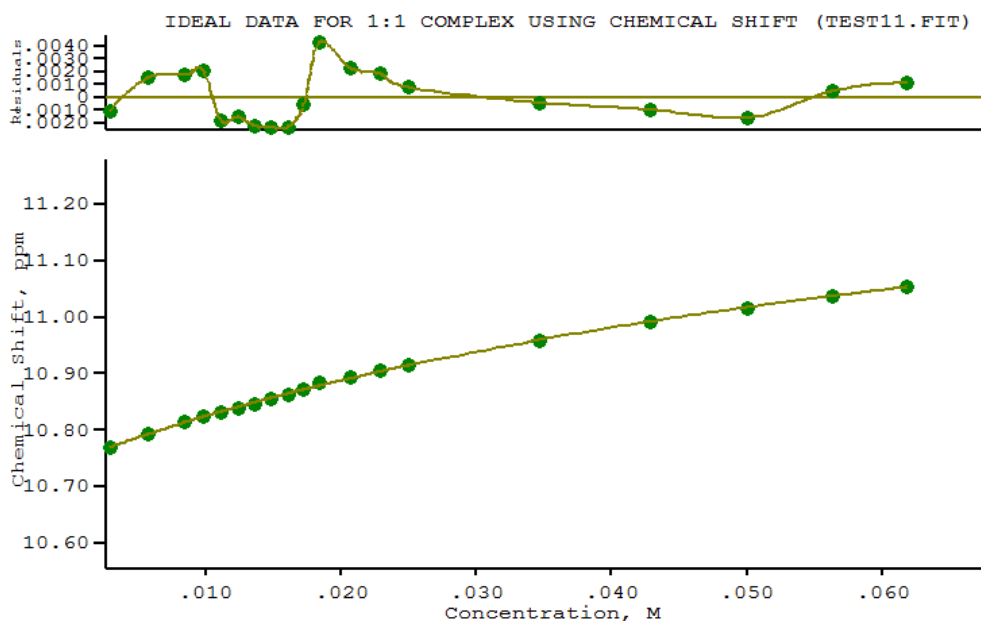


Figure S91: Binding curve generated from the ^1H NMR titration of **5** with TBANO_3 in $\text{DMSO-d}_6/0.5\% \text{H}_2\text{O}$. The data was fitted to a 1:1 receptor:anion binding model using WinEQNMR2. A binding constant could not be accurately obtained due to small change in chemical shift.



$$K_1 = 9.2 \text{ M}^{-1} \pm 10\%$$

Figure S92: Binding curve generated from the ^1H NMR titration of **5** with TMAHCO_3 in $\text{DMSO-d}_6/0.5\% \text{H}_2\text{O}$. The data was fitted to a 1:1 receptor:anion binding model using WinEQNMR2.



$$K_1 = 8.7 \text{ M}^{-1} \pm 15\%$$

Figure S93: Binding curve generated from the ^1H NMR titration of **6** with TBACl in $\text{DMSO-d}_6/0.5\% \text{H}_2\text{O}$. The data was fitted to a 1:1 receptor:anion binding model using WinEQNMR2.

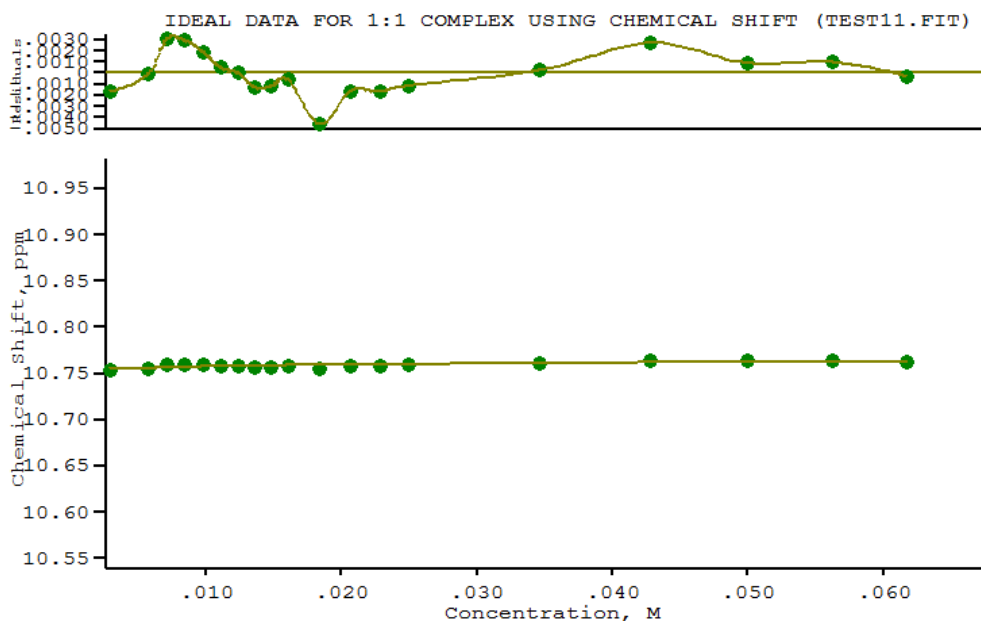
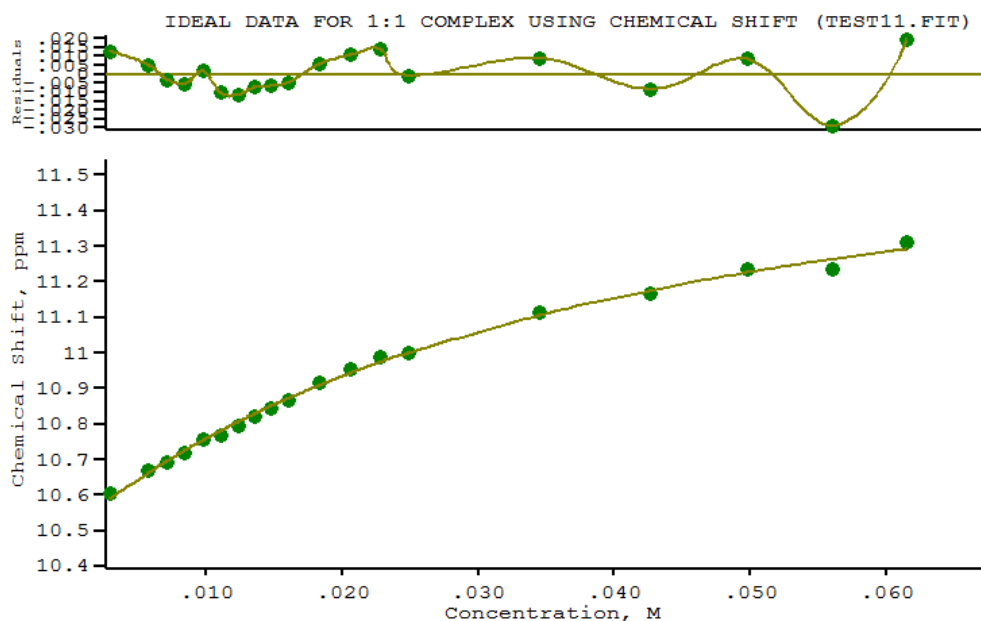


Figure S94: Binding curve generated from the ^1H NMR titration of **5** with TBANO_3 in $\text{DMSO-d}_6/0.5\% \text{H}_2\text{O}$. The data was fitted to a 1:1 receptor:anion binding model using WinEQNMR2. A binding constant could not be accurately obtained due to small change in chemical shift.



$$K_1 = 14.1 \text{ M}^{-1} \pm 15\%$$

Figure S95: Binding curve generated from the ^1H NMR titration of **6** with TEAHCO_3 in $\text{DMSO-d}_6/0.5\% \text{H}_2\text{O}$. The data was fitted to a 1:1 receptor:anion binding model using WinEQNMR2.

Fluorescence Studies

Fluorescence titration protocol: The fluorescence emission intensity for compound **3** was found to be maximal for all wavelengths with $\lambda_{\text{ex}} = 365 \text{ nm}$ when both slits were 5 nm. The fluorescence emission was recorded using a *Varian Cary Eclipse Fluorescence Spectrophotometer*. The compound was titrated into either a) Methanol, b) 0.5 mM unilamellar POPC vesicles (prepared as described previously) suspended in aqueous 489 mM NaCl solution, buffered to pH 7.2 with sodium phosphate salts, or c) 0.5 mM unilamellar POPC:Cholesterol vesicles 7:3 molar ratio suspended in aqueous 489 mM NaCl solution, buffered to pH 7.2 with sodium phosphate salts. The compound was added as a Methanol solution (maximum 50 μL methanol added due to solubility reasons) and fluorescence spectra taken over a 0-100 μL concentration range. To show no change in fluorescence spectra was observed over time, each concentration was an average of three separate scans taken at 0 mins, 1 min and 2 mins, although no change in fluorescence spectra was observed over this time scale.

Excimer spectra in water. Fluorescence spectra was taken for compound **3** as mentioned above when the compound was added as a methanol solution to aqueous sodium chloride buffer (489 mM buffered to pH 7.2 with sodium phosphate salts).

Figure S96 shows that the intensity of the excimer spectra changed over the period of 1 minute. The fluorescence spectra **3** added to vesicles did not change over time.

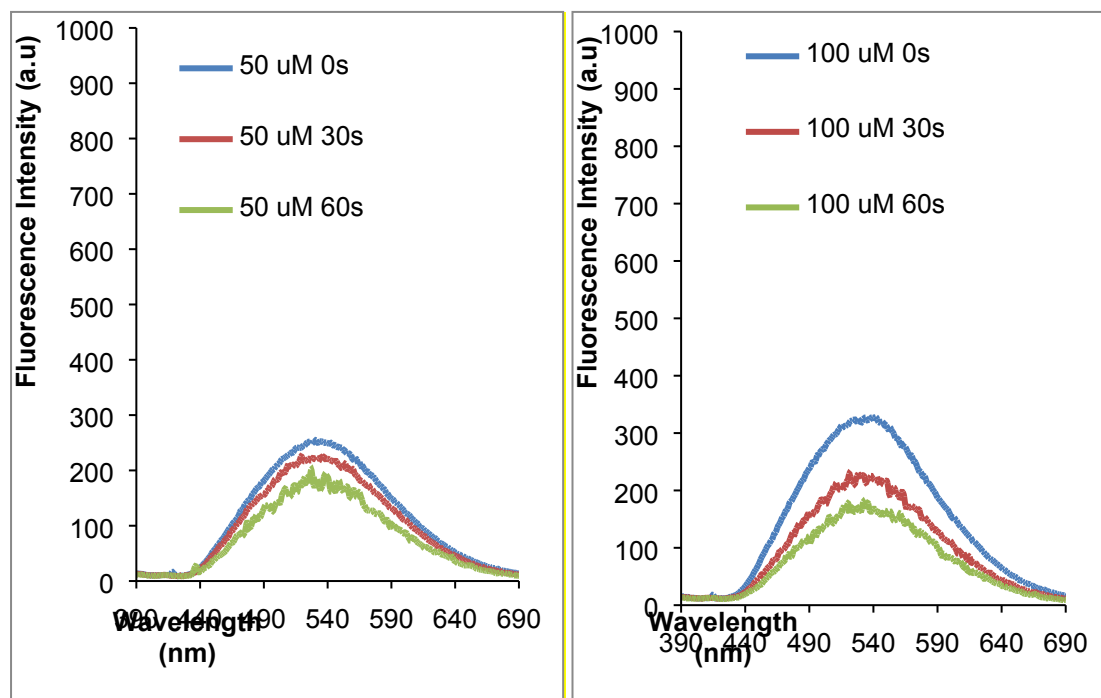


Figure S96: Fluorescence spectra of **3** added as a methanol solution to aqueous sodium chloride buffer. Spectra recorded for a) 50 uM **3** over a period of 60 s and b) 100 uM **3** over a period of 60 s. The intensity of the single peak at 540 nm decreases over time as the compound visibly precipitated out of solution in this time scale.

Kinetic Study:

To monitor whether the intensity of the monomer or excimer emission peaks of **3** changed over time, we carried out a fluorescence study where the intensity of the wavelength at 456 nm and 540 nm were monitored for a period of 10 minutes. The receptor was added as a methanol solution after 30s. The study showed that the compound rapidly aggregates in the phospholipid bilayer and then this does not change over time, implying that the degree of aggregation stays the same. This suggests that the compound rapidly enters the phospholipid bilayer and then

aggregates into its transporting unit. The study was repeated at 50 uM and 100 uM of

3. The study at 50 uM figure (**S97a**) shows a quick spike of the aggregated 540 nm which disappears over the course of ~30 s whilst the monomer peak increases over this time. This suggests the compound initially aggregates in the aqueous medium, and subsequently partitions into the lipid bilayer. This is visible to a lesser extent in the 100 uM study (**S97b**)

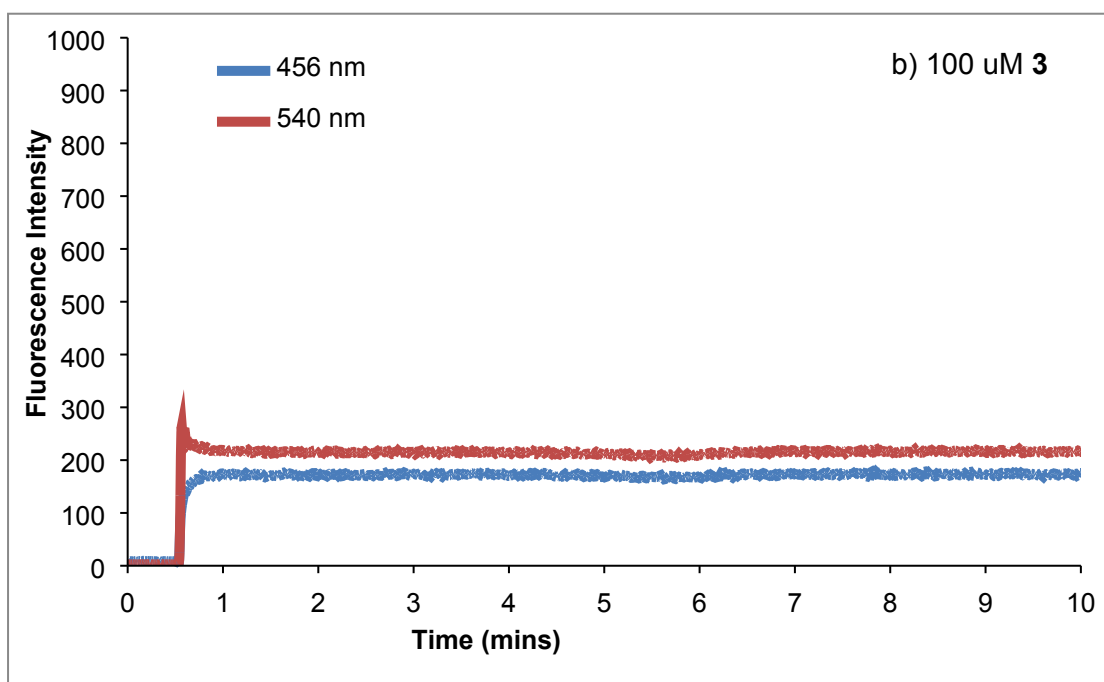
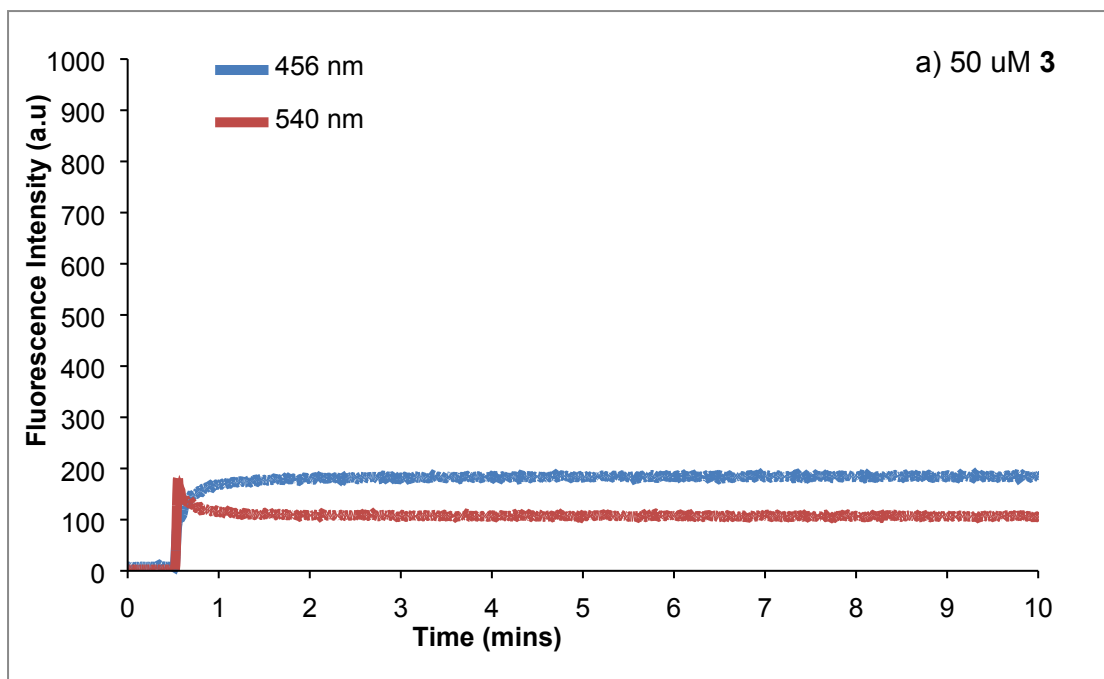


Figure S97: Fluorescence spectra monitoring the change in intensity of the monomer and excimer peaks at 456 nm and 540 nm respectively over time. $\lambda_{\text{ex}} = 365$ nm and both slits were 5 nm. The compound was added as a methanol solution at 30 s to a solution of 0.5 M unilamellar POPC vesicles suspended in aqueous 489 mM NaCl buffered to pH 7.2 with sodium phosphate salts. Spectra shows a) 50 μM **3** and b) 100 μM **3**.

References

1. M. P. Hughes and B. D. Smith, *J. Org. Chem.*, 1997, **62**, 4492–4499.
2. Y. J. Im, K. Y. Lee, T. H. Kim and J. N. Kim, *Tetrahedron Lett.*, 2002, **43**, 4675–4678.
3. S. Brooks, C. Caltagirone, A. Cossins, P. Gale and M. Light, *Supramol. Chem.*, 2008, **20**, 349–355.
4. J. P. Larocca and M. A. Y. Sharkawi, *J. Pharm. Sci.*, 1967, **56**, 916–918.
5. R. C. MacDonald, R. I. MacDonald, B. P. M. Menco, K. Takeshita, N. K. Subbarao and L. Hu, *Biochim. Biophys. Acta - Biomembr.*, 1991, **1061**, 297–303.
6. M. J. Hynes, *J. Chem. Soc. Dalton Trans.*, 1993, 311.